Received: 19 March 2021 | Revised: 23 September 2021 | Accepted: 25 September 2021

DOI: 10.1111/gcb.15922

Global Change Biology WILEY

PRIMARY RESEARCH ARTICLE

Trends in climatically driven extreme growth reductions of *Picea abies* and *Pinus sylvestris* in Central Europe

Václav Treml[1] | Jiří Mašek[1] | Jan Tumajer[1] | Miloš Rydval[2] | Vojtěch Čada[2] | Ondřej Ledvinka[3] | Miroslav Svoboda[2]

[1]Department of Physical Geography and Geoecology, Faculty of Science, Charles University, Prague, Czechia

[2]Department of Forest Ecology, Faculty of Forestry and Wood Science, Czech University of Life Science, Prague, Czechia

[3]Czech Hydrometeorological Institute, Prague, Czechia

Correspondence
Václav Treml, Department of Physical Geography and Geoecology, Faculty of Science, Charles University, Prague, Czechia.
Email: treml@natur.cuni.cz

Funding information
Grantová Agentura České Republiky, Grant/Award Number: 19-138076S

Abstract

Extreme tree growth reductions represent events of abrupt forest productivity decline and carbon sequestration reduction. An increase in their magnitude can represent an early warning signal of impending tree mortality. Yet the long-term trends in extreme growth reductions remain largely unknown. We analyzed the trends in the proportion of trees exhibiting extreme growth reductions in two Central-European conifer species—*Pinus sylvestris* (PISY) and *Picea abies* (PCAB)—between 1901 and 2018. We used a novel approach for extreme growth reduction quantification by relating their size to their mean recurrence interval. Twenty-eight sites throughout Czechia and Slovakia with 1120 ring width series representing high- and low-elevation forests were inspected for extreme growth reductions with recurrence intervals of 15 and 50 years along with their link to climatic drivers. Our results show the greatest growth reductions at low-elevation PCAB sites, indicating high vulnerability of PCAB to drought. The proportions of trees exhibiting extreme growth reductions increased over time at low-elevation PCAB, decreased recently following an abrupt increase in the 1970–1980s at high-elevation PCAB, and showed nonsignificant trends in high- and low-elevation PISY. Climatic drivers of extreme growth reductions, however, shifted over time for all site categories as the proportion of low-temperature-induced extreme growth reductions declined since the 1990s, whereas events caused by drought consistently increased in frequency during the same period. We observed higher growth volatility at the lower range of distribution compared with the upper range margin of PISY and PCAB. This will undoubtedly considerably impact tree growth and vitality as temperatures and incidence of drought in Central Europe are expected to further increase with ongoing climate change.

KEYWORDS
cold spell, conifers, drought, Norway spruce, Scots pine, tree growth, tree rings

1 | INTRODUCTION

Due to climate change, temperate forests are facing the growing frequency and magnitude of extreme climatic events such as heat waves or seasonal droughts with detrimental impacts on tree growth (Dannenberg et al., 2019; Sánchez-Salguero et al., 2017; Scharnweber et al., 2020), tree mortality (Camarero et al., 2015; DeSoto et al., 2020; Vanoni et al., 2016) and ecosystem productivity (Kolus et al., 2019). By contrast, the ongoing warming is reflected by increasing growth trends and improved tree vigor in cold-limited

boreal and mountain forests (D'Orangeville et al., 2018; Ponocná et al., 2016; Silva et al., 2016). High spatial and inter-annual variability in tree growth and changing size and frequency of extreme tree growth reductions (EGRs) and their regional variability represent an important source of uncertainty in global carbon budgets (Tei et al., 2017). However, representative data on long-term trends in EGRs for major forest ecosystems and their climatic drivers remain poorly understood.

Time series of annual stem growth closely mirror climatic factors including extreme events, which has, for example, been illustrated by the use of extremely narrow tree rings as indicators of abrupt cooling (Battipaglia et al., 2010; D'Arrigo et al., 2013; Pearson et al., 2020) or major droughts (Cook et al., 2015). The size of EGRs depends not only on the nature of the extreme climatic event (or other sources of disturbances; Anderegg et al., 2015) but also on legacy effects due to previous tree growth history, vigor, and within-stand interactions (Bose et al., 2020; Linares et al., 2010; Serra-Maluquer et al., 2018). The probability of EGR occurrence in conifers increases after two or more subsequent extreme climatic events (Anderegg et al., 2020; Gao et al., 2018). Trees with high growth rates prior to an extreme climatic event often exhibit stronger growth reductions compared with slow-growing trees and vice versa as slow-growing individuals prioritize investments in defense mechanisms and root biomass and are thus better prepared for extreme climatic events (Martínez-Vilalta et al., 2012; Zang et al., 2014). Furthermore, dominant trees are more resistant to drought compared with suppressed individuals because the large trees can more efficiently compete for soil moisture (Zang et al., 2012). Drought resistance can also be influenced by growth variability before a drought event, with higher growth variability typically resulting in more pronounced EGRs (Bose et al., 2020). All the abovementioned alterations of tree growth responses to drought might change over time as the potential for some degree of acclimation after a series of extreme climatic events has previously been reported (Pretzsch et al., 2020).

In temperate parts of Europe, EGRs have recently caused severe drops in net ecosystem productivity (Trotsiuk et al., 2020). Specific climatic conditions usually result in inverse tree growth responses between high- and low-elevation forests given their position relative to the species climatic optimum (Neuwirth et al., 2007; Zang et al., 2014). Indeed, warm and dry events typically have a negative effect in lowlands (formation of narrow tree rings) and a positive influence in mountain regions (formation of wide tree rings) and vice-versa for cold and wet events (Charru et al., 2017; Lebourgeois et al., 2010; Neuwirth et al., 2007; Rolland et al., 2000). Over the past century, several years characterized by extremely reduced growth (e.g., 1906, 1921, 1947, 1962, 1976, 2003, and 2018) have been reported across lowland areas of Western and Central Europe (Lebourgeois et al., 2010; Neuwirth et al., 2007; Rammig et al., 2015; Vitali et al., 2017; Vitasse et al., 2019). Conversely, 1913, 1942, 1948, 1954, 1974, and 1992 were reported as extremely narrow tree rings in mountain regions of Central and Eastern Europe (Hartl-Meier et al., 2014; Rammig et al., 2015; Treml et al., 2015). This suggests that European forests experienced periods of both regional EGR events with tree growth affected across large spatial scales (e.g., 1940s, 1970s) as well as events restricted to specific sites.

In Central Europe, average temperatures have increased since the beginning of the 20th century by about 1°C (IPCC, 2021) leading to higher evapotranspiration rates (Mozny et al., 2020) and soil moisture deficits (Hanel et al., 2018). Together with recent summer heat waves (e.g., 2003, 2015, 2018; Scharnweber et al., 2020) these changes have been manifested as EGRs and an overall decrease of tree vigor across vast areas of Central Europe (Brun et al., 2020; Etzold et al., 2019; Sidor et al., 2019). However, whether recent EGRs represent a continuation of a 20th century trend or they are unprecedented in the century-wide context remains unclear. Furthermore, only limited information has been available on species-specific trends in EGRs and differences in these trends between warm and cold ranges of species distribution.

In this study, we analyze the trends in the proportion of trees exhibiting EGRs based on 118-year tree-ring width series from 28 low- and high-elevation sites of *Picea abies* and *Pinus sylvestris* in Central Europe. Because individual trees from the same forest stand might show variable sensitivity to climate (Carrer, 2011), we build tree-specific distribution functions describing the relationship between the size of EGRs and their recurrence interval (i.e., mean period between two EGRs with the same intensity). We focus our analyses on medium as well as high magnitude EGRs based on recurrence intervals of 15 and 50 years, respectively. We hypothesize that during the 1901–2018 period the proportion of trees with EGRs has been increasing at drought-limited sites as a consequence of recent more frequent droughts (Brázdil et al., 2015), whereas EGRs have decreased at temperature-limited sites as a consequence of increasing temperature (Tumajer et al., 2021). We further hypothesize that both PISY and PCAB high-elevation sites exhibit temperature-induced EGRs, whereas low-elevation sites of both species show EGRs caused by drought.

2 | MATERIALS AND METHODS

2.1 | Study species and sampling site network

In Central Europe, conifer forests dominated by PCAB and PISY represent the major forest ecosystems covering large areas that are of considerable economic importance (Spiecker, 2000). Across the Czech Republic and Slovakia, PCAB dominates in mountain regions at elevations above 1000 m a.s.l. PCAB can, however, also be naturally found in lowlands, typically occurring in valley floors and lower parts of slopes (Chytrý, 2013; Szabó et al., 2017). PISY occurs from lowlands to highlands usually at less productive sites (sandstone areas, river terraces, rocky slopes) or at waterlogged locations (Chytrý, 2013). For this study, we sampled 28 natural stands of PCAB and PISY distributed at the margins of their elevation distribution—at low and high-elevation sites throughout the Czech Republic and Slovakia

(Figure 1; Table 1). Sites were classified based on their relative position as high elevation PCAB and PISY (PCAB high, PISY high) and low elevation PCAB and PISY (PCAB low and PISY low). PCAB high were situated on moderate slopes, whereas PCAB low were located on steep slopes near valley bottoms. PISY stands were located either in areas with sandstone bedrock or on rocky (often steep) slopes. All stands represent near-natural forests in natural reserves with probable occasional logging in the past. The studied stands comprised trees old enough to record tree-ring variability since the beginning of the 20th century. We acquired data from 40 to 60 dominant and co-dominant trees from each stand (Table 1) with the final data set containing 1120 tree-ring series.

2.2 | Growth data processing

From each tree we collected one to two increment cores at breast height. Cores were processed following standard dendrochronological procedures (Speer, 2011). Tree-ring widths were measured and visually and statistically cross-dated (Stokes & Smiley, 1998).

Abrupt growth changes were subsequently calculated on raw series using the method of Schweingruber et al. (1990) called "relative growth change" (Jetschke et al., 2019) as follows:

$$\mathrm{RGC}_t = \frac{R_t}{\frac{1}{6} \cdot \sum_{n=t-6}^{t-1} R_n},$$

where RGC is relative growth change, R is tree-ring width and t represents years. RGC for a given year is defined as the ratio of the tree-ring width in that year to the mean tree-ring width during the previous 6 years. A 6-year window was selected as a trade-off between window length (long window preferred) and avoidance of the age trend (short window preferred; Jetschke et al., 2019). Furthermore, spectral analysis indicated that a 6-year period effectively captured short-term growth variations (decreasing or increasing sections, peaks or depressions) over 8–12 year cycles inherent in our time series (Supporting Information 1).

Because we were interested in the effect of extreme climatic events triggering growth reductions, we retained negative RGC values for subsequent analysis. Because young trees are typically more sensitive to extreme events than old and big trees (Schweingruber, 1996; Vieira et al., 2009) we adjusted the RGC values to account for age effects. For each site, we computed mixed effect linear models to explain RGC (dependent variable) using cambial age (fixed effect) and tree (random effect). Residuals from these models were then re-scaled to mean negative RGC for each site, and these values represented negative RGCs free of the age effect.

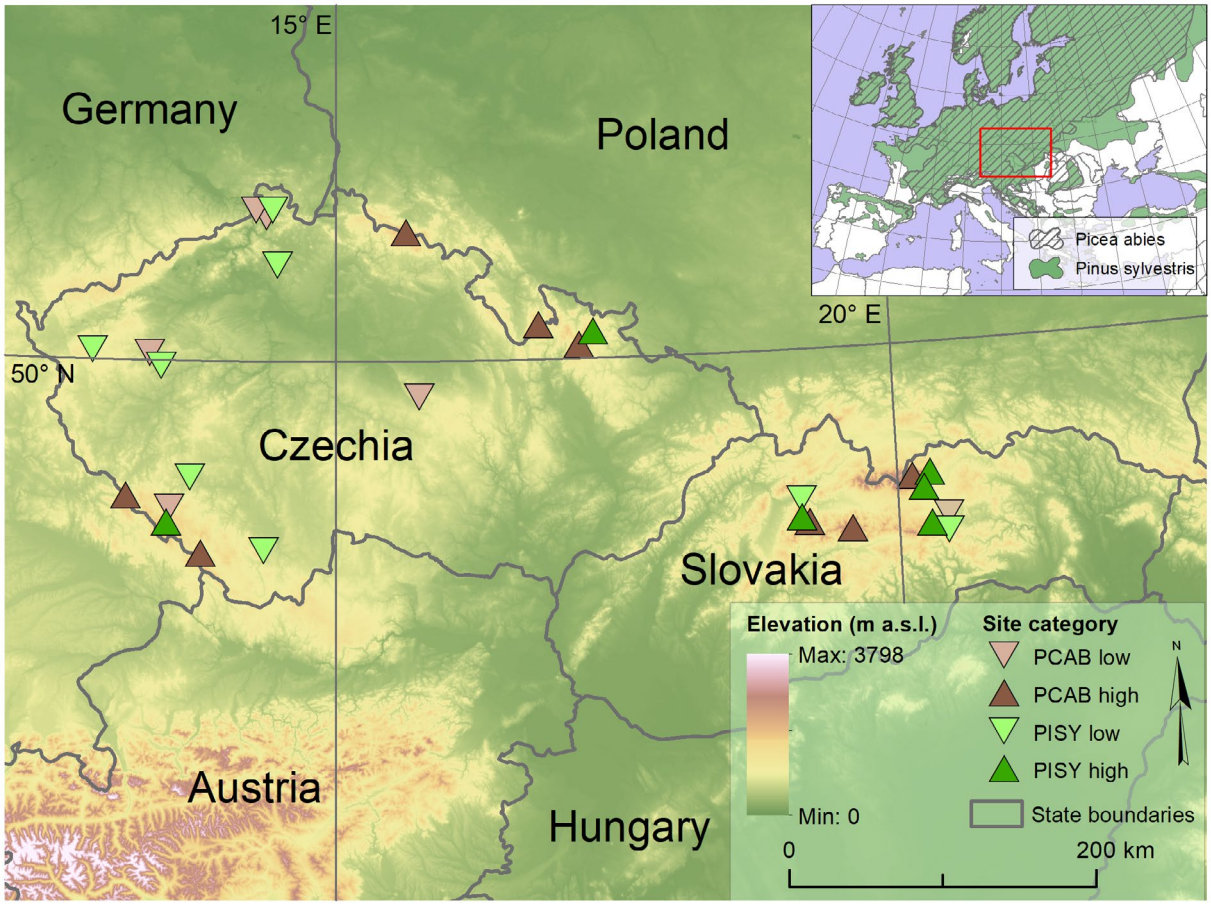

FIGURE 1 Map of the studied stands. Inset shows distribution ranges of *Picea abies* (PCAB) and *Pinus sylvestris* (PISY) in Europe

TABLE 1 Basic characteristics of investigated stands

Site code	Site category	Coordinates (Lat; Long)	Elevation (m a.s.l.)	No. of trees	Average growth rate (mm)	Mean sample length (±SD)
HAV	PCAB low	48.95; 20.42	540	42	0.69	124 ± 15
JET	PCAB low	50.85; 14.35	200	38	1.20	170 ± 39
POL	PCAB low	49.79; 15.75	580	40	2.17	120 ± 20
RAA	PCAB low	50.04; 13.29	460	41	0.91	144 ± 26
REJ	PCAB low	49.13; 13.50	650	41	1.07	185 ± 34
STR	PCAB low	50.88; 14.25	470	35	1.12	113 ± 17
CEZ	PCAB high	48.87; 13.79	950	36	1.33	152 ± 50
DIV	PCAB high	50.07; 17.21	1300	45	0.74	151 ± 30
CHO	PCAB high	48.93; 19.60	1450	43	0.90	136 ± 40
JAV	PCAB high	49.21; 20.16	1400	60	0.64	187 ± 42
KRA	PCAB high	50.20; 16.84	1300	42	0.89	136 ± 61
OST	PCAB high	49.20; 13.11	1200	40	1.01	177 ± 39
SMR	PCAB high	48.98; 19.22	1450	48	1.01	182 ± 42
SIS	PCAB high	50.75; 15.64	1320	44	0.76	109 ± 31
DIK	PISY low	48.89; 14.35	480	34	0.49	124 ± 26
PLU	PISY low	50.05; 12.77	760	41	0.79	119 ± 9
KOS	PISY low	50.56; 14.45	400	43	0.50	203 ± 36
LET	PISY low	48.95; 20.44	550	59	0.48	145 ± 26
LUB	PISY low	49.12; 19.16	620	44	0.51	164 ± 25
PRA	PISY low	49.31; 13.68	470	47	0.49	185 ± 27
RAS	PISY low	50.04; 13.29	460	49	0.72	165 ± 45
RUZ	PISY low	50.88; 14.41	425	47	0.39	122 ± 62
BRE	PISY high	49.04; 13.47	1000	47	0.66	122 ± 62
PAL	PISY high	49.23; 20.32	950	42	0.43	245 ± 16
SUV	PISY high	50.15; 17.34	940	35	0.61	270 ± 66
TAL	PISY high	49.14; 20.25	910	45	0.72	141 ± 8
TMA	PISY high	49.01; 19.15	1100	39	0.52	245 ± 22
TRK	PISY high	48.93; 20.31	910	52	0.45	211 ± 43

The next step involved the identification of years with exceptionally high growth reductions exceeding common year-to-year variability. We applied a recurrence interval method, which identifies theoretical frequencies of extreme events (Dingman, 2002; Figure 2). A long recurrence interval characterizes highly anomalous events, whereas a short recurrence interval can be used to identify high-frequency events. Because the individual sensitivity of trees to extreme events can vary considerably (Hacket-Pain et al., 2019), we performed this analysis at the individual tree level. Inverse RGC values represented input into the calculation (RGC_{inv} in Figure 2a), with higher values representing greater negative deviations in growth. For each tree, all RGCs were ranked from the highest (theoretical recurrence interval of one occurrence over the tree lifespan) to the lowest (2-year recurrence interval on average; Figure 2b). The relationship between recurrence intervals and the respective RGC values was estimated by fitting an exponential curve, and the theoretical magnitudes of high-frequency (15 years) and low-frequency (50 years) RGCs were extracted for each tree (Figure 2d). The selected recurrence intervals were chosen to illustrate trends of relatively high-frequency (i.e., less extreme) and low-frequency (i.e., highly extreme) events. Our results were consistent irrespective of any slight adjustments of the interval size (i.e. 10–25 years for 15-year, or 40–60 years for 50-year recurrence intervals).

Relative growth changes exceeding values of RGC with 15-year or 50-year recurrence intervals are hereafter referred to as extreme growth reductions (EGR15 and EGR50 for 15- a 50-year recurrence intervals respectively; Figure 2e). Differences in the size of EGR15 and EGR50 between site categories were tested using analysis of variance and the Tukey post hoc test.

For each site the proportion of trees exhibiting EGR15 or EGR50 in each year between 1901 and 2018 was calculated. Time series of the proportion of trees with EGR15 or EGR50 were then

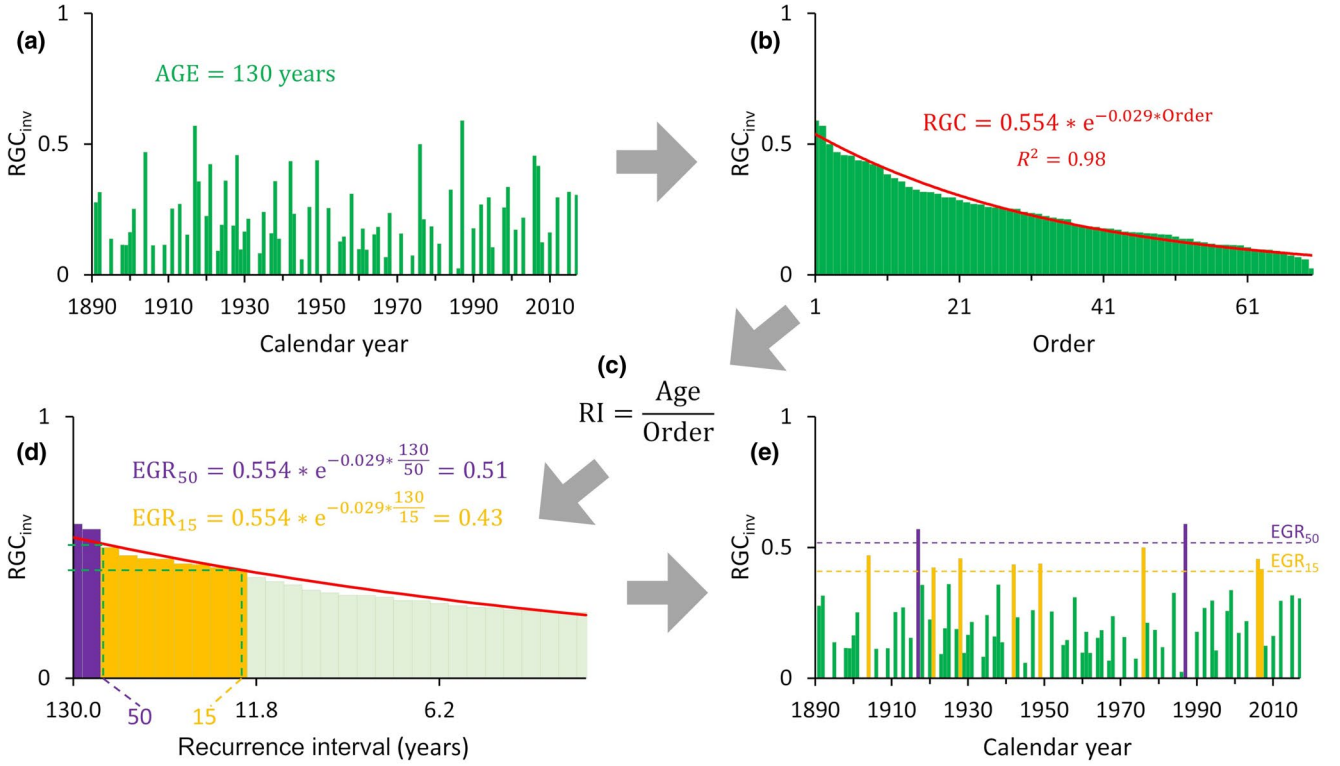

FIGURE 2 Illustration of recurrence interval (RI) calculation starting from original time series of relative growth changes ("RGC_{inv}"; a). Relative growth change (RGCs) were ranked according to their size and fitted with an exponential function (b). The theoretical recurrence interval of RGC_{inv} event with given intensity (order) depends on tree age (i.e., the length of the series; c). RGC_{inv} values corresponding to 15- or 50-year recurrence intervals were computed using a theoretical fitted exponential distribution (d). All RGCs exceeding 15- or 50-year recurrence interval threshold values were defined as extreme growth reductions (e)

fitted using generalized additive mixed effect models (GAMMs; Wood, 2017) to represent the relationship between EGR15, EGR50 and calendar years for each site category (i.e., PCAB high and low, PISY high and low). The structure of the models was as follows:

$$\text{EGR} = s(\text{calender year}) + \text{site} + \varepsilon,$$

where s is a smoothing term, site was considered as a random effect and ε is the error term with an AR1 correlation structure (as mean site EGRs showed some degree of autocorrelation possibly due to legacy effects of drought events on growth in subsequent years; Anderegg et al., 2015). Thin regression splines represented the smoothing term, and the degree of smoothing was defined by internal cross-validation (Wood, 2017). Significance of the site random effect was tested by a comparison of the model with and without random effect using likelihood ratio test. The models were also fitted for an alternative shorter time interval (1960–2018) to assess their temporal stationarity.

To supplement the analysis of extreme growth reductions, we also computed mean stem growth trends using site tree-ring width chronologies derived from regional curve standardization (RCS; Briffa & Melvin, 2011) as RCS standardization is a reliable method for the characterization of long-term growth trends (Peters et al., 2015; Supporting Information 2).

2.3 | Climatic data

We used local climatic data to attribute each EGR to the climatic variable that most likely led to its formation. Climatic data sets for all sites cover 1901–2018 and are based on meteorological station data. All climatic data were provided by Czech and Slovak hydrometeorological institutes and the German meteorological service. Monthly mean temperatures were first interpolated from the nearest set of meteorological stations using orographic regression, which assumes a relationship between temperature and log-transformed elevation (R package gstat; Pebesma, 2004). Precipitation was interpolated from station data using the inverse-distance weighted method with an exponent of two. At least three stations (temperature) or seven stations (precipitation) were always used for interpolation and the number of available stations increased over time. The maximum distance between a meteorological station and a given site was 50 km. Based on the monthly precipitation and temperature data, the standardized precipitation evaporation index (SPEI) was computed

(Vicente-Serrano et al., 2010). For a particular month, four preceding months were considered in calculating the ratio between precipitation and evapotranspiration as part of the Thornthwaite method.

2.4 | Identification of climatic drivers of EGR trends

In the next step, we identified the climatic trigger of each EGR event and separated trends for EGRs with different climatic triggers. First, we determined the dominant climatic drivers based on inter-annual tree-ring width variability for each site using the site tree-ring width chronologies. For this purpose, each tree-ring series was standardized and the age trend removed using a 70-year cubic spline (Cook & Peters, 1981), and a mean site chronology was developed by averaging the detrended series. Based on climate-growth correlations (Fritts, 1976), the main climatic variables influencing stem growth were summer SPEI (June–August) predominantly at low-elevation sites and summer temperature (June–July) at high-elevation sites (Supporting Information 3). Additional seasonal periods with significant effects on tree growth at some sites included spring (either low spring temperature or drought) and late winter temperature (especially low temperatures in February and March; Supporting Information 3).

Second, we assigned each EGR to a climatic driver, including (1) summer drought (June–August SPEI), (2) low summer temperature (June–July mean temperature), (3) low spring temperature (April–May mean temperature), (4) spring drought (April–May SPEI), and (5) winter low temperature (mean temperature February–March). Years that experienced temperature or SPEI with 1SD below the mean of the specific climatic variable were considered as years potentially triggering a reduction in tree growth. The mean and SD were computed over a 50-year window to account for possible acclimation of plants to climatic trends. For summer droughts and summer low temperatures, we also considered the year prior to respective growing season due to lagged tree responses to preceding growing season (Fritts, 1976).

We matched each EGR with its potential climatic driver and classified EGRs as low-temperature-induced (i.e., linked to low summer, spring, or winter temperature) or drought-induced (i.e., linked to spring or summer drought). Some events could not be associated with any climatic driver (classified as "other"), and some EGR events could be related to a combination of drought and cold temperature. For each site category, the differences in the proportion of trees exhibiting EGRs induced by drought or low temperature were tested using analysis of variance to identify a dominant driver of growth reductions. Analysis of variance was also used to test differences in proportions of trees exhibiting EGR between years with unfavorable weather (mean − 1SD for all climatic variables) and remaining years (all years with values > mean − 1SD). The analyses mentioned above were performed both for EGR15 and EGR50; however, because differences between the two groups were negligible, we predominantly focus on the EGR15 results and only present the EGR50 results when necessary.

To inspect trends in EGRs separated according to their respective climatic driver, we again fitted GAMMs (Wood, 2017) for each site category (PCAB high and low, PISY high and low) and the climatic drivers. The models were constructed to represent the relationship between the proportion of trees exhibiting EGRs (with temperature-induced or drought-induced EGRs considered separately) and calendar years with the site as a random variable.

All statistical analyses were performed using R (R Core Team, 2019), namely packages dplR (Bunn, 2008), pointRes (van der Maaten-Theunissen et al., 2015), lme4 (Bates et al., 2015), mgcv (Wood, 2017), and gstat (Pebesma, 2004).

3 | RESULTS

For both EGR15 and EGR50, PCAB high exhibited the lowest values of growth reductions whereas the low-elevation PCAB and PISY sites were characterized by relatively high EGRs (Figure 3). Differences were highly significant between site categories ($p \approx 0.001$). The average EGR with a 15-year recurrence interval was 0.39 for PCAB high (i.e. one event with a growth reduction of at least 39% occurs every 15 years on average). For PCAB low, the average EGR15 was markedly higher (0.49) with significant differences compared with PCAB high and PISY high (0.45). PISY low showed significantly greater EGR15 (0.48) than PISY high (0.45). In general, EGR50 experienced more pronounced between-category differences (Figure 3). Differences were significant between all category combinations ($p \approx 0.001$) with the lowest EGR50 exhibited by PCAB high (with a mean value of 0.53) and the highest for PCAB low (0.63; Figure 3).

Trends in the proportion of trees showing EGR15 for PCAB high were stable until the 1960s followed by a pronounced increase (1970–1980s) and then a decreasing trend since the 1990s (Figure 4; Supporting Information 4). The effect of the smooth term (year) was significant both for the entire (1901–2018) and shortened (1960–2018) period (Figure 4). PCAB low showed a slightly decreasing long-term trend in the proportion of trees with EGR15 followed by an increase since the 2000s. The effect of the smooth term was significant only for the shorter 1960–2018 period, random effect of site played a significant role for EGR15 (Figure 4; Supporting Information 5). Proportions of trees with EGRs in PISY low increased slightly over time, whereas the opposite trend was observed for PISY high. However, the effect of the smoothing term year was not significant both for PISY high and low (Figure 4). The trends in EGR50 mimic those of EGR15 (Figure 4; Supporting Information 5), with a lower proportion of trees exhibiting a more extreme response in the case of EGR50.

Between 66% and 95% of EGR15 events were associated with some type of climatic extreme at each site (Supporting Information 6; Figure 5a). PCAB high experienced the highest proportion of low-temperature-driven EGRs (36%) and the lowest proportion of drought-driven EGRs (21%, significantly lower than all other

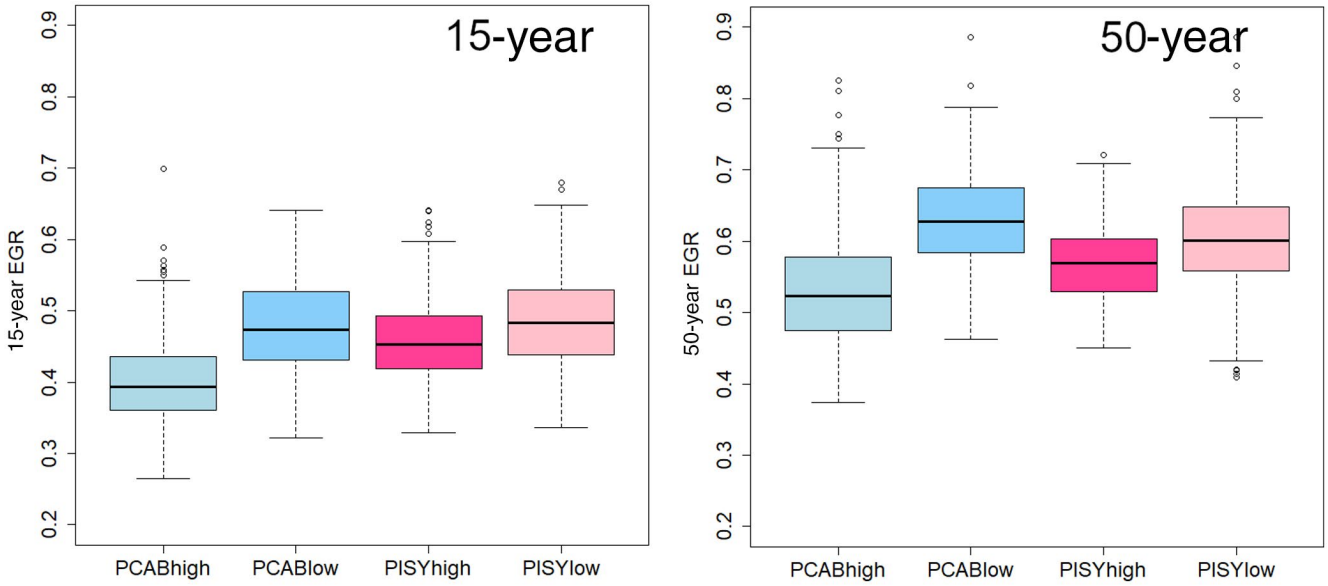

FIGURE 3 Extreme growth reductions with 15- and 50-year recurrence intervals. Boxplots indicate the median (line), interquartile range (boxes) and 1.5 times the interquartile range (whiskers). Note that all between-site differences were significant ($p < 0.05$, Tukey HSD test) with the exception of PCAB low versus PISY low for 15-year EGRs

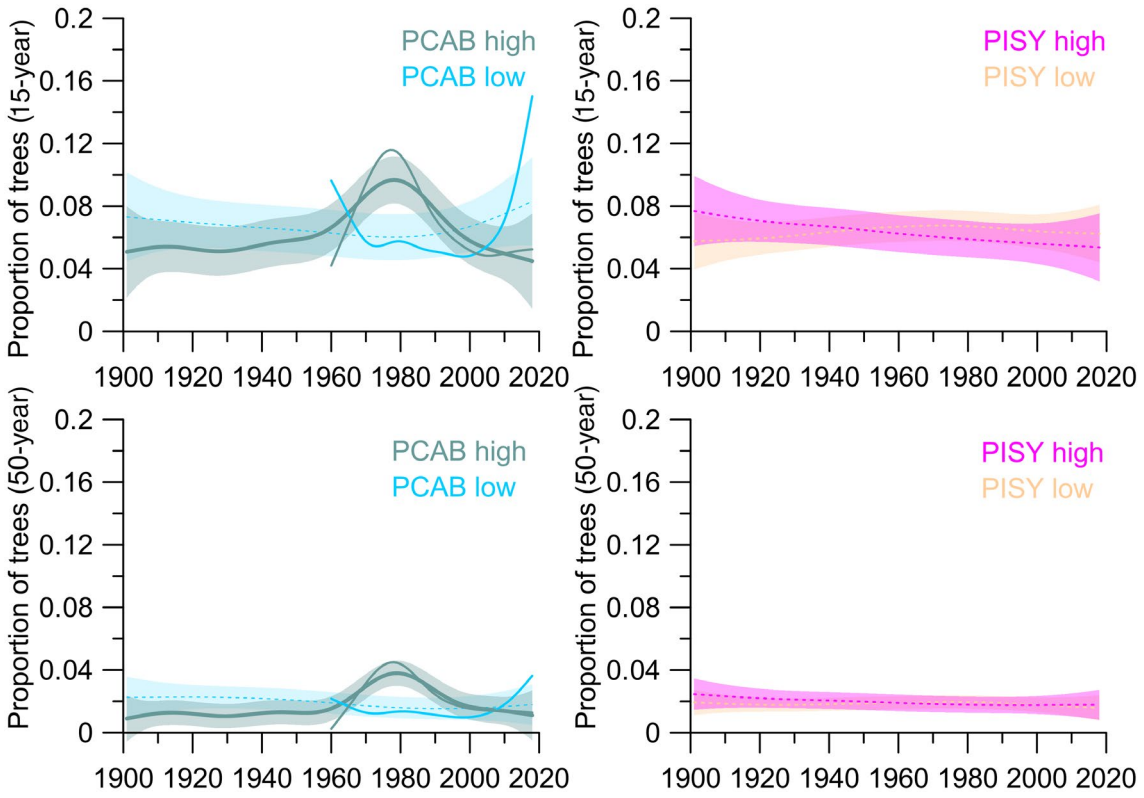

FIGURE 4 Trends in the proportion of trees showing extreme growth reductions (upper panel: 15-year recurrence interval, lower panel: 50-year recurrence interval) as modeled by generalized additive models (bold lines with confidence limits indicating ±1SE). Full and dotted lines denote significant and insignificant effects of the smooth term (year), respectively, for the period 1901–2018. Only significant GAMM fits for the 1960–2018 period are shown (thin line without confidence buffer)

categories, $p < 0.05$; Figure 5a). The lowest incidence of low-temperature driven EGRs was observed for PISY high (19%). The highest proportion of drought-driven EGRs was observed for PCAB low (36% on average; Figure 5a). The proportion of climatic drivers associated with EGR50 did not differ from that of EGR15 ($p > 0.05$; Supporting Information 6).

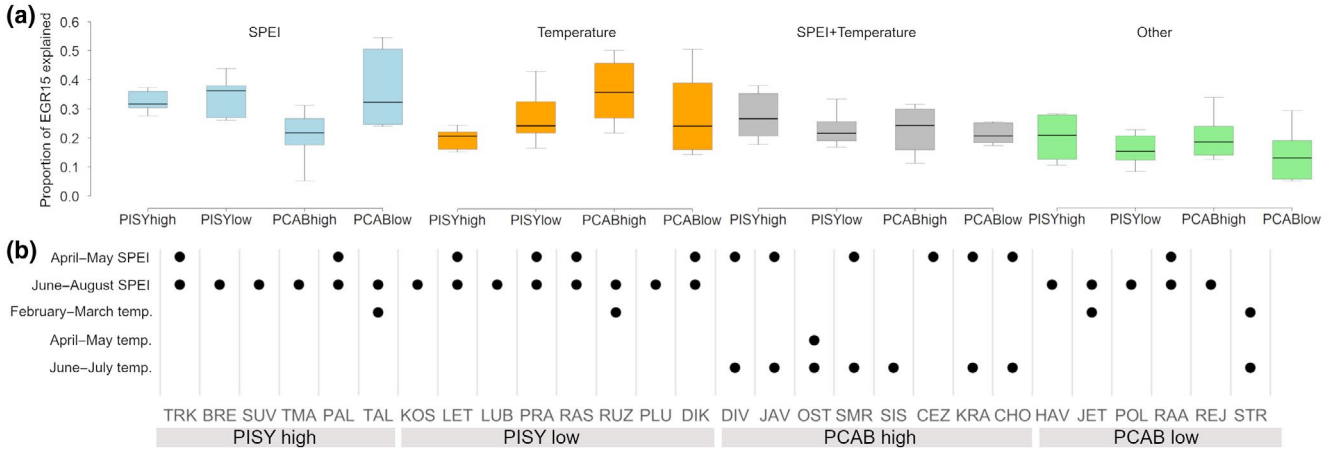

FIGURE 5 (a) The proportion of extreme growth reductions with a 15-year recurrence interval assigned to potential triggers: drought (standardized precipitation evaporation index), low temperature, a combination of low temperature and drought, or extreme growth reductions not explained by these climatic variables ("other"). Boxplots indicate the median (line), interquartile range (boxes) and 1.5 times the interquartile range (whiskers). (b) Significance assessment of the higher proportion of trees exhibiting EGR15 in years with unfavorable weather conditions (1SD below the mean) compared with years with favorable weather as tested by analysis of variance. Dots denote significant relationships ($p < 0.05$). For site abbreviations, see Table 1

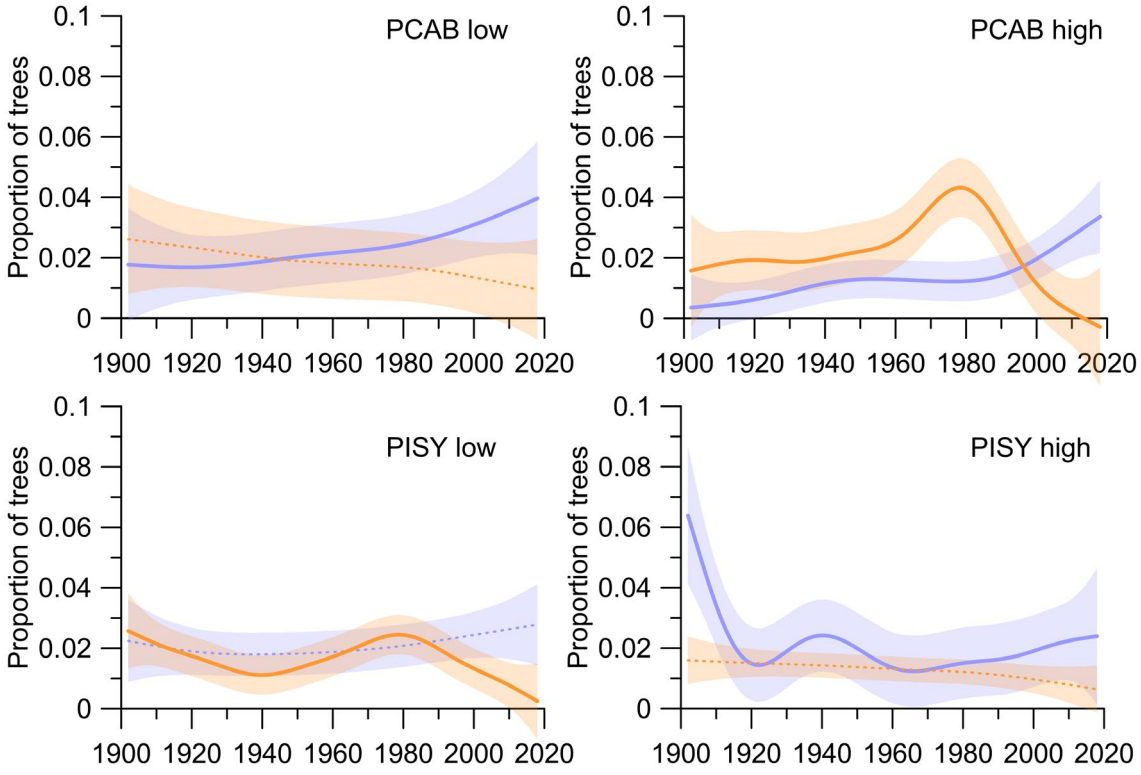

FIGURE 6 Trends in the proportion of trees exhibiting extreme growth reductions with a 15-year recurrence interval categorized according to the type of climatic trigger. Predictions based on generalized additive models show drought representing low SPEI in June–August and/or in April–May (blue), and low temperatures for the June–July and/or April–May and/or February–March periods (red). Error buffers indicate ±1SE. Full and dotted lines denote significant or insignificant effects of the smooth term (year), respectively

The significant effect of low June-July temperature on the proportion of trees exhibiting EGR15 was identified for PCAB high (seven out of eight sites) and also for one PCAB low site (Figure 5b). June–August drought was the predominant cause of EGR15 in all remaining site categories (PCAB low—five out of six sites, PISY high and PISY low—all sites; Figure 5b). Surprisingly, April-May drought was also identified as a common driver of EGR15 in PCAB high (five out of eight sites), and it was frequently associated with EGR15 at PISY low sites (four out of eight sites). From the remaining potential EGR triggers, only low February–March

temperatures were occasionally significant at PCAB low, and PISY high and low (Figure 5b).

For PCAB low, the proportion of trees exhibiting EGR15 caused by cool temperatures gradually decreased over time (Figure 6). In contrast, the proportion of trees with EGRs attributed to drought increased over the same period and droughts have become a dominant driver of EGRs since the 1990s (Figure 6) with about 5% of trees showing EGRs triggered by drought in each recent year. The effect of the smooth term (year) was significant for drought and insignificant for low temperature EGRs (Figure 6).

For PCAB high, the dominant driver accounting for the majority of EGR15 was low temperature with a prominent peak in the 1970s and 1980s followed, however, by a substantial decrease of importance of cool temperatures in the 2000s and 2010s (Figure 6). The proportion of trees with EGR15 attributed to drought increased gradually and acceleration of this trend was observed in the most recent period. EGR15 caused by drought showed a higher contribution to overall EGR15 than low-temperature-driven EGR15 since 2000. The effects of the smooth terms were significant for both low temperature and drought-driven EGRs (Figure 6).

For PISY low sites, the proportion of trees with EGR15 attributed to drought increased over time and low-temperature driven EGR15 showed unstable trends and subsequently diminished in the 2000s. Although the effect of the smooth term (year) was significant for temperature-triggered EGR15, it was insignificant for drought-driven EGR15 (Figure 6).

At PISY high, we observed a sharp decrease in the proportion of trees exhibiting drought-driven EGR15 at the beginning of the 20th century, followed by a culmination in the 1940s and gradual rise since the 1980s (Figure 6). Low-temperature-triggered EGR15 gradually decreased over the entire study period with substantial between-site variability (Supporting Information 5). Although the effect of the smooth term (year) was insignificant for low temperature-driven EGR15, it was significant for drought-driven EGR15 (Figure 6). With the exception of PCAB low drought-triggered EGRs and PISY high EGRs triggered by low temperatures, no other site random effect played a significant role in influencing trends in climate-driven EGRs (Supporting Information 5).

4 | DISCUSSION

Our results highlight trends in climatically driven EGRs for the distribution margins of PISY and PCAB, which are considered to be among the most sensitive environments to ongoing warming (Peterson et al., 2019). We found a clear differentiation in EGR trends and their climatic drivers between high and low-elevation PCAB stands, which represent dominant forest species in Central European mountains and lowlands. By contrast, the between-site differences were less obvious for PISY stands with an azonal and highly discontinuous distribution restricted to low-productivity environments. The overall size of EGRs was greater at low-elevation moisture-limited sites than at high-elevation temperature-limited sites, and this difference was also more prominent in the case of PCAB compared with PISY stands. This indicates the combined effect of local climatic conditions and species-specific niches in determining EGR patterns.

4.1 | Trends in extreme growth reductions

We found that the highest values of EGRs occurred in PCAB low stands corresponding to the high drought sensitivity of this species (Lebourgeois et al., 2010; Spiecker, 2000). We also observed a recent increase in the proportion of PCAB low trees exhibiting EGRs (both for 15- and 50-year recurrence intervals). Our observation is consistent with recently reported waves of increased spruce mortality or declines following droughts and bark-beetle outbreaks in Central Europe (Krejza et al., 2021; Schuldt et al., 2020). However, our data also show that there were many isolated extreme growth reductions in the past with even greater impact at stand-level compared with the recent instances (e.g., 1947–1948, 1921–1924, 1964, 1974–1976). The majority were associated with strong droughts, even stronger than those observed recently (Hanel et al., 2018; Trnka et al., 2016). The main driver behind the recent increase in EGRs is the high concentration of successive extreme events, which makes the recent increase in EGRs in PCAB low distinct at the century scale. The identified EGRs at PCAB low also varied a lot between sites so their recent increase can be considered as a predominant trend but not unified for all low-elevation PCAB stands.

At PCAB high, the proportion of trees exhibiting EGRs was lowest among all site categories. PCAB high sites represent the central part of the climatic niche of PCAB in Central Europe and are thus well adapted to relatively cool summers. The only exception is represented by the distinct culmination of EGRs in the 1970s and 1980s. June-July temperatures between 1974 and 1984 were among the coldest in the 20th century (Dubicka & Glowicki, 2000). In addition, the 1970s and 1980s were characterized by high levels of atmospheric pollution and spatially varying intensity of acid deposition with the strongest impact on northwestern parts of the studied region, which significantly contributed to the increase in EGRs in that period (Kolář et al., 2015; Rydval & Wilson, 2012). In the last 20 years (after 2000), we observed a decrease in EGRs below levels recorded in the 20th century, which might be related to substantially increased growth of the majority of PCAB high sites driven by increasing temperatures (Ponocná et al., 2016; Tumajer et al., 2021).

P. sylvestris sites exhibited ambiguous trends between high elevations (predominantly decreasing proportion of trees with EGRs) and low elevations (predominantly increasing proportion of trees with EGRs). However, the slope of the EGR trends was weak, which is in line with the observations of Bose et al. (2020) demonstrating no difference in growth resistance of German PISY to drought between the 1980s and 2000s. Less-pronounced trends in PISY compared with PCAB are in accordance with the wider climatic range that PISY occupies compared with PCAB and thus probably also

reflect greater plasticity of this species in response to climatic extremes (van Kleunen & Fischer, 2007).

In accordance with other studies focusing on PCAB (e.g., Cienciala et al., 2018; Pretzsch et al., 2014; Tumajer et al., 2017) we observed increasing growth over the last 40 (PCAB low) to 30 years (PCAB high; Supplementary Information 2). The effect of the observed growth increase on EGRs may be twofold—it could partly compensate for the growth reduction in response to extreme droughts, but trees could subsequently also become more sensitive to future extreme drought events since trees with a larger aboveground structure (stems, crowns) and with roots distributed in shallow soil horizons are more sensitive to evaporative losses (McGregor et al., 2021; Stovall et al., 2019). We observed the highest EGRs in the PCAB low-site category followed by PISY low and PISY high. The determined ranking in EGR size is also consistent with the magnitude of gradual growth reduction observed in the late 2010s, which is highest in PCAB low, followed by PISY low and PISY high (Supporting Information 2). High EGRs and decadal growth depressions might serve as warning signals of forthcoming high mortality rates such as those reported in PCAB high in the 1970s and 1980s (Kolář et al., 2015), in PCAB low during the early 1950s (Schelhaas et al., 2003) and probably also more recently (2010s) in PCAB low and PISY low (Buras et al., 2018; Cienciala et al., 2017).

4.2 | Climatic drivers of extreme growth reductions

Spatially explicit and species-specific trends in climatic drivers of EGRs were identified for the 1901–2018 period. EGRs triggered by low temperatures gradually declined after the 1990s for all site categories. At the same time, the proportion of drought-driven EGRs increased. Consequently, EGRs attributed to drought occurred more frequently in the recent period than EGRs triggered by low temperature in all site categories. For PCAB high, this switch of the dominant climatic driver of EGRs during the 2000s was the first such occurrence since 1901. This means that summer drought-driven EGRs recently become important across the entire elevation range of PCAB, which conforms to already reported reactions of PCAB to recent extreme drought events such as 2003 (Hartl-Meier et al., 2014) and increasing moisture limitation of spruce across elevation gradients (Bosela et al., 2021; Ponocná et al., 2016; Schurman et al., 2019).

For low-elevation PISY, the drought-induced EGRs exhibited an increasing trend. However, this was less steep than for PCAB low, supporting the observation that, in a long-term context, PISY is more drought tolerant than PCAB (Lévesque et al., 2013; Oberhuber, 2017). The trends in the proportion of trees exhibiting EGRs at PISY high showed a recent increase, but this was not as pronounced as for other site categories. The climatic signal in the tree rings of PISY high is complex and varies more between sites compared with other site categories (Supporting Information 3), which may provide a possible explanation for the less pronounced trends.

We observed profound differences in the climatic drivers of EGRs between PCAB and PISY along an elevation gradient. While PCAB demonstrated a distinct separation of high-elevation sites with EGRs driven mainly by low June–July temperature and EGRs at low-elevation sites triggered by summer and spring drought events, PISY was characterized by drought-driven EGRs at both margins of its elevation distribution. For PCAB the observed differentiation of climatic drivers is consistent with expected patterns of climate-growth response determined by elevation (Kolář et al., 2017; Mäkinen et al., 2002; Tumajer et al., 2017). For PISY, the identified homogeneity in drivers of EGRs is probably related to site properties. Natural PISY stands in Central Europe occupy a discontinuous ecological niche mostly comprising rocky substrates, steep slopes, or locations with shallow nutrient-poor soils (Chytrý, 2013). The majority of these sites are characterized by low water-holding capacity and are thus prone to the effects of drought, even at high elevations. In fact, the climatic signals of relict PISY stands across lowlands and mountains in Central Europe exhibit rather strong associations with summer moisture (Bauwe et al., 2013; Büntgen et al., 2012; Oberhuber et al., 1998). The identified pattern of drought-triggered EGRs has implications for the future growth dynamics of natural forests under climate change. While PISY stands will probably show extreme responses to droughts across their entire elevation span, PCAB stands will continue to be much more vulnerable in low elevations.

Interestingly, we found a high degree of coincidence of spring droughts and EGRs for PCAB high. Whether this represents a causal relationship remains uncertain. Low spring precipitation can delay snow melt, which can, in turn, lead to later growing season onset with a corresponding reduction in annual growth.

For all sites, we found a certain percentage of EGRs not explained by our climatic variables (usually between 10% and 30%). Some of these EGRs could be ascribed to non-climatic influences (e.g., pests or other disturbances, Honkaniemi et al., 2018; Huang et al., 2020). However, the remainder of EGRs was probably caused by climatic extremes other than those explicitly considered in this study. Temperate conifers of Central Europe also react to spring droughts and frosts at relatively short timescales (e.g., cold spells) which are not represented in data with monthly resolution (Suvanto et al., 2017; Trotsiuk et al., 2020; Vitasse et al., 2019). Assignment of EGRs to climatic triggers was supported by statistical tests, which means that this assignment also has a certain degree of associated uncertainty. We cannot, thus, exclude that in individual rare cases the true cause of an EGR can be different (e.g., a disturbance instead of a climatic variable).

4.3 | Methodological considerations

The EGRs are based on the "relative growth change" methodology, which scales current growth in relation to growth in a preceding time interval (Jetschke et al., 2019; Schweingruber, 1996). The trend component of EGR time series, thus, quantifies the occurrence of increasingly more (or less) extreme events relative to prior growth.

The recurrence interval method, widely used in hydrology, climatology, or fire ecology (e.g., Dingman, 2002; Rodríguez et al.,

2014; Tepley & Veblen, 2015), was applied to derive EGRs with their magnitude corresponding to the average period over which the EGR occurred. To our knowledge, this was the first employment of the recurrence interval method in order to determine extreme events in tree rings. The method accounts for differences in growth plasticity among trees since recurrence intervals are computed at the tree level. We propose that the recurrence interval method can be a useful tool in future studies when applied together with other approaches (e.g., growth resilience metrics; Lloret et al., 2011) to evaluate extreme events recorded in tree rings.

In this study, we focused on size of year-to-year growth reductions. We are aware that this is merely one part of the reaction of trees to extreme events, which can be studied relatively objectively. Other important components of the response of trees include the duration of the response and the ability to recover to previous rates of growth (Lloret et al., 2011).

4.4 | Conclusions

In this study, we demonstrated pronounced species-specific differences regarding the trends and drivers of EGRs between lower and upper species distribution margins. There is a clear differentiation between high- and low-elevation PCAB and less-pronounced differences along the elevation gradient for PISY. As a result, the magnitude of EGRs characterized by the same recurrence interval differed considerably between PCAB low (the largest) and PCAB high (the smallest), while differences in the size of EGRs were smaller for PISY. Because the EGRs at low-elevation PCAB were mainly drought-driven, this site category exhibited a recent increase in the proportion of trees with EGRs. The occurrence of low temperature-driven EGRs faded away after the 1990s in all site categories while at the same time the proportion of EGRs triggered by drought increased. EGRs were greatest in low-elevation sites, indicating high vulnerability of PCAB and, to a lesser extent, also PISY stands to growth declines or even diebacks since high growth variability is considered one of the preconditions for increased mortality. Declining growth trends since the 2010s together with high EGRs imply a high risk for lowland PCAB and PISY stands. We found that recent EGRs of low-elevation PCAB are at the margin of the range of variability observed in the 20th century, whereas all remaining site categories (PCAB high, PISY low and high) remain still within this range.

ACKNOWLEDGMENTS

This research was supported by the Czech Science Foundation (19-138076S). We thank the administrators of the protected areas for permission to carry out our research and for their logistical support. Two anonymous reviewers are acknowledged for valuable comments on earlier version of the manuscript.

CONFLICT OF INTEREST

The author declares no conflict of interest.

DATA AVAILABILITY STATEMENT

Raw tree-ring width series for individual sites are openly available in a public repository at https://www.ncei.noaa.gov/products/paleoclimatology/tree-ring.

ORCID

Václav Treml https://orcid.org/0000-0001-5067-3308
Jiří Mašek https://orcid.org/0000-0002-3494-9113
Jan Tumajer https://orcid.org/0000-0002-7773-7081
Miloš Rydval https://orcid.org/0000-0001-5079-2534
Vojtěch Čada https://orcid.org/0000-0002-3922-2108
Ondřej Ledvinka https://orcid.org/0000-0002-0203-7064
Miroslav Svoboda https://orcid.org/0000-0003-4050-3422

REFERENCES

Anderegg, W. R. L., Schwalm, C., Biondi, F., Camarero, J. J., Koch, G., Litvak, M., Ogle, K., Shaw, J. D., Shevliakova, E., Williams, A. P., Wolf, A., Ziaco, E., & Pacala, S. (2015). Pervasive drought legacies in forest ecosystems and their implications for carbon cycle models. *Science*, *349*(6247), 528–532. https://doi.org/10.1126/science.aab1833

Anderegg, W. R. L., Trugman, A. T., Badgley, G., Konings, A. G., & Shaw, J. (2020). Divergent forest sensitivity to repeated extreme droughts. *Nature Climate Change*, *10*(12), 1091–1095. https://doi.org/10.1038/s41558-020-00919-1

Bates, D., Mächler, M., Bolker, B. M., & Walker, S. C. (2015). Fitting linear mixed-effects models using lme4. *Journal of Statistical Software*, *67*(1). https://doi.org/10.18637/jss.v067.i01

Battipaglia, G., Frank, D., Büntgen, U., Dobrovolnỳ, P., Brázdil, R., Pfister, C., & Esper, J. (2010). Five centuries of Central European temperature extremes reconstructed from tree-ring density and documentary evidence. *Global and Planetary Change*, *72*(3), 182–191. https://doi.org/10.1016/j.gloplacha.2010.02.004

Bauwe, A., Koch, M., Kallweit, R., Konopatzky, A., Strohbach, B., & Lennartz, B. (2013). Tree-ring growth response of scots pine (*Pinus sylvestris* L.) to climate and soil water availability in the lowlands of north-eastern Germany. *Baltic Forestry*, *19*(2), 212–225.

Bose, A. K., Gessler, A., Bolte, A., Bottero, A., Buras, A., Cailleret, M., Camarero, J. J., Haeni, M., Hereş, A. M., Hevia, A., Lévesque, M., Linares, J. C., Martinez-Vilalta, J., Matías, L., Menzel, A., Sánchez-Salguero, R., Saurer, M., Vennetier, M., Ziche, D., & Rigling, A. (2020). Growth and resilience responses of Scots pine to extreme droughts across Europe depend on predrought growth conditions. *Global Change Biology*, *26*(8), 4521–4537. https://doi.org/10.1111/gcb.15153

Bosela, M., Tumajer, J., Cienciala, E., Dobor, L., Kulla, L., Marčiš, P., Popa, I., Sedmák, R., Sedmáková, D., Sitko, R., Šebeň, V., Štěpánek, P., & Büntgen, U. (2021). Climate warming induced synchronous growth decline in Norway spruce populations across biogeographical gradients since 2000. *Science of the Total Environment*, *752*, 141794. https://doi.org/10.1016/j.scitotenv.2020.141794

Brázdil, R., Trnka, M., Mikšovský, J., Řezníčková, L., & Dobrovolný, P. (2015). Spring-summer droughts in the Czech Land in 1805–2012 and their forcings. *International Journal of Climatology*, *35*(7), 1405–1421. https://doi.org/10.1002/joc.4065

Briffa, K. R., & Melvin, T. M. (2011). A closer look at regional curve standardization of tree-ring records: Justification of the need, a warning of some pitfalls, and suggested improvements in its application. *Dendroclimatology*, *5*, 113–145. https://doi.org/10.1007/978-1-4020-5725-0_5

Brun, P., Psomas, A., Ginzler, C., Thuiller, W., Zappa, M., & Zimmermann, N. E. (2020). Large-scale early-wilting response of Central European

forests to the 2018 extreme drought. *Global Change Biology*, *26*(12), 7021–7035. https://doi.org/10.1111/gcb.15360

Bunn, A. G. (2008). A dendrochronology program library in R (dplR). *Dendrochronologia*, *26*(2), 115–124. https://doi.org/10.1016/j.dendro.2008.01.002

Büntgen, U., Kaczka, R. J., Trnka, M., & Rigling, A. (2012). Ensemble estimates reveal a complex hydroclimatic sensitivity of pine growth at Carpathian cliff sites. *Agricultural and Forest Meteorology*, *160*, 100–109. https://doi.org/10.1016/j.agrformet.2012.02.011

Buras, A., Schunk, C., Zeitrg, C., Herrmann, C., Kaiser, L., Lemme, H., Straub, C., Taeger, S., Gößwein, S., Klemmt, H. J., & Menzel, A. (2018). Are Scots pine forest edges particularly prone to drought-induced mortality? *Environmental Research Letters*, *13*(2), 025001. https://doi.org/10.1088/1748-9326/aaa0b4

Camarero, J. J., Gazol, A., Sangüesa-Barreda, G., Oliva, J., & Vicente-Serrano, S. M. (2015). To die or not to die: Early warnings of tree dieback in response to a severe drought. *Journal of Ecology*, *103*(1), 44–57. https://doi.org/10.1111/1365-2745.12295

Carrer, M. (2011). Individualistic and time-varying tree-ring growth to climate sensitivity. *Plos One*, *6*, e22813. https://doi.org/10.1371/journal.pone.0022813

Charru, M., Seynave, I., Hervé, J. C., Bertrand, R., & Bontemps, J. D. (2017). Recent growth changes in Western European forests are driven by climate warming and structured across tree species climatic habitats. *Annals of Forest Science*, *74*(2), 33. https://doi.org/10.1007/s13595-017-0626-1

Chytrý, M. (2013). Vegetation of the Czech Republic 4. *Forest and scrub vegetation*. Academia.

Cienciala, E., Altman, J., Doležal, J., Kopáček, J., Štěpánek, P., Ståhl, G., & Tumajer, J. (2018). Increased spruce tree growth in Central Europe since 1960s. *Science of the Total Environment*, *619–620*, 1637–1647. https://doi.org/10.1016/j.scitotenv.2017.10.138

Cienciala, E., Tumajer, J., Zatloukal, V., Beranová, J., Holá, Š., Hůnová, I., & Russ, R. (2017). Recent spruce decline with biotic pathogen infestation as a result of interacting climate, deposition and soil variables. *European Journal of Forest Research*, *136*(2), 307–317. https://doi.org/10.1007/s10342-017-1032-9

Cook, E., & Peters, K. (1981). The smoothing spline, a new approach to standardising forest interior tree-ring. *Trre-Ring Bulletin*, *41*, 45–53.

Cook, E. R., Seager, R., Kushnir, Y., Briffa, K. R., Büntgen, U., Frank, D., Krusic, P. J., Tegel, W., van der Schrier, G., Andreu-Hayles, L., Baillie, M., Baittinger, C., Bleicher, N., Bonde, N., Brown, D., Carrer, M., Cooper, R., Čufar, K., Dittmar, C., … Zang, C. (2015). Old World megadroughts and pluvials during the Common Era. *Science Advances*, *1*(10), 1–10. https://doi.org/10.1126/sciadv.1500561

Dannenberg, M. P., Wise, E. K., & Smith, W. K. (2019). Reduced tree growth in the semiarid United States due to asymmetric responses to intensifying precipitation extremes. *Science Advances*, *5*(10), 1–11. https://doi.org/10.1126/sciadv.aaw0667

D'Arrigo, R., Wilson, R., & Anchukaitis, K. J. (2013). Volcanic cooling signal in tree ring temperature records for the past millennium. *Journal of Geophysical Research: Atmospheres*, *118*(16), 9000–9010. https://doi.org/10.1002/jgrd.50692

DeSoto, L., Cailleret, M., Sterck, F., Jansen, S., Kramer, K., Robert, E. M. R., Aakala, T., Amoroso, M. M., Bigler, C., Camarero, J. J., Čufar, K., Gea-Izquierdo, G., Gillner, S., Haavik, L. J., Hereş, A.-M., Kane, J. M., Kharuk, V. I., Kitzberger, T., Klein, T., … Martínez-Vilalta, J. (2020). Low growth resilience to drought is related to future mortality risk in trees. *Nature Communications*, *11*(1), 1–9. https://doi.org/10.1038/s41467-020-14300-5

Dingman, S. L. (2002). *Physical hydrology*. Waveland Press.

D'Orangeville, L., Houle, D., Duchesne, L., Phillips, R. P., Bergeron, Y., & Kneeshaw, D. (2018). Beneficial effects of climate warming on boreal tree growth may be transitory. *Nature Communications*, *9*(1), 1–10. https://doi.org/10.1038/s41467-018-05705-4

Dubicka, M., & Glowicki, B. (2000). Air temperature and cloudiness at Sniezka between 1901 and 1998. *Prace Geograficzne*, *107*, 205–212.

Etzold, S., Ziemińska, K., Rohner, B., Bottero, A., Bose, A. K., Ruehr, N. K., Zingg, A., & Rigling, A. (2019). One century of forest monitoring data in Switzerland reveals species- and site-specific trends of climate-induced tree mortality. *Frontiers in Plant Science*, *10*, 307. https://doi.org/10.3389/fpls.2019.00307

Fritts, H. C. (1976). *Tree rings and climate*. Academic Press, https://doi.org/10.1016/b978-0-12-268450-0.x5001-0

Gao, S., Liu, R., Zhou, T., Fang, W., Yi, C., Lu, R., Zhao, X., & Luo, H. (2018). Dynamic responses of tree-ring growth to multiple dimensions of drought. *Global Change Biology*, *24*(11), 5380–5390. https://doi.org/10.1111/gcb.14367

Hacket-Pain, A., Ascoli, D., Berretti, R., Mencuccini, M., Motta, R., Nola, P., Piussi, P., Ruffinatto, P., & Vacchiano, G. (2019). Temperature and masting control Norway spruce growth, but with high individual tree variability. *Forest Ecology and Management*, *438*, 142–150. https://doi.org/10.1016/j.foreco.2019.02.014

Hanel, M., Rakovec, O., Markonis, Y., Máca, P., Samaniego, L., Kyselý, J., & Kumar, R. (2018). Revisiting the recent European droughts from a long-term perspective. *Scientific Reports*, *8*(1), 1–11. https://doi.org/10.1038/s41598-018-27464-4

Hartl-Meier, C., Dittmar, C., Zang, C., & Rothe, A. (2014). Mountain forest growth response to climate change in the Northern Limestone Alps. *Trees – Structure and Function*, *28*(3), 819–829. https://doi.org/10.1007/s00468-014-0994-1

Honkaniemi, J., Ojansuu, R., Kasanen, R., & Heliövaara, K. (2018). Interaction of disturbance agents on Norway spruce: A mechanistic model of bark beetle dynamics integrated in simulation framework WINDROT. *Ecological Modelling*, *388*, 45–60. https://doi.org/10.1016/j.ecolmodel.2018.09.014

Huang, J., Kautz, M., Trowbridge, A. M., Hammerbacher, A., Raffa, K. F., Adams, H. D., Goodsman, D. W., Xu, C., Meddens, A. J. H., Kandasamy, D., Gershenzon, J., Seidl, R., & Hartmann, H. (2020). Tree defence and bark beetles in a drying world: Carbon partitioning, functioning and modelling. *New Phytologist*, *225*(1), 26–36. https://doi.org/10.1111/nph.16173

IPCC. (2021). Climate change 2021: The physical science basis. In V. Masson-Delmotte, P. Zhai, A. Pirani, S. L. Connors, C. Péan, S. Berger, N. Caud, Y. Chen, L. Goldfarb, M. I. Gomis, M. Huang, K. Leitzell, E. Lonnoy, J. B. R. Matthews, T. K. Maycock, T. Waterfield, O. Yelekçi, R. Yu, & B. Zhou (Eds.), *Contribution of working group I to the sixth assessment report of the Intergovernmental Panel on Climate Change*. Cambridge University Press.

Jetschke, G., van der Maaten, E., & van der Maaten-Theunissen, M. (2019). Towards the extremes: A critical analysis of pointer year detection methods. *Dendrochronologia*, *53*, 55–62. https://doi.org/10.1016/j.dendro.2018.11.004

Kolář, T., Čermák, P., Oulehle, F., Trnka, M., Štěpánek, P., Cudlín, P., Hruška, J., Büntgen, U., & Rybníček, M. (2015). Pollution control enhanced spruce growth in the "Black Triangle" near the Czech-Polish border. *Science of the Total Environment*, *538*, 703–711. https://doi.org/10.1016/j.scitotenv.2015.08.105

Kolář, T., Čermák, P., Trnka, M., Žid, T., & Rybníček, M. (2017). Temporal changes in the climate sensitivity of Norway spruce and European beech along an elevation gradient in Central Europe. *Agricultural and Forest Meteorology*, *239*, 24–33. https://doi.org/10.1016/j.agrformet.2017.02.028

Kolus, H. R., Huntzinger, D. N., Schwalm, C. R., Fisher, J. B., McKay, N., Fang, Y., Michalak, A. M., Schaefer, K., Wei, Y., Poulter, B., Mao, J., Parazoo, N. C., & Shi, X. (2019). Land carbon models underestimate the severity and duration of drought's impact on plant productivity. *Scientific Reports*, *9*(1), 1–10. https://doi.org/10.1038/s41598-019-39373-1

Krejza, J., Cienciala, E., Světlík, J., Bellan, M., Noyer, E., Horáček, P., Štěpánek, P., & Marek, M. V. (2021). Evidence of climate-induced

stress of Norway spruce along elevation gradient preceding the current dieback in Central Europe. *Trees – Structure and Function*, *35*(1), 103–119. https://doi.org/10.1007/s00468-020-02022-6

Lebourgeois, F., Rathgeber, C. B. K., & Ulrich, E. (2010). Sensitivity of French temperate coniferous forests to climate variability and extreme events (*Abies alba*, *Picea abies* and *Pinus sylvestris*). *Journal of Vegetation Science*, *21*(2), 364–376. https://doi.org/10.1111/j.1654-1103.2009.01148.x

Lévesque, M., Saurer, M., Siegwolf, R., Eilmann, B., Brang, P., Bugmann, H., & Rigling, A. (2013). Drought response of five conifer species under contrasting water availability suggests high vulnerability of Norway spruce and European larch. *Global Change Biology*, *19*(10), 3184–3199. https://doi.org/10.1111/gcb.12268

Linares, J. C., Camarero, J. J., & Carreira, J. A. (2010). Competition modulates the adaptation capacity of forests to climatic stress: Insights from recent growth decline and death in relict stands of the Mediterranean fir Abies pinsapo. *Journal of Ecology*, *98*(3), 592–603. https://doi.org/10.1111/j.1365-2745.2010.01645.x

Lloret, F., Keeling, E. G., & Sala, A. (2011). Components of tree resilience: Effects of successive low-growth episodes in old ponderosa pine forests. *Oikos*, *120*, 1909–1920. https://doi.org/10.1111/j.1600-0706.2011.19372.x

Mäkinen, H., Nöjd, P., Kahle, H. P., Neumann, U., Tveite, B., Mielikäinen, K., Röhle, H., & Spiecker, H. (2002). Radial growth variation of Norway spruce (*Picea abies* (L.) Karst.) across latitudinal and altitudinal gradients in central and northern Europe. *Forest Ecology and Management*, *171*(3), 243–259. https://doi.org/10.1016/S0378-1127(01)00786-1

Martínez-Vilalta, J., López, B. C., Loepfe, L., & Lloret, F. (2012). Stand- and tree-level determinants of the drought response of Scots pine radial growth. *Oecologia*, *168*(3), 877–888. https://doi.org/10.1007/s00442-011-2132-8

McGregor, I. R., Helcoski, R., Kunert, N., Tepley, A. J., Gonzalez-Akre, E. B., Herrmann, V., Zailaa, J., Stovall, A. E. L., Bourg, N. A., McShea, W. A., Pederson, N., Sack, L., & Anderson-Teixeira, K. J. (2021). Tree height and leaf drought tolerance traits shape growth responses across droughts in a temperate broadleaf forest. *New Phytologist*, *231*, 601–616. https://doi.org/10.1111/nph.16996

Mozny, M., Trnka, M., Vlach, V., Vizina, A., Potopova, V., Zahradnicek, P., Stepanek, P., Hajkova, L., Staponites, L., & Zalud, Z. (2020). Past (1971–2018) and future (2021–2100) pan evaporation rates in the Czech Republic. *Journal of Hydrology*, *590*, 125390. https://doi.org/10.1016/j.jhydrol.2020.125390

Neuwirth, B., Schweingruber, F. H., & Winiger, M. (2007). Spatial patterns of central European pointer years from 1901 to 1971. *Dendrochronologia*, *24*(2–3), 79–89. https://doi.org/10.1016/j.dendro.2006.05.004

Oberhuber, W. (2017). Soil water availability and evaporative demand affect seasonal growth dynamics and use of stored water in co-occurring saplings and mature conifers under drought. *Trees – Structure and Function*, *31*(2), 467–478. https://doi.org/10.1007/s00468-016-1468-4

Oberhuber, W., Stumböck, M., & Kofler, W. (1998). Climate-tree-growth relationships of Scots pine stands (*Pinus sylvestris* L.) exposed to soil dryness. *Trees – Structure and Function*, *13*(1), 19–27. https://doi.org/10.1007/s004680050183

Pearson, C., Salzer, M., Wacker, L., Brewer, P., Sookdeo, A., & Kuniholm, P. (2020). Securing timelines in the ancient Mediterranean using multiproxy annual tree-ring data. *Proceedings of the National Academy of Sciences of the United States of America*, *117*(31), 8410–8415. https://doi.org/10.1073/pnas.2013168117

Pebesma, E. J. (2004). Multivariable geostatistics in S: The gstat package. *Computers & Geosciences*, *30*(7), 683–691. https://doi.org/10.1016/j.cageo.2004.03.012

Peters, R. L., Groenendijk, P., Vlam, M., & Zuidema, P. A. (2015). Detecting long-term growth trends using tree rings: A critical evaluation of methods. *Global Change Biology*, *21*(5), 2040–2054. https://doi.org/10.1111/gcb.12826

Peterson, M. L., Doak, D. F., & Morris, W. F. (2019). Incorporating local adaptation into forecasts of species' distribution and abundance under climate change. *Global Change Biology*, *25*(3), 775–793. https://doi.org/10.1111/gcb.14562

Ponocná, T., Spyt, B., Kaczka, R., Büntgen, U., & Treml, V. (2016). Growth trends and climate responses of Norway spruce along elevational gradients in East-Central Europe. *Trees – Structure and Function*, *30*(5), 1633–1646. https://doi.org/10.1007/s00468-016-1396-3

Pretzsch, H., Biber, P., Schütze, G., Uhl, E., & Rötzer, T. (2014). Forest stand growth dynamics in Central Europe have accelerated since 1870. *Nature Communications*, *5*, 1–10. https://doi.org/10.1038/ncomms5967

Pretzsch, H., Grams, T., Häberle, K. H., Pritsch, K., Bauerle, T., & Rötzer, T. (2020). Growth and mortality of Norway spruce and European beech in monospecific and mixed-species stands under natural episodic and experimentally extended drought. Results of the KROOF throughfall exclusion experiment. *Trees – Structure and Function*, *34*(4), 957–970. https://doi.org/10.1007/s00468-020-01973-0

R Core Team. (2019). *R: A language and environment for statistical computing (3.5.1)*. R Foundation for Statistical Computing. Retrieved from http://www.r-project.org/

Rammig, A., Wiedermann, M., Donges, J. F., Babst, F., Von Bloh, W., Frank, D., Thonicke, K., & Mahecha, M. D. (2015). Coincidences of climate extremes and anomalous vegetation responses: Comparing tree ring patterns to simulated productivity. *Biogeosciences*, *12*(2), 373–385. https://doi.org/10.5194/bg-12-373-2015.

Rodríguez, R., Navarro, X., Casas, M. C., Ribalaygua, J., Russo, B., Pouget, L., & Redaño-Rodriguez, A. (2014). Influence of climate change on IDF curves for the metropolitan area of Barcelona (Spain). *International Journal of Climatology*, *34*, 643–654. https://doi.org/10.1002/joc.3712

Rolland, C., Desplanque, C., & Schweingruber, F. H. (2000). Extreme tree rings in spruce (*Picea abies* [L.] Karst.) and fir (*Abies alba* Mill.) stands in relation to climate, site, and space in the Southern French and Italian Alps. *Arctic, Antarctic, and Alpine Research*, *32*(1), 1–13.

Rydval, M., & Wilson, R. (2012). The impact of industrial SO_2 pollution on North Bohemia conifers. *Water, Air, and Soil Pollution*, *223*(9), 5727–5744. https://doi.org/10.1007/s11270-012-1310-6

Sánchez-Salguero, R., Camarero, J. J., Carrer, M., Gutiérrez, E., Alla, A. Q., Andreu-Hayles, L., Hevia, A., Koutavas, A., Martínez-Sancho, E., Nola, P., Papadopoulos, A., Pasho, E., Toromani, E., Carreira, J. A., & Linares, J. C. (2017). Climate extremes and predicted warming threaten Mediterranean Holocene firs forests refugia. *Proceedings of the National Academy of Sciences of the United States of America*, *114*(47), 10142–10150. https://doi.org/10.1073/pnas.1708109114

Scharnweber, T., Smiljanic, M., Cruz-García, R., Manthey, M., & Wilmking, M. (2020). Tree growth at the end of the 21st century – The extreme years 2018/19 as template for future growth conditions. *Environmental Research Letters*, *15*(7), 074022. https://doi.org/10.1088/1748-9326/ab865d

Schelhaas, M. J., Nabuurs, G. J., & Schuck, A. (2003). Natural disturbances in the European forests in the 19th and 20th centuries. *Global Change Biology*, *9*(11), 1620–1633. https://doi.org/10.1046/j.1365-2486.2003.00684.x

Schuldt, B., Buras, A., Arend, M., Vitasse, Y., Beierkuhnlein, C., Damm, A., Gharun, M., Grams, T. E. E., Hauck, M., Hajek, P., Hartmann, H., Hiltbrunner, E., Hoch, G., Holloway-Phillips, M., Körner, C., Larysch, E., Lübbe, T., Nelson, D. B., Rammig, A., … Kahmen, A. (2020). A first assessment of the impact of the extreme 2018 summer drought on Central European forests. *Basic and Applied Ecology*, *45*, 86–103. https://doi.org/10.1016/j.baae.2020.04.003

Schurman, J. S., Babst, F., Björklund, J., Rydval, M., Bače, R., Čada, V., Janda, P., Mikolas, M., Saulnier, M., Trotsiuk, V., & Svoboda, M. (2019). The

climatic drivers of primary Picea forest growth along the Carpathian arc are changing under rising temperatures. *Global Change Biology*, *25*(9), 3136–3150. https://doi.org/10.1111/gcb.14721

Schweingruber, F. H. (1996). *Tree rings and environment dendroecology*. Paul Haupt.

Schweingruber, F. H., Eckstein, D., Serre-Bachet, F., & Bräker, O. U. (1990). Identification, presentation and interpretation of event years and pointer years in dendrochronology. *Dendrochronologia*, *8*, 9–38.

Serra-Maluquer, X., Mencuccini, M., & Martínez-Vilalta, J. (2018). Changes in tree resistance, recovery and resilience across three successive extreme droughts in the northeast Iberian Peninsula. *Oecologia*, *187*(1), 343–354. https://doi.org/10.1007/s00442-018-4118-2

Sidor, C. G., Camarero, J. J., Popa, I., Badea, O., Apostol, E. N., & Vlad, R. (2019). Forest vulnerability to extreme climatic events in Romanian Scots pine forests. *Science of the Total Environment*, *678*, 721–727. https://doi.org/10.1016/j.scitotenv.2019.05.021

Silva, L. C. R., Sun, G., Zhu-Barker, X., Liang, Q., Wu, N., & Horwath, W. R. (2016). Tree growth acceleration and expansion of alpine forests: The synergistic effect of atmospheric and edaphic change. *Science Advances*, *2*(8), e1501302. https://doi.org/10.1126/sciadv.1501302

Speer, J. H. (2011). *Fundamentals of tree-ring research*. The University of Arizona Press. https://doi.org/10.1002/gea.20357

Spiecker, H. (2000). *Spruce monocultures in Central Europe – Problems and prospects (Issue 33)*. European Forest Institute.

Stokes, M. A., & Smiley, L. T. (1998). *An introduction to tree-ring dating*. The University of Chicago Press, https://doi.org/10.1016/b978-0-444-54304-2.03001-3

Stovall, A., Shugart, H., & Yang, X. (2019). Tree height explains mortality risk during an intense drought. *Nature Communications*, *10*, 4385. https://doi.org/10.1038/s41467-019-12380-6

Suvanto, S., Henttonen, H. M., Nöjd, P., Helama, S., Repo, T., Timonen, M., & Mäkinen, H. (2017). Connecting potential frost damage events identified from meteorological records to radial growth variation in Norway spruce and Scots pine. *Trees – Structure and Function*, *31*(6), 2023–2034. https://doi.org/10.1007/s00468-017-1590-y

Szabó, P., Kuneš, P., Svobodová-Svitavská, H., Švarcová, M. G., Křížová, L., Suchánková, S., Müllerová, J., & Hédl, R. (2017). Using historical ecology to reassess the conservation status of coniferous forests in Central Europe. *Conservation Biology*, *31*(1), 150–160. https://doi.org/10.1111/cobi.12763

Tei, S., Sugimoto, A., Yonenobu, H., Matsuura, Y., Osawa, A., Sato, H., Fujinuma, J., & Maximov, T. (2017). Tree-ring analysis and modeling approaches yield contrary response of circumboreal forest productivity to climate change. *Global Change Biology*, *23*(12), 5179–5188. https://doi.org/10.1111/gcb.13780

Tepley, A., & Veblen, T. T. (2015). Spatiotemporal fire dynamics in mixed-conifer and aspen forests in the San Juan Mountains of southwestern Colorado, USA. *Ecological Monographs*, *85*, 583–603. https://doi.org/10.1890/14-1496.1

Treml, V., Ponocná, T., King, G. M., & Büntgen, U. (2015). A new tree-ring-based summer temperature reconstruction over the last three centuries for east-central Europe. *International Journal of Climatology*, *35*(10), 3160–3171. https://doi.org/10.1002/joc.4201

Trnka, M., Balek, J., Štepánek, P., Zahradnícek, P., Možný, M., Eitzinger, J., Žalud, Z., Formayer, H., Turna, M., Nejedlík, P., Semerádová, D., Hlavinka, P., & Brázdil, R. (2016). Drought trends over part of Central Europe between 1961 and 2014. *Climate Research*, *70*(2–3), 143–160. https://doi.org/10.3354/cr01420

Trotsiuk, V., Hartig, F., Cailleret, M., Babst, F., Forrester, D. I., Baltensweiler, A., Buchmann, N., Bugmann, H., Gessler, A., Gharun, M., Minunno, F., Rigling, A., Rohner, B., Stillhard, J., Thürig, E., Waldner, P., Ferretti, M., Eugster, W., & Schaub, M. (2020). Assessing the response of forest productivity to climate extremes in Switzerland using model–data fusion. *Global Change Biology*, *26*(4), 2463–2476. https://doi.org/10.1111/gcb.15011

Tumajer, J., Altman, J., Štěpánek, P., Treml, V., Doležal, J., & Cienciala, E. (2017). Increasing moisture limitation of Norway spruce in Central Europe revealed by forward modelling of tree growth in tree-ring network. *Agricultural and Forest Meteorology*, *247*, 56–64. https://doi.org/10.1016/j.agrformet.2017.07.015

Tumajer, J., Kašpar, J., Kuželová, H., Shishov, V. V., Tychkov, I. I., Popkova, M. I., Vaganov, E. A., & Treml, V. (2021). Forward modeling reveals multidecadal trends in cambial kinetics and phenology at treeline. *Frontiers in Plant Science*, *12*, 613643. https://doi.org/10.3389/fpls.2021.613643

Van der Maaten-Theunissen, M., van der Maaten, E., & Bouriaud, O. (2015). PointRes: An R package to analyze pointer years and components of resilience. *Dendrochronologia*, *35*, 34–38. https://doi.org/10.1016/j.dendro.2015.05.006

Van Kleunen, M., & Fischer, M. (2007). Progress in the detection of costs of phenotypic plasticity in plants. *New Phytologist*, *176*, 727–730. https://doi.org/10.1111/j.1469-8137.2007.02296.x

Vanoni, M., Bugmann, H., Nötzli, M., & Bigler, C. (2016). Quantifying the effects of drought on abrupt growth decreases of major tree species in Switzerland. *Ecology and Evolution*, *6*(11), 3555–3570. https://doi.org/10.1002/ece3.2146

Vicente-Serrano, S. M., Beguería, S., & López-Moreno, J. I. (2010). A multiscalar drought index sensitive to global warming: The standardized precipitation evapotranspiration index. *Journal of Climate*, *23*(7), 1696–1718. https://doi.org/10.1175/2009JCLI2909.1

Vieira, J., Campelo, F., & Nabais, C. (2009). Age-dependent responses of tree-ring growth and intra-annual density fluctuations of *Pinus pinaster* to Mediterranean climate. *Trees – Structure and Function*, *23*(2), 257–265. https://doi.org/10.1007/s00468-008-0273-0

Vitali, V., Büntgen, U., & Bauhus, J. (2017). Silver fir and Douglas fir are more tolerant to extreme droughts than Norway spruce in south-western Germany. *Global Change Biology*, *23*(12), 5108–5119. https://doi.org/10.1111/gcb.13774

Vitasse, Y., Bottero, A., Cailleret, M., Bigler, C., Fonti, P., Gessler, A., Lévesque, M., Rohner, B., Weber, P., Rigling, A., & Wohlgemuth, T. (2019). Contrasting resistance and resilience to extreme drought and late spring frost in five major European tree species. *Global Change Biology*, *25*(11), 3781–3792. https://doi.org/10.1111/gcb.14803

Wood, S. N. (2017). *Generalized additive models: An introduction with R* (2nd ed.). Chapman and Hall/CRC.

Zang, C., Hartl-Meier, C., Dittmar, C., Rothe, A., & Menzel, A. (2014). Patterns of drought tolerance in major European temperate forest trees: Climatic drivers and levels of variability. *Global Change Biology*, *20*(12), 3767–3779. https://doi.org/10.1111/gcb.12637

Zang, C., Pretzsch, H., & Rothe, A. (2012). Size-dependent responses to summer drought in Scots pine, Norway spruce and common oak. *Trees – Structure and Function*, *26*(2), 557–569. https://doi.org/10.1007/s00468-011-0617-z

SUPPORTING INFORMATION

Additional supporting information may be found in the online version of the article at the publisher's website.

How to cite this article: Treml, V., Mašek, J., Tumajer, J., Rydval, M., Čada, V., Ledvinka, O., & Svoboda, M. (2021). Trends in climatically driven extreme growth reductions of *Picea abies* and *Pinus sylvestris* in Central Europe. *Global Change Biology*, 00, 1–14. https://doi.org/10.1111/gcb.15922

Ecosystems
https://doi.org/10.1007/s10021-023-00822-8

Variability in Tree-ring Width and NDVI Responses to Climate at a Landscape Level

Jiří Mašek,* Jan Tumajer, Jelena Lange, Ryszard Kaczka, Petr Fišer, and Václav Treml

Department of Physical Geography and Geoecology, Faculty of Science, Charles University, Albertov 6, 128 43 Prague, Czech Republic

Abstract

Inter-annual climatically driven growth variability of above-ground biomass compartments (for example, tree stems and foliage) controls the intensity of carbon sequestration into forest ecosystems. However, understanding the differences between the climatic response of stem and foliage at the landscape level is limited. In this study, we examined the climate-growth response of stem and leaf biomass and their relationship for *Pinus sylvestris* (PISY) and *Picea abies* (PCAB) in topographically complex landscapes. We used tree-ring width chronologies and time series of the normalized difference vegetation index (NDVI) derived from high-resolution Landsat scenes as proxies for stem and leaf biomass, respectively. We then compared growth variability and climate-growth relationships of both biomass proxies between topographical categories. Our results show that the responses of tree rings to climate differ significantly from those found in NDVI, with the stronger climatic signal observed in tree rings. Topography had distinct but species-specific effects: At moisture-limited PISY stands, stem biomass (tree rings) was strongly topographically driven, and leaf biomass (NDVI) was relatively insensitive to topographic variability. In landscapes close to the climatic optimum of PCAB, the relationship between stem and leaf biomass was weak, and their correlations with climate were often inverse, with no significant effects of topography. Different climatic signals from NDVI and tree rings suggest that the response of canopy and stem growth to climate change might be decoupled. Furthermore, our results hint toward different prioritizations of biomass allocation in trees under stressful conditions which might change allometric relationships between individual tree compartments in the long term.

Highlights

- Tree rings showed a stronger climatic signal than NDVI
- Response of tree rings differ from NDVI for *P. abies*
- Coherent tree rings and NDVI of *P. sylvestris* strongly influenced by topography

Received 21 June 2022; accepted 8 January 2023

Supplementary Information: The online version contains supplementary material available at https://doi.org/10.1007/s10021-023-00822-8.

Author contributions: J.M. conceived of or designed study, contributed new methods or models, performed research, analyzed data, and wrote the paper. J.T. contributed new methods or models and wrote the paper. J.L. contributed new methods or models and wrote the paper. R.K. contributed new methods or models and wrote the paper. P.F. performed research and analyzed data. V.T. conceived of or designed study, contributed new methods or models, and wrote the paper.

**Corresponding author; e-mail:* jiri.masek@natur.cuni.cz

Published online: 26 January 2023

Introduction

Carbon sequestration in terrestrial ecosystems exhibits high inter-annual variability that depends on weather conditions (Anderegg and others 2012). This variability represents a significant uncertainty in global carbon cycle models (Le Quéré and others 2009; Pan and others 2011; Babst and others 2014). Carbon is stored in various segments of trees: For example, conifers in temperate forests sequester a large amount of carbon in stems (~ 45% of annually formed tree biomass), leaves (~ 15%), and the remaining about 40% are divided into roots (~ 25%) and branches (~ 15%) (Bernoulli and Körner 1999). Annual ring-width chronologies can be used to analyze the influence of climate on stem biomass formation (Girardin and others 2016, Babst and others 2017). Trends in leaf biomass can be assessed by remote sensing data, which are available for the entire Earth for recent decades at fine temporal and spatial resolution (Vicente-Serrano and others 2016; Song 2012).

Stem and leaf biomass increment tend to be correlated, which potentially allows linking information from both data sources (Babst and others 2018; Vicente-Serrano and others 2020). Vegetation greenness and leaf biomass represented by NDVI have been shown to correlate with tree-ring width and basal area increment (Vicente-Serrano and others 2016; Zhang and others 2018; Liang and others 2005; Schröder and Körner 2018; Berner and others 2013), wood density (Beck and others 2013; D'Arrigo and others 2000; Bunn and others 2013), earlywood and latewood width (Pompa-García and others 2021; Pasho and Alla 2015), seed production, apical increment (Wang and others 2004), and carbon isotope ratios in wood (del Castillo and others 2015; Leavitt and others 2008). On the other hand, this relationship may vary in time, space, and along various environmental gradients. For instance, temporal variability in the relationship between radial growth and canopy conditions might be caused by extreme drought events, either through direct (Gazol and others 2018b; Kannenberg and others 2019) or legacy effects (Wu and others 2017; Anderegg and others 2015). On a global scale, the links between canopy conditions and radial growth were shown to systematically differ between bioclimatic zones (Wong and others 2021; Kaufmann and others 2008; Seftigen and others 2018; Bhuyan and others 2017; Bunn and others 2013).

At a landscape level, the terrain morphology may significantly modulate the link between radial growth and canopy dynamics (Wang and others 2021; Kannenberg and others 2019; Coulthard and others 2017) because it influences water balance and topoclimate (Vicente-Serrano and others 2012, Vicente-Serrano and others 2016). Tree growth and NDVI are influenced by topographical factors such as slope orientation and inclination (Montpellier and others 2018; Zhan and others 2012; Oberhuber and Kofler 2000), elevation (Ponocná and others 2016; Zhan and others 2012), solar radiation (Riihimäki and others 2017), and soil water availability (Rabbel and others 2018; Adams and others 2014; Del-Toro-Guerrero and others 2019). Additional factors driving the relationship between tree rings and NDVI include species composition (Berner and others 2011; Lopatin and others 2006), canopy age structure (Alla and others 2017; Bhuyan and others 2017; Correa–Díaz and others 2019), and phenology (Bhuyan and others 2017; Gazol and others 2018a). Despite all this knowledge, there is a lack of studies combining tree rings and NDVI analyses covering several distinct topographic features and investigating the influence of topography on the climatic signal and the relationship between NDVI and tree rings.

A combination of tree-ring and remote sensing data has been used before to reveal trends in ecosystem productivity, but solely at regional (Vicente-Serrano and others 2020; Xu and others 2019), or continental to global scales (Bunn and others 2013; Kaufmann and others 2008; Vicente-Serrano and others 2012). Accordingly, most studies used satellite data with large spatial coverage but a low spatial resolution from hundreds of meters to a few kilometers per pixel (Vicente-Serrano and others 2020; Wang and others 2004; D'Arrigo and others 2000). However, low spatial resolution masks potential differences at a landscape level (Bhuyan and others 2017; Berner and others 2011) which can be vital for determining forest response to climate change (Correa–Díaz and others 2019; Bhuyan and others 2017). Both forest mortality and growth trends preserve topographic patterns, which are averaged out in large-pixel scenes (Wang and others 2021; Bhuyan and others 2017).

In this study, we aim to compare climate signals in leaf biomass (represented by NDVI derived from high-resolution satellite data) and stem biomass (represented by tree rings) in topographically complex landscapes. For this purpose, we sampled 40 sites of *P. abies* and *P. sylvestris* in areas representing lowland and mountain forests of the temperate zone. We hypothesize that growth trends in wood and leaf biomass and their climatic responses are correlated. We further expect that the strength

of this relationship varies according to topography due to differences in moisture accumulation and the amount of incoming radiation.

Methods

Study Areas and Study Species

P. abies (PCAB) and *P. sylvestris* (PISY) account for about 30% and 20% of the species composition in Central Europe, respectively (Spiecker 2000; Durrant and others 2016). PCAB is characterized by a shallow root system taking up moisture from upper soil horizons. This species naturally occurs in mountainous uplands with nutrient-poor soils where it forms dense stands. PISY is a light-demanding species with a deep rooting system and high ecological tolerance; hence, it primarily occupies less productive sites, where it forms open-canopy stands (Durrant and others 2016).

To represent typical areas with a prevalence of either PISY or PCAB forests, we selected two landscapes in Central Europe (Czech Republic)—Kokořínsko hills (dominated by PISY) and Šumava Mts. (dominated by PCAB) (Figure 1). The Kokořínsko hills are a topographically complex area (Figure 1) formed by sandstone rock massif and dissected by narrow canyon-shaped valleys of approximately 100 m depth (Bína and Demek 2012). The highest peaks (614 m a. s. l.) are formed by volcanic intrusions and parts of consolidated sandstones (Ložek and others 2005). PCAB sites were situated in the Šumava Mts. (elevation of the local highest peak is 1235 m a. s. l.) in a mountain landscape composed of old metamorphic rocks forming gently inclined slopes (Demek and others 1965). Slope inclination in Kokořínsko hills is variable (mean of 15°), which contrasts with Šumava Mts., where slopes are uniform with a mean inclination of 10° (Table S1). While Kokořínsko hills are located in the mild temperate zone with annual precipitation totals of about 500–650 mm and a mean annual temperature of 8 °C, Šumava Mts. are located in the wet temperate zone with annual precipitation totals of 1200 mm and a mean annual temperature of approximately 4 °C (Figure 1). Winter snow cover lasts for about 80 days in Kokořínsko hills and almost 160 days in Šumava Mts. (period 1961–2000; Tolasz and others 2007). Soils in both areas are typically nutrient-poor leptosols, podzols, and cambisols (Ložek and others 2005; Albrecht and others 2003).

Sample Collection and Processing

We sampled 20 sites in each study area to cover the variability of the landscape in terms of moisture availability and solar irradiation, involving the following four categories: south-facing slopes, north-facing slopes, plateaus, and valley bottoms (further referred to as site categories; Figure 1). Each site category was represented by five sites in each study area. At each site, we delineated a circular inventory plot with a radius of 16 m to

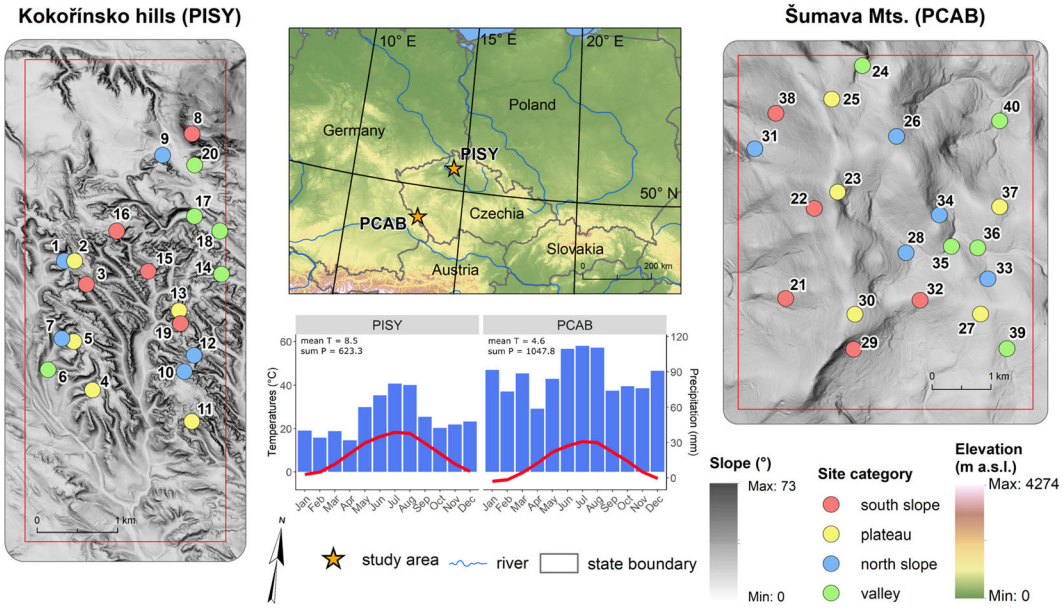

Figure 1. Study areas, location of sampled sites, and climate diagrams (1985–2017) for PCAB and PISY. Sites are numbered according to Table S2.

approximate the size of one pixel of the Landsat scene (30 m × 30 m). Plots were characterized by monospecific stands of the respective species. We sampled at least 26 canopy-level trees within each inventory plot using an increment borer. Additionally, at one site per each site category and species, we sampled all trees with a diameter at breast height (DBH) greater than 10 cm to consider the influence of tree age on the climatic response of tree compartments (Carrer and Urbinati 2004). Our dataset contains 1147 trees, 639 for PISY, and 508 for PCAB (Table S2).

Tree cores were dried, glued onto wooden laths, and sanded to improve the visibility of tree rings. Measuring tree-ring widths as a proxy for stem biomass increment was performed in WinDENDRO (Regent Instruments 2011) on scans with a resolution of 1200 dpi. Tree rings were automatically detected and then visually checked and corrected if necessary. We used PAST4 (Knibbe 2004) for cross-dating of the tree-ring series. Since we were interested in high-frequency variability, we removed age trends from individual series using a smoothing spline with a 50% frequency cutoff at a 30-year-long window. Tree-ring indices (TRI) were calculated as ratios of observed tree-ring width and the value predicted by the spline (Cook and Peters 1981). Because the detrending approach might influence the resulting climatic signal (D'Arrigo and others 2006), we also tested the trend removal using a spline with a 70-year-long window. The climatic signal was similar for both versions of the spline; therefore, all the following analyses were carried out using tree-ring series detrended with a 30-year-long window spline. Standard chronologies (Figure S1A) were built for each site using Tukey's Biweight Robust Mean in R (R Core Team 2019) and the package dplR (1.7.2; Bunn, 2008).

NDVI Data

We used Landsat (high-quality T1_SR scenes) satellite data to calculate NDVI (normalized difference vegetation index) as a proxy for leaf biomass for the window 1985–2021 (Shabanov and others 2005) because these data provide the longest currently available time series of multispectral scenes with high resolution (30 m per pixel since 1984) (Zhu and others 2018). Landsat 5, 7, and 8 are each using different sensors, TM (Thematic Mapper), ETM + (Enhanced Thematic Mapper Plus), and OLI (Operational Land Imager), respectively, and they cover different time windows. Hence, datasets of Landsat 5 and 7 were recalculated by regression to be comparable with Landsat 8 (Roy and others 2016) by using Google Earth Engine (Gorelick and others 2017). We erased clouds and their shadows from all scenes to avoid distortion of spectral data (Zhu and others 2015). All available scenes for the growing season were selected. The start of the growing season for individual years was set to the first day in the year with a mean temperature of five preceding days over 12 °C, and 9 °C for PISY and PCAB, respectively, that is, mean temperature triggering bud burst reported for these species in a similar environment (Hájková and others 2012). The end of the growing season was set to 30th September (DOY 274), when trees in the temperate forests of Central Europe approximately complete their radial growth (Etzold and others 2021; Tumajer and others 2022; Krejza and others 2021). The leaf formation is usually completed before July with only limited subsequent changes in leaf biomass (Kraus and others 2016; Fajstavr and others 2019). Iterations with various lengths of the growing season revealed the negligible impact on climate-NDVI correlations. NDVI was calculated for each pixel of the selected scenes as follows:

$$NDVI = \frac{NIR - Red}{NIR + Red}$$

where 'Red' indicates reflectance in the red spectrum and 'NIR' refers to the reflectance in the near-infrared spectrum (NASA 2022). In the next step, the median NDVI from all scenes within the vegetation period was calculated for each year, and an annually resolved time series of these values was extracted for our sites. To relate these values to our study sites in the field, we computed the mean of all pixels overlapping with a respective study site (2 or 4 pixels in most cases) weighted by the proportion of sampling site area located inside a specific pixel.

Long-term trends in the time series of vegetation indices can be affected by various factors, including forest densification as trees are getting larger (Vicente-Serrano and others 2004) and CO_2 fertilization (Donohue and others 2013). To remove these trends, we fitted linear regressions to the NDVI time series and used the residuals for further analyses (Figure S2). Although our study sites are located in evergreen forests, the values of NDVI during the vegetation period in each year are slowly increasing and never reach full saturation (Figure S3).

Climate Data

For both study areas, daily and monthly (Figure S1B) mean temperatures and precipitation to-

tals were obtained by interpolating data from the nearest meteorological stations of the Czech Hydrometeorological Institute. Stations with a maximum distance of 50 km from the sampling sites were considered for interpolation. The timespan of available climatic data covers the 1901–2018 period. Mean temperatures were interpolated by orographic regression, assuming the dependence of temperature on elevation (*R* package gstat 2.0–9; Pebesma 2004). Interpolation of precipitation was done using the inverse distance weighting method (Lu and Wong 2008). At least three stations were used to interpolate mean monthly temperatures and seven for precipitation, with an increasing number of stations over time. The standardized precipitation evapotranspiration index (SPEI, Vicente-Serrano and others 2010) was calculated in twelve different time steps with 1 to 12 considered preceding months in the calculation of the ratio between precipitation and evapotranspiration (*R* package SPEI 1.7; Beguería and Vicente-Serrano 2017). Evapotranspiration was computed using the Thornthwaite method (Thornthwaite 1948). We found that correlations between TRI or NDVI and the SPEI did not differ considerably between the various versions of SPEI. Therefore, we decided to use SPEI based on the four preceding months for final analyses since it was reported that SPEI 3–6 usually shows the best fit with NDVI (Vicente-Serrano and others 2012). SPEI 4 reflects a balance between deeply rooting species (PISY) which use water retained in the soil for most of the year, and shallow rooting species (PCAB), reaching soil layers with a relatively fast turnover of infiltrating water (Sprenger and others 2019).

Statistical Analysis

All analyses were based on the time window 1985–2017 as the longest possible common period covered by TRI and NDVI data. Calculations were performed in R 4.2.0 (R Core Team 2022).

To assess the coherency of growth patterns, we employed a principal component gradient analysis (PCGA; *R* package dendRolAB; Buras and others 2016) for both TRI and NDVI. Using the 20 site chronologies per species, we determined the proportion of variability explained by the first principal component (PC1) as an indication of a common signal in the chronologies. We assumed that the second and third principal components (PC2 and PC3) capture growth variability attributed to the four site categories (valleys, plateaus, northern and southern slopes). Therefore, differences in loadings on PC2 and PC3 were tested between site categories using ANOVA. Since there were significant differences in the age of trees between sites and site categories, we also ran a PCGA on a dataset containing solely adult trees with an age of 80–150 years. The results did not differ considerably; hence, all following analyses were carried out on the entire dataset.

To analyze climate-growth responses for each site, Pearson's correlations of TRI and NDVI with monthly mean temperatures and SPEI were computed. We included months that potentially have strong effects on tree growth, that is, the months from June of the year preceding tree-ring (leaf) formation until September of the ring-formation year (Fritts, 1976). We used the *R* package 'treeclim' for dendroclimatic analysis (version 2.0.6.0; Zang and Biondi 2015). To examine how topography influenced the climatic signal in the TRI (as a proxy for stem biomass) and in the NDVI (as a proxy for leaf biomass) chronologies, differences in climate-growth correlations were compared between site categories using ANOVA. To assess similarities in climatic responses between TRI and NDVI from the same site category, we computed t tests of correlation coefficients between site categories and species.

To test how sensitivity to climate is influenced by topography, we calculated the correlation with the main driving variable for each site (for PISY mean SPEI from June to August, for PCAB mean SPEI of the previous year from June to August). Then, we fitted the linear model with climate-growth correlations (response variable) and altitude, slope, north deviation, and topographic wetness index (TWI; Beven and Kirkby 1979) as explanatory variables for each species and TRI and NDVI, respectively. Topographic variables were derived from LIDAR-based surface topography models with a regular grid of 5 × 5 m (DMR 4G; ČÚZK 2013) using ArcMap 10.7.1 (ESRI 2020). See Supplementary material for more information.

To quantify the relationship between wood and leaf biomass, we correlated the time series of TRI and NDVI for each site and tested differences in correlation coefficients between site categories using ANOVA.

Results

Growth Variability Within TRI and NDVI

Growth coherency of both TRI and NDVI was strong: PC1 explained 58–74% of the variability between individual site chronologies both for PCAB and PISY. For PISY, the coherency was larger

for NDVI, while for PCAB, radial growth represented by the TRI was substantially more coherent than NDVI (Figure 2).

With respect to site categories, PCGA revealed significant differences for PISY TRI, clearly distinguishing plateaus and valleys (Figure 2A, Table S3) and between northern and southern slopes (Figure 2B). Valleys and northern slopes differed substantially, and plateaus and southern slopes revealed a nearly significant difference (Table S3). For PCAB, TRI and NDVI showed no systematic pattern and no significant differences between site categories along any PC (Figure 2).

Topographic Variability in the Climatic Signal of TRI and NDVI

The climatic signal differed between biomass proxies, climate variables, species, and site categories. PISY TRI chronologies from plateaus showed the strongest correlations with both previous and current-year summer SPEI, followed by sites from southern and northern slopes, while responses in valleys were always weak and mostly insignificant (Figure 3). By contrast, the correlations of PISY TRI with temperature were strongest for valleys, followed by slopes, peaking from January to March of the current year. Plateaus showed non-significant or even significant negative TRI correlations with temperature during the previous June and December. Differences in climate-growth correlations between plateaus and valleys were statistically significant for both temperature and SPEI in most tested months (Table S4). NDVI of PISY was mainly positively correlated with current-year summer SPEI (Figure 3). Plateaus and north slopes exhibited the strongest relationship with SPEI. Peak correlations of PISY NDVI with SPEI (culminating in current June and July) occurred about one month earlier compared to TRI (peak in current July and August). Relationships of NDVI with temperature showed two periods with statistically significant correlations: positive correlations with the previous October and negative correlations with March of the leaf-formation year.

PCAB TRI exhibited significant negative correlations with temperature in the previous summer and positive correlations with current January and March. PCAB TRI correlations with SPEI were mostly weak and insignificant (Figure 3). In contrast, NDVI was significantly negatively influenced by SPEI during the previous summer and autumn for all site categories. NDVI of PCAB revealed significant positive correlations with temperature during the previous August and December. Overall, there were no systematic differences caused by topography in the climatic signal of PCAB chronologies (Table S5).

Although the response of PISY TRI and NDVI to SPEI revealed very similar patterns (Figure 3), there were significant differences in absolute values of correlation coefficients. Specifically, the most prominent differences occurred for plateaus during the previous summer (correlations with TRI

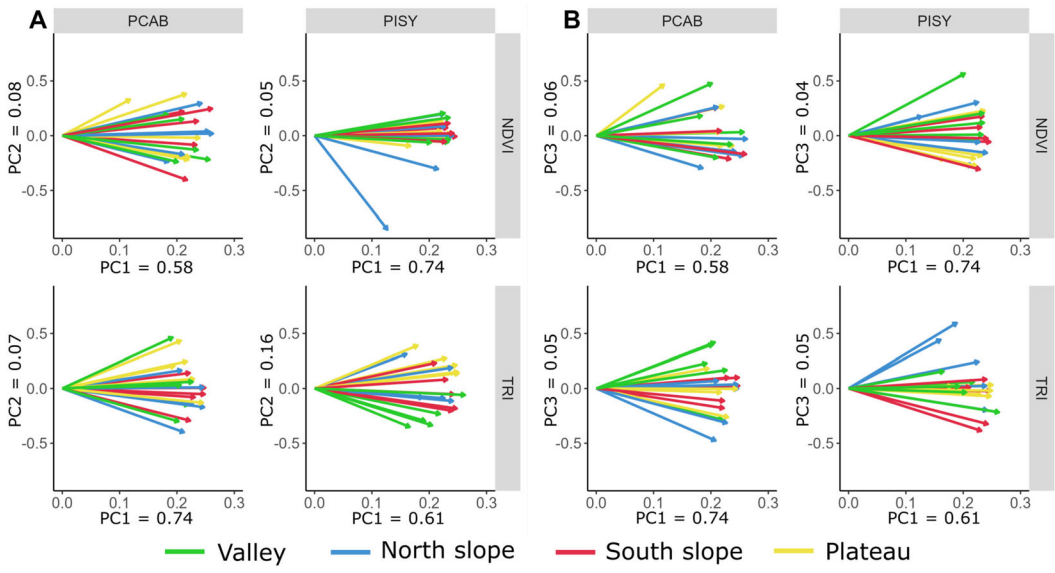

Figure 2. Biplots of principal component gradient analysis showing growth variability in TRI and NDVI time series covering the 1985–2017 period separately for PCAB and PISY sites. The color coding of site categories is indicated in the legend below. Panel A: PC1 versus PC2, panel B: PC1 versus PC3.

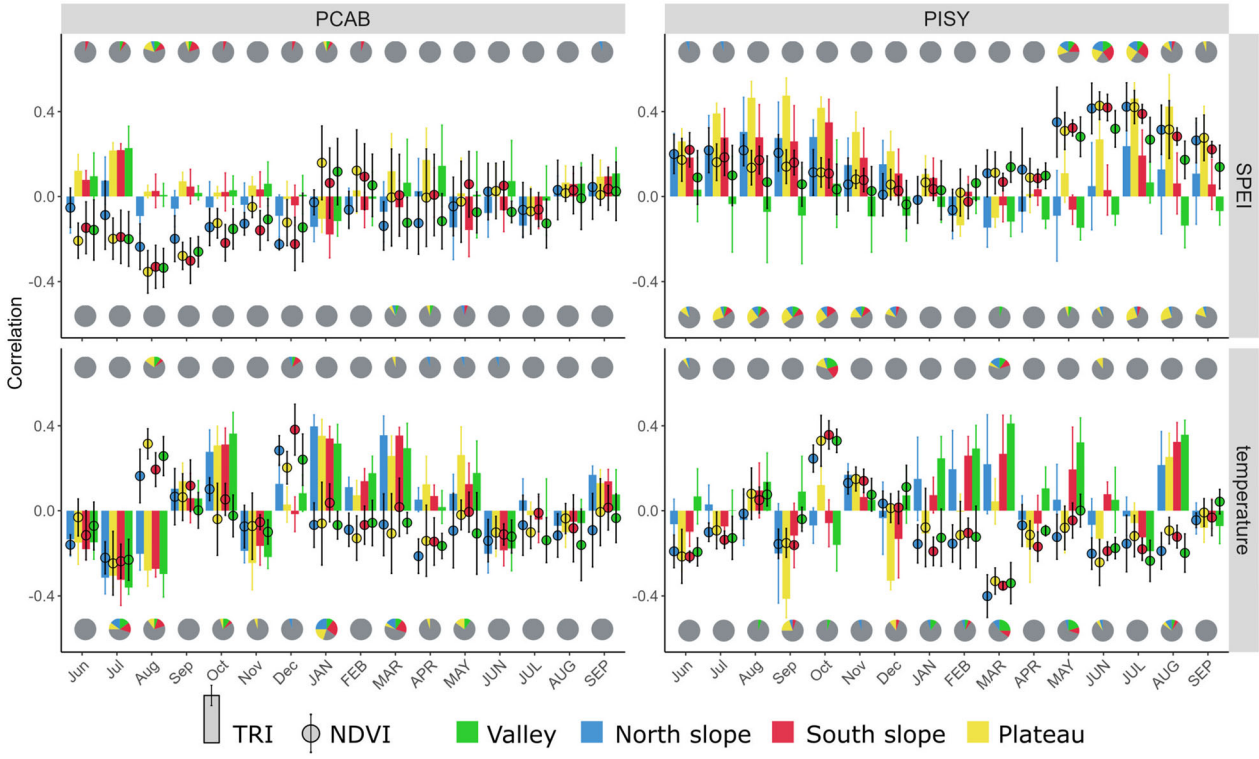

Figure 3. Mean correlations of TRI (bars) and NDVI (circles) with monthly mean temperatures (bottom) and SPEI (top) for PCAB (left) and PISY (right). Error bars show standard deviations between individual sites. Pie graphs denote the percentage of significant correlations observed for individual sites ($p < 0.05$), upper row: NDVI, bottom row: TRI. The gray area represents non-significant correlations, and colors denote individual site categories (see legend below). Small letters indicate months of the previous year, and capital letters denote months of the current year.

stronger than with NDVI) and for valleys in the current spring (correlations with NDVI stronger than with TRI) (Table S6). For temperature, climate-growth correlations differed substantially between TRI and NDVI of PISY. There were opposite responses for TRI and NDVI, namely in the previous October (TRI negative, NDVI positive) and the current March (NDVI negative and TRI positive) (Table S6, Figure 3). For PCAB stands of all site categories, TRI and NDVI correlations with temperature and SPEI differed across almost all months of the previous year, winter, and spring of the ring-formation year (Table S6).

The linear model explaining correlations of PISY TRI with SPEI was statistically significant ($R^2 = 0.85$, p value < 0.05) with a strong influence of slope, TWI, and altitude on climatic sensitivity. A relatively high amount of explained variability ($R^2 = 0.4$, p value $= 0.09$) was observed for a model explaining correlations of PISY NDVI and SPEI, where TWI revealed a significant effect. For PCAB both models were insignificant with a low coefficient of determination (Table S7).

Relationship Between TRI and NDVI

Correlations between the time series of TRI and NDVI were statistically significant for 20% of the sites for PISY. Correlations were strongest for plateaus and generally decreased in the following order: south slopes, north slopes, and valleys (Figure 4). However, there was no statistically sig-

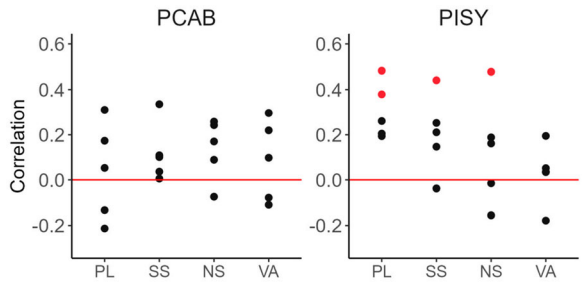

Figure 4. Correlations between TRI and NDVI chronologies per species and site category (SS—south slopes, NS—north slopes, PL—plateaus, VA—valleys). Red dots denote statistically significant correlations ($p < 0.05$).

nificant difference between site categories with respect to mean TRI-NDVI correlations. For PCAB, all correlations between TRI and NDVI were non-significant.

Discussion

Our results highlight a complex pattern in climatic responses of tree-ring widths and NDVI that are driven by interactions of site climatic conditions, species, and topography. By combining analyses of tree-ring width (as a proxy for stem biomass) and NDVI (as a proxy for leaf biomass), we found that the climatic limitation of stem and leaf biomass can be significantly different close to a species' ecological optimum (our PCAB sites). On the other hand, climate-growth responses of tree rings and NDVI were more similar at the moisture-limited PISY sites, mainly for the SPEI drought index. Overall, the climatic limitation of tree rings was stronger and partly modulated by topographic conditions, while NDVI was less affected by topography in our study.

Growth Coherency and Relationships of TRI and NDVI

The high levels of common variability determined by PCGA both for TRI and NDVI chronologies are in line with previous observations (Galván and others 2014; Fang and others 2012; Bunn and others 2013; Pesaresi and others 2020; Ivanova and others 2021). We found, however, species-specific differences. The relatively less coherent growth pattern of PISY TRI compared to PISY NDVI might have been caused by the more variable topography of PISY sites (Montpellier and others 2018; Oberhuber and Kofler 2000). Additionally, there was a higher variability in age among PISY sites compared to PCAB, which can affect the common growth signal (Konter and others 2016; Mašek and others 2021). PCAB forests in Šumava Mts. are known for disturbance dynamics (wind throws, bark beetle), which might have caused the relatively high variance in NDVI, even though we had cautiously placed our plots in stable and undisturbed areas of the forest stands. Overall, the growth coherence among both TRI and NDVI was anyway high enough to represent the prevailing common signal since PC1 always captured more than 50% of the variance.

Although it has been shown that correlations between NDVI and TRI increase with a spatial resolution (250 m compared to 8 km; Bhuyan and others 2017), our correlation coefficients between TRI and NDVI ranged from −0.27 to 0.50 (based on a resolution of 30 m), which is comparable to other studies that used lower (250 m) resolution MODIS data (Wang and others 2021; Correa–Díaz and others 2019; Schröder and Körner 2018). It is possible that a resolution of 250 m is high enough to obtain ecologically realistic correlations between TRI and NDVI, while spatially more detailed data do not enhance the signal considerably. This suggests that the general pattern of NDVI, and thus leaf biomass production, is captured even with lower-resolution data (250 m).

Overall, PISY sites, particularly plateaus, showed higher correlations between TRI and NDVI than PCAB, probably due to a common climatic driver (drought) for both biomass proxies. The decline of correlations for PISY from plateaus to slopes and valleys was likely caused by increasing moisture availability along the topographic gradient. At PCAB sites, stem and leaf biomass differed in their climatic signal (Table S6), except for the summer months from June to September, which probably led to the low correlations between PCAB TRI and NDVI. It has been demonstrated that correlations between TRI and NDVI tend to increase toward the margins of a species' climatic niche (Alla and others 2017; Coulthard and others 2017; Liang and others 2009). Although PCAB stands in Šumava Mts. are near the climatic optimum of this species (Mäkinen and others 2002), our PISY stands occur in an area experiencing frequent droughts, which can be even more severe at plateaus with shallow soils. Considering the significant correlations between TRI and NDVI for PISY and the clear influence of topography, NDVI, and digital elevation models could be used to spatially interpolate growth dynamics and thus the intensity of carbon sequestration at a landscape level. For our PCAB sites, where the growth patterns of TRI and NDVI were heterogeneous and free of topographic effects, the spatial extrapolation would be highly uncertain.

Effects of Climate and Topography on TRI and NDVI

Site topographic categories were distinguished by the second or third principal component for PISY TRI but not for any biomass proxy of PCAB. Climatic conditions reflect topographical characteristics, resulting in topographically varying temperature (slope orientation) and water availability (terrain curvature), which is then recorded in tree rings and NDVI (Rabbel and others 2018; Riihimäki and others 2017). PISY sites at plateaus were strongly drought-limited due to high solar

radiation and flat terrain unfavorable for long-term moisture accumulation as previously shown for similar areas in Central Europe (Mácová 2008). By contrast, PISY sites in the valleys revealed much less drought limitation and even showed a positive effect of summer temperature, which is likely due to moisture accumulation and a common topographically induced temperature inversion (Cílek 2007). In contrast, site categories of PCAB did not differ in their climatic responses, which is probably due to the generally less climatically limited growth and relatively low topographical variability of Šumava Mts. compared to Kokořínsko hills (Figure 1). The topographically different climatic limitations thus presumably were translated into different growth patterns at each PISY site category; by contrast, the landscape-scale growth variability of PCAB was driven by different effects than site climatic conditions.

Interestingly, the seasonal response pattern of PISY NDVI to SPEI was very similar to that of the tree rings, but it was shifted back by one month. This shift suggests that tree-ring formation lags behind needle production by approximately one month, probably due to the onset of growth occurring first in terminal shoots and leaves and its delay toward the stem base (Petit and others 2018). This relationship might have important implications with respect to a temporal decoupling of carbon assimilation in leaves and carbon sequestration in wood biomass (Teets and others 2022; Kannenberg and others 2022; Anderson-Teixeira and others 2022). Leaf biomass production seems to be influenced by climatic conditions at a different time of the year than xylogenesis. Studies have shown that while carbon assimilation (hence vegetation greenness) may start with temperatures of over 0 °C, the growth of trees is limited by temperatures of 5–6 °C (Fatichi and others 2014). These findings may also explain the lag in climate responses of NDVI and TRI in our study. During drought years, the growth (carbon sink) is interrupted earlier than photosynthesis (carbon assimilation) because of low turgor in cells; therefore, assimilated carbon is stored in non-structural carbohydrates which might be used for root production (Teets and others 2022) or for the growth in the following year. This might explain the high correlations of PISY TRI and the low correlations of PISY NDVI with SPEI in the previous year. Overall, the stronger climatic signal of TRI compared to NDVI suggests that wood formation is more strongly driven by climatic constraints than by the availability of source sugars from leaves (Dow and others 2022; Cabon and others 2022; Fatichi and others 2014).

The response of PCAB (both biomass proxies) to SPEI was generally weak, most likely because moisture is not a growth-limiting factor in the humid environment of Šumava Mts. However, high moisture availability in the preceding summer caused a decrease in NDVI. This could result from wet and cloudy conditions, which might have caused low photosynthesis rates and consequently less available resources invested in bud formation (Alton 2008). PCAB NDVI was also rather insensitive to temperature, except for positive correlations in the previous August and to a larger extent previous December, which can be associated with suitable conditions for bud formation (August) and favorable conditions for soil processes leading to higher accessibility of nitrogen (Weigel and others 2021).

NDVI showed hardly any significant differences between site categories since it is a generally less climate-sensitive proxy than tree-ring width (Peña-Gallardo and others 2018; Liang and others 2009; Gazol and others 2018a). Adult trees preferably allocate biomass to roots during drought periods, mainly at the expense of the stem (Dybzinski and others 2011; Zhang and others 2015; Sevanto and Dickman 2015). This holds the explanation for NDVI and stem growth topographical patterns for PISY in the drought-limited region of Kokořínsko hills, where PISY exhibited less topographical differences of NDVI compared to tree rings. During droughts, trees probably adjusted their biomass allocation at plateaus, while the allocation remained unaffected in valleys. With this, our results suggest that toward the moisture-limited part of the species range, the limitation of sink processes becomes important (Cabon and others 2022). In dry years, the sugar investments in leaves remain less affected and thus the potential intensity of photosynthesis is also not reduced. However, the investment of sugars into stem growth is depressed because cambial cell expansion and division need sufficient delivery of water (Cabon and others 2020). Relatively weaker response of leaf biomass to climate was compared to stem wood biomass thus indirectly corroborating outcomes of studies highlighting the importance of not only source but also sink-limitation processes of tree growth (Fatichi and others 2014; Friend and others 2019; Körner 2015).

Furthermore, it was also argued that a stronger climatic sensitivity of tree rings compared to NDVI may result from partial distortion of the spectral signal due to the limited spatial resolution and due

to noise from other vegetation, which can imprint into the resulting pixel values (Gazol and others 2018a). We tried to avoid artifacts due to admixed species by selecting monospecific sites. Also, soil wetness might imprint into the NDVI signal since it influences spectral reflectance (positively for dry soils; Demattê and others 2004). Unfortunately, canopies of PISY growing in an open stand might not fully cover the ground, and consequently, NDVI estimates might be biased by the presence of ground vegetation. Another explanation for the lower sensitivity of NDVI to climate might be that actual meteorological conditions affecting cambium and needles differ because of the height difference and because the crown shelters the stem. It is likely that the importance of topographical variability in terms of temperature effects is lower at 30 m above the ground than at 1.3 m, where the tree core was taken (Kollas and others 2014). Averaging the NDVI into seasonal values (covering the entire vegetation period May–September) might also have influenced the climatic sensitivity of NDVI. However, data at monthly or biweekly resolution (Brehaut and Danby 2018; Correa–Díaz and others 2019; Wu and others 2017; Wang and others 2021) were not available for high-quality Landsat scenes with no cloud cover in our study areas.

Conclusions

Relationships between stem (tree-ring width) and leaf biomass (NDVI) and their climatic signals have so far been studied using low-resolution satellite images masking local topographical differences in forest responses to climate. In this study, we analyzed climate-growth responses of tree-ring widths and NDVI for two main Central European species (*P. abies*, and *P. sylvestris*) at a landscape level using high-resolution Landsat data and systematically taking into account topographic differences. We conclude that the link between tree-ring and NDVI chronologies was generally stronger for *P. sylvestris* compared to *P. abies* and reflected a topographical pattern. Climatic responses of tree rings and NDVI significantly differed in areas near the climatic optimum of a species (*P. abies* in Šumava Mts.). On the other hand, the direction of climate responses of tree rings and NDVI for drought-limited *P. sylvestris* in Kokořínsko hills was similar, but the strength of these responses was strongly modulated by the landscape topography. Overall, tree rings showed a closer link to climatic drivers than NDVI for both species, probably due to a combination of effects such as biomass allocation changes during droughts, spectral distortion of remote sensing data, and different meteorological conditions influencing the stem and crown. Further research is needed to improve our understanding of the decoupling of the climate signal of different tree compartments. This knowledge is important for forecasting climate change effects on the entire above-ground forest biomass and, consequently, on ecosystems and the carbon cycle.

Acknowledgements

We appreciate the permission and help of the administrators of the protected areas Kokořínsko hills and Šumava Mts. to carry out our research. We are grateful to Charles University Grant Agency (GAUK 548120) for the financial support.

Funding

Open access publishing supported by the National Technical Library in Prague. The study was funded by the Charles University Grant Agency (GAUK 548120).

Data Availability

Tree-ring width data have been uploaded to the International Tree-Ring Data Bank (ITRDB). Codes for NDVI time-series calculation in Google Earth Engine are provided here: PCAB: https://code.earthengine.google.com/ddb1fc420d3be0f01719effb1facfa2b, and PISY: https://code.earthengine.google.com/8a54269c4279d7795aeec9cc5873d109. All used data (climate, ring width, and NDVI) are freely available for download on GitHub (https://github.com/JirkaSkaut/Topographic-variability) including the R script for all calculations and figure drawings.

Declarations

Conflict of interest The authors declare no conflict of interest.

REFERENCES

Adams HR, Barnard HR, Loomis AK. 2014. Topography alters tree growth-climate relationships in a semi-arid forested catchment. Ecosphere 5:1–16.

Albrecht J. 2003. Českobudějovicko. In: Mackovčin P, Sedláček M (eds.): Chráněná území ČR, svazek VIII. Agentura ochrany přírody a krajiny ČR a EkoCentrum Brno, Praha, 808 pp.

Alla AQ, Pasho E, Marku V. 2017. Growth variability and contrasting climatic responses of two Quercus macrolepis stands from Southern Albania. Trees - Struct Funct 31:1491–1504.

Alton PB. 2008. Reduced carbon sequestration in terrestrial ecosystems under overcast skies compared to clear skies. Agric for Meteorol 148:1641–1653.

Anderegg WRL, Berry JA, Smith DD, Sperry JS, Anderegg LDL, Field CB. 2012. The roles of hydraulic and carbon stress in a widespread climate-induced forest die-off. Proc Natl Acad Sci U S A 109:233–237.

Anderegg WRL, Schwalm C, Biondi F, Camarero JJ, Koch G, Litvak M, Ogle K, Shaw JD, Shevliakova E, Williams AP, Wolf A, Ziaco E, Pacala S. 2015. Pervasive drought legacies in forest ecosystems and their implications for carbon cycle models. Science (80-) 349:528–32.

Anderson-Teixeira KJ, Kannenberg SA. 2022. What drives forest carbon storage? The ramifications of source–sink decoupling. New Phytol 236:5–8.

Tolasz R (ed.). 2007. Atlas podnebí Česka. ČHMÚ, Praha, Olomouc, 255 s.

Babst F, Alexander MR, Szejner P, Bouriaud O, Klesse S, Roden J, Ciais P, Poulter B, Frank D, Moore DJP, Trouet V. 2014. A tree-ring perspective on the terrestrial carbon cycle. Oecologia 176:307–322.

Babst F, Poulter B, Bodesheim P, Mahecha MD, Frank DC. 2017. Improved tree-ring archives will support earth-system science. Nat Ecol Evol 1:1–2. https://doi.org/10.1038/s41559-016-0008.

Babst F, Bodesheim P, Charney N, Friend AD, Girardin MP, Klesse S, Moore DJP, Seftigen K, Björklund J, Bouriaud O, Dawson A, DeRose RJ, Dietze MC, Eckes AH, Enquist B, Frank DC, Mahecha MD, Poulter B, Record S, Trouet V, Turton RH, Zhang Z, Evans MEK. 2018. When tree rings go global: Challenges and opportunities for retro- and prospective insight. Quat Sci Rev 197:1–20.

Beck PSA, Andreu-Hayles L, D'Arrigo R, Anchukaitis KJ, Tucker CJ, Pinzón JE, Goetz SJ. 2013. A large-scale coherent signal of canopy status in maximum latewood density of tree rings at arctic treeline in North America. Glob Planet Change 100:109–118. https://doi.org/10.1016/j.gloplacha.2012.10.005.

Beguería S, Vicente-Serrano SM. (2017). SPEI: Calculation of the Standardised Precipitation-Evapotranspiration Index. R package version 1.7. https://CRAN.R-project.org/package=SPEI

Berner LT, Beck PSA, Bunn AG, Lloyd AH, Goetz SJ. 2011. High-latitude tree growth and satellite vegetation indices: Correlations and trends in Russia and Canada (1982–2008). J Geophys Res Biogeosciences 116:1–13.

Berner LT, Beck PSA, Bunn AG, Goetz SJ. 2013. Plant response to climate change along the forest-tundra ecotone in northeastern Siberia. Glob Chang Biol 19:3449–3462.

Bernoulli M, Körner C. 1999. Dry matter allocation in treeline trees. Phyt - Ann Rei Bot 39:7–12.

Beven KJ, Kirkby MJ. 1979. A physically based, variable contributing area model of basin hydrology. Hydrol. Sci. Bull. 24:43–69. https://doi.org/10.1080/02626667909491834.

Bhuyan U, Zang C, Vicente-Serrano SM, Menzel A. 2017. Exploring relationships among tree-ring growth, climate variability, and seasonal leaf activity on varying timescales and spatial resolutions. Remote Sens 9.

Bína J, Demek J (2012) Z nížin do hor: Geomorfologické jednotky České republiky. Academia Praha. ISBN: 978-802-0020-260, 343s

Brehaut L, Danby RK. 2018. Inconsistent relationships between annual tree ring-widths and satellite-measured NDVI in a mountainous subarctic environment. Ecol Indic 91:698–711. https://doi.org/10.1016/j.ecolind.2018.04.052.

Bunn AG. 2008. A dendrochronology program library in R (dplR). Dendrochronologia 26:115–124.

Bunn AG, Hughes MK, Kirdyanov A V., Losleben M, Shishov V V., Berner LT, Oltchev A, Vaganov EA. 2013. Comparing forest measurements from tree rings and a space-based index of vegetation activity in Siberia. Environ Res Lett 8.

Buras A, Van Der Maaten-Theunissen M, Van Der Maaten E, Ahlgrimm S, Hermann P, Simard S, Heinrich I, Helle G, Unterseher M, Schnittler M, Eusemann P, Wilmking M. 2016. Tuning the voices of a choir: Detecting ecological gradients in time-series populations. PLoS One 11:1–21.

Cabon A, Peters RL, Fonti P, Martínez-Vilalta J, De Cáceres M. 2020. Temperature and water potential co-limit stem cambial activity along a steep elevational gradient. New Phytol 226:1325–1340.

Cabon A, Kannenberg SA, Arain A, Babst F, Baldocchi D, Belmecheri S, Delpierre N, Guerrieri R, Maxwell JT, McKenzie S, Meinzer FC, Moore DJP, Pappas C, Rocha A V., Szejner P, Ueyama M, Ulrich D, Vincke C, Voelker SL, Wei J, Woodruff D, Anderegg WRL. 2022. Cross-biome synthesis of source versus sink limits to tree growth. Science (80-) 761:758–61.

Carrer M, Urbinati C. 2004. Age-Dependent Tree-Ring Growth Responses to Climate in Larix decidua and *Pinus cembra* Author(s): Marco Carrer and Carlo Urbinati Published by: Wiley Stabl URL: http://www.jstor.org/stable/3450399 REFERENCES Linked references are available on JSTOR f. Ecology 85:730–40.

Cílek V. 2007. Climate, microclimate and paleoclimate of sandstone areas of Central and Northern Bohemia (Czech republic). In: Härtel H, Cílek V, Herben T, Jackson A, Williams R (eds.): Sandstone landscapes. Academia, Praha, s. 97–103.

Cook E, Peters K. 1981. The smoothing spline, a new approach to standardising forest interior tree-ring. Trre-Ring Bull 41:45–53.

Correa-Díaz A, Silva LCR, Horwath WR, Gómez-Guerrero A, Vargas-Hernández J, Villanueva-Díaz J, Velázquez-Martínez A, Suárez-Espinoza J. 2019. Linking Remote Sensing and Dendrochronology to Quantify Climate-Induced Shifts in High-Elevation Forests Over Space and Time. J Geophys Res Biogeosciences 124:166–183.

Coulthard BL, Touchan R, Anchukaitis KJ, Meko DM, Sivrikaya F. 2017. Tree growth and vegetation activity at the ecosystem-scale in the eastern Mediterranean. Environ Res Lett 12.

ČÚZK (Czech Office for Surveying, Mapping and Cadastre), 2013. Digitální model reliéfu ČR 4. generace.

D'Arrigo RD, Jacoby GC, Bunker DE, Malmstrom CM, Los SO. 2000. Correlation between maximum latewood density of annual tree rings and NDVI based estimates of forest productivity. Int J Remote Sens 21:2329–2336.

D'Arrigo R, Wilson R, Jacoby G. 2006. On the long-term context for late twentieth century warming. J Geophys Res Atmos 111:1–12.

del Castillo J, Voltas J, Ferrio JP. 2015. Carbon isotope discrimination, radial growth, and NDVI share spatiotemporal responses to precipitation in Aleppo pine. Trees - Struct Funct 29:223–233.

Del-Toro-Guerrero FJ, Kretzschmar T, Bullock SH. 2019. Precipitation and topography modulate vegetation greenness in the mountains of Baja California, México. Int J Biometeorol 63:1425–1435.

Demattê JAM, Campos RC, Alves MC, Fiorio PR, Nanni MR. 2004. Visible-NIR reflectance: A new approach on soil evaluation. Geoderma 121:95–112.

Demek J, Balatka B, Czudek T, Láznička Z, Linhart J, Loučková J, Panoš V, Raušer J, Seichterová H, Sládek J, Stehlík O, Štecl O, Vlček V. 1965. Geomorfologie českých zemí. Nakladatelství Československé akademie věd, Praha, 335 s.

Donohue RJ, Roderick ML, McVicar TR, Farquhar GD. 2013. Impact of CO2 fertilization on maximum foliage cover across the globe's warm, arid environments. Geophys Res Lett 40:3031–3035.

Dow C, Kim AY, D'Orangeville L, Gonzalez-Akre EB, Helcoski R, Herrmann V, Harley GL, Maxwell JT, McGregor IR, McShea WJ, McMahon SM, Pederson N, Tepley AJ, Anderson-Teixeira KJ. 2022. Warm springs alter timing but not total growth of temperate deciduous trees. Nature 608:552–557.

Durrant TH, de Rigo D, Caudullo G. 2016. *P. sylvestris* in Europe: distribution, habitat, usage and threats. In: San-Miguel-Ayanz J, de Rigo D, Caudullo G, Houston Durrant T, Mauri A. (Eds.). 2016. European Atlas of Forest Tree Species. Publication Office of the European Union, Luxembourg.

Dybzinski R, Farrior C, Wolf A, Reich PB, Pacala SW. 2011. Evolutionarily stable strategy carbon allocation to foliage, wood, and fine roots in trees competing for light and nitrogen: An analytically tractable, individual-based model and quantitative comparisons to data. Am Nat 177:153–166.

ESRI, 2020. ArcGIS Desktop: Release 10.7.1. Redlands. Environmental Systems Research Institute, CA.

Etzold S, Sterck F, Bose AK, Braun S, Buchmann N, Eugster W, Gessler A, Kahmen A, Peters RL, Vitasse Y, Walthert L, Ziemińska K, Zweifel R. 2022. Number of growth days and not length of the growth period determines radial stem growth of temperate trees. Ecol Lett 25:427–439.

Fajstavr M, Bednářová E, Nezval O, Giagli K, Gryc V, Vavrčík H, Horáček P, Urban J. 2019. How needle phenology indicates the changes of xylem cell formation during drought stress in *P. sylvestris* L. Dendrochronologia 56.

Fang K, Gou X, Chen F, Li Y, Zhang F, Kazmer M. 2012. Tree growth and its association with climate between individual tree-ring series at three mountain ranges in north central China. Dendrochronologia 30:113–119. https://doi.org/10.1016/j.dendro.2011.04.003.

Fatichi S, Leuzinger S, Körner C. 2014. Moving beyond photosynthesis: From carbon source to sink-driven vegetation modeling. New Phytol 201:1086–1095.

Friend AD, Patrick AHE, Tim F, Rathgeber CBK, Richardson AD, Turton RH. 2019. On the need to consider wood formation processes in global vegetation models and a suggested approach. Ann for Sci 76:49.

Frittz HC. 1976. Tree Rings and Climate. New York: Academic Press.

Galván JD, Camarero JJ, Gutiérrez E. 2014. Seeing the trees for the forest: Drivers of individual growth responses to climate in *Pinus uncinata* mountain forests. J Ecol 102:1244–1257.

Gazol A, Camarero JJ, Vicente-Serrano SM, Sánchez-Salguero R, Gutiérrez E, de Luis M, Sangüesa-Barreda G, Novak K, Rozas V, Tíscar PA, Linares JC, Martín-Hernández N, Martínez del Castillo E, Ribas M, García-González I, Silla F, Camisón A, Génova M, Olano JM, Longares LA, Hevia A, Tomás-Burguera M, Galván JD. 2018a. Forest resilience to drought varies across biomes. Glob Chang Biol 24:2143–2158.

Gazol A, Camarero JJ, Sangüesa-Barreda G, Vicente-Serrano SM. 2018b. Post-drought resilience after forest die-off: Shifts in regeneration, composition, growth and productivity. Front Plant Sci 871:1–12.

Girardin MP, Bouriaud O, Hogg EH, Kurz W, Zimmermann NE, Metsaranta JM, De Jong R, Frank DC, Esper J, Büntgen U, Guo XJ, Bhatti J. 2016. No growth stimulation of Canada's boreal forest under half-century of combined warming and CO2 fertilization. Proc Natl Acad Sci U S A 113:E8406–E8414.

Gorelick N, Hancher M, Dixon M, Ilyushchenko S, Thau D, Moore R. 2017. Google Earth Engine: Planetary-scale geospatial analysis for everyone. Remote Sens Environ 202:18–27. https://doi.org/10.1016/j.rse.2017.06.031.

Hájková L (ed.). 2012. Atlas fenologických poměrů Česka. Praha: Český hydrometeorologický ústav; Olomouc, 2012. ISBN 978–80–86690–98–8.

Instruments Regent. 2011. WinDendro Image Analysis System. Québec: Regent Instruments Inc.

Ivanova Y, Kovalev A, Soukhovolsky V. 2021. Modeling the radial stem growth of the pine (*P. sylvestris* l.) forests using the satellite-derived ndvi and lst (modis/aqua) data. Atmosphere (basel) 12:1–15.

Kannenberg SA, Novick KA, Alexander MR, Maxwell JT, Moore DJP, Phillips RP, Anderegg WRL. 2019. Linking drought legacy effects across scales: From leaves to tree rings to ecosystems. Glob Chang Biol 25:2978–2992.

Kannenberg SA, Cabon A, Babst F, Belmecheri S, Delpierre N, Guerrieri R, Maxwell JT, Meinzer FC, Moore DJP, Pappas C, Ueyama M, Ulrich DEM, Voelker SL, Woodruff DR, Anderegg WRL. 2022. Drought-induced decoupling between carbon uptake and tree growth impacts forest carbon turnover time. Agric For Meteorol 322:108996. https://doi.org/10.1016/j.agrformet.2022.108996

Kaufmann RK, D'Arrigo RD, Paletta LF, Tian HQ, Jolly WM, Myneni RB. 2008. Identifying climatic controls on ring width: The timing of correlations between tree rings and NDVI. Earth Interact 12:1–14.

Knibbe B. 2004. Personal Analysis System for Tree-ring Research 4 - Instruction Manual. Vienna: SCIEM.

Kollas C, Randin CF, Vitasse Y, Körner C. 2014. How accurately can minimum temperatures at the cold limits of tree species be extrapolated from weather station data? Agric for Meteorol

184:257–266. https://doi.org/10.1016/j.agrformet.2013.10.001.

Konter O, Büntgen U, Carrer M, Timonen M, Esper J. 2016. Climate signal age effects in boreal tree-rings: Lessons to be learned for paleoclimatic reconstructions. Quat Sci Rev 142:164–172. https://doi.org/10.1016/j.quascirev.2016.04.020.

Körner C. 2015. Paradigm shift in plant growth control. Curr Opin Plant Biol 25:107–114.

Kraus C, Zang C, Menzel A. 2016. Elevational response in leaf and xylem phenology reveals different prolongation of growing period of common beech and Norway spruce under warming conditions in the Bavarian Alps. Eur J for Res 135:1011–1023.

Krejza J, Cienciala E, Světlík J, Bellan M, Noyer E, Horáček P, Štěpánek P, Marek MV. 2021. Evidence of climate-induced stress of Norway spruce along elevation gradient preceding the current dieback in Central Europe. Trees - Struct Funct 35:103–119. https://doi.org/10.1007/s00468-020-02022-6.

Le Quéré C, Raupach MR, Canadell JG, Marland G, Bopp L, Ciais P, Conway TJ, Doney SC, Feely RA, Foster P, Friedlingstein P, Gurney K, Houghton RA, House JI, Huntingford C, Levy PE, Lomas MR, Majkut J, Metzl N, Ometto JP, Peters GP, Prentice IC, Randerson JT, Running SW, Sarmiento JL, Schuster U, Sitch S, Takahashi T, Viovy N, Van Der Werf GR, Woodward FI. 2009. Trends in the sources and sinks of carbon dioxide. Nat Geosci 2:831–836.

Leavitt SW, Chase TN, Rajagopalan B, Lee E, Lawrence PJ. 2008. Southwestern U.S. tree-ring carbon isotope indices as a possible proxy for reconstruction of greenness of vegetation. Geophys Res Lett 35:1–5.

Liang EY, Shao XM, He JC. 2005. Relationships between tree growth and NDVI of grassland in the semi-arid grassland of north China. Int J Remote Sens 26:2901–2908.

Liang E, Eckstein D, Liu H. 2009. Assessing the recent grassland greening trend in a long-term context based on tree-ring analysis: A case study in North China. Ecol Indic 9:1280–1283.

Lopatin E, Kolström T, Spiecker H. 2006. Determination of forest growth trends in Komi Republic (northwestern Russia): Combination of tree-ring analysis and remote sensing data. Boreal Environ Res 11:341–353.

Ložek V, Kubíková J, Spryňar P. 2005. Střední Čechy. In: Mackovčin P, Sedláček M (eds.): Chráněná území ČR, svazek XIII. Agentura ochrany přírody a krajiny ČR a EkoCentrum Brno, Praha, 904 pp.

Lu GY, Wong DW. 2008. An adaptive inverse-distance weighting spatial interpolation technique. Comput Geosci 34:1044–1055.

Mácová M. 2008. Dendroclimatological comparison of native *P. sylvestris* and invasive *Pinus strobus* in different habitats in the Czech Republic. Preslia 80:277–289.

Mäkinen H, Nöjd P, Kahle HP, Neumann U, Tveite B, Mielikäinen K, Röhle H, Spiecker H. 2002. Radial growth variation of Norway spruce (*P. abies* (L.) Karst.) across latitudinal and altitudinal gradients in central and northern Europe. For Ecol Manage 171:243–259.

Mašek J, Tumajer J, Rydval M, Lange J, Treml V. 2021. Age and size outperform topographic effects on growth-climate responses of trees in two Central European coniferous forest types. Dendrochronologia 68:125845.

Montpellier EE, Soulé PT, Knapp PA, Shelly JS. 2018. Divergent growth rates of alpine larch trees (Larix lyallii Parl.) in response to microenvironmental variability. Arctic, Antarct Alp Res 50:1–9. https://doi.org/10.1080/15230430.2017.1415626.

NASA. 2022. Measuring vegetation NDVI & EVI. Normalized Difference Vegetation Index (NDVI). http://earthobservatory.nasa.gov/Features/MeasuringVegetation/measuring_vegetation_2.php (12.5.2022)

Oberhuber W, Kofler W. 2000. Topographic influences on radial growth of Scots pine (*P. sylvestris* L.) at small spatial scales. Plant Ecol 146:231–240.

Pan Y, Birdsey RA, Fang J, Houghton R, Kauppi PE, Kurz WA, Phillips OL, Shvidenko A, Lewis SL, Canadell JG, Ciais P, Jackson RB, Pacala SW, McGuire AD, Piao S, Rautiainen A, Sitch S, Hayes D. 2011. A large and persistent carbon sink in the world's forests. Science 333:988–993.

Pasho E, Alla AQ. 2015. Climate impacts on radial growth and vegetation activity of two co-existing Mediterranean pine species. Can J for Res 45:1748–1756.

Pebesma EJ. 2004. Multivariable geostatistics in S: The gstat package. Comput Geosci 30:683–691.

Peña-Gallardo M, Vicente-Serrano SM, Camarero JJ, Gazol A, Sánchez-Salguero R, Domínguez-Castro F, El Kenawy A, Beguería-Portugés S, Gutiérrez E, de Luis M, Sangüesa-Barreda G, Novak K, Rozas V, Tíscar PA, Linares JC, del Castillo EM, Matamoros MR, García-González I, Silla F, Camisón Á, Génova M, Olano JM, Longares LA, Hevia A, Galván JD. 2018. Drought sensitiveness on forest growth in peninsular Spain and the Balearic Islands. Forests 9:1–20.

Pesaresi S, Mancini A, Quattrini G, Casavecchia S. 2020. Mapping mediterranean forest plant associations and habitats with functional principal component analysis using Landsat 8 NDVI time series. Remote Sens 12.

Petit G, von Arx G, Kiorapostolou N, Lechthaler S, Prendin AL, Anfodillo T, Caldeira MC, Cochard H, Copini P, Crivellaro A, Delzon S, Gebauer R, Gričar J, Grönholm L, Hölttä T, Jyske T, Lavrič M, Lintunen A, Lobo-do-Vale R, Peltoniemi M, Peters RL, Robert EMR, Roig Juan S, Senfeldr M, Steppe K, Urban J, Van Camp J, Sterck F. 2018. Tree differences in primary and secondary growth drive convergent scaling in leaf area to sapwood area across Europe. New Phytol 218:1383–1392.

Pompa-García M, Camarero JJ, Colangelo M, González-Cásares M. 2021. Inter and intra-annual links between climate, tree growth and NDVI: improving the resolution of drought proxies in conifer forests. Int J Biometeorol 65:2111–2121. https://doi.org/10.1007/s00484-021-02170-5.

Ponocná T, Spyt B, Kaczka R, Büntgen U, Treml V. 2016. Growth trends and climate responses of Norway spruce along elevational gradients in East-Central Europe. Trees - Struct Funct 30:1633–1646.

R Core Team. 2019. R: A language and environment for statistical computing. R Foundation for Statistical Computing, Vienna, Austria. URL https://www.R-project.org/.

Rabbel I, Neuwirth B, Bogena H, Diekkrüger B. 2018. Exploring the growth response of Norway spruce (*P. abies*) along a small-scale gradient of soil water supply. Dendrochronologia 52:123–130. https://doi.org/10.1016/j.dendro.2018.10.007.

Riihimäki H, Heiskanen J, Luoto M. 2017. The effect of topography on arctic-alpine aboveground biomass and NDVI patterns. Int J Appl Earth Obs Geoinf 56:44–53. https://doi.org/10.1016/j.jag.2016.11.005.

Roy DP, Kovalskyy V, Zhang HK, Vermote EF, Yan L, Kumar SS, Egorov A. 2016. Characterization of Landsat-7 to Landsat-8 reflective wavelength and normalized difference vegetation index continuity. Remote Sens Environ 185:57–70.

Schroeder J, Körner M. 2018. Remote-sensing data are closely related to growth information in tree-ring index chronologies. TRACE—Tree Rings Archaeol Climatol Ecol Vol 7 Proc DENDROSYMPOSIUM 2008, April 27th–30th 2008. Zakopane, Poland 16:14–24.

Seftigen K, Frank DC, Björklund J, Babst F, Poulter B. 2018. The climatic drivers of normalized difference vegetation index and tree-ring-based estimates of forest productivity are spatially coherent but temporally decoupled in Northern Hemispheric forests. Glob Ecol Biogeogr 27:1352–1365.

Sevanto S, Dickman LT. 2015. Where does the carbon go?-Plant carbon allocation under climate change. Tree Physiol 35:581–584.

Shabanov NV, Huang D, Yang W, Tan B, Knyazikhin Y, Myneni RB, Ahl DE, Gower ST, Huete AR, Aragão LEOC, Shimabukuro YE. 2005. Analysis and optimization of the MODIS leaf area index algorithm retrievals over broadleaf forests. IEEE Trans Geosci Remote Sens 43:1855–1865.

Song C. 2012. Optical remote sensing of forest leaf area index and biomass. Prog Phys Geogr 37:98–113.

Spiecker H. 2000. Spruce monocultures in Central Europe – Problems and prospects (Issue 33). European Forest Institute.

Sprenger M, Stumpp C, Weiler M, Aeschbach W, Allen ST, Benettin P, Dubbert M, Hartmann A, Hrachowitz M, Kirchner JW, McDonnell JJ, Orlowski N, Penna D, Pfahl S, Rinderer M, Rodriguez N, Schmidt M, Werner C. 2019. The Demographics of Water: A Review of Water Ages in the Critical Zone. Rev Geophys 57:800–834.

Teets A, Moore DJP, Alexander MR, Blanken PD, Bohrer G, Burns SP, Carbone MS, Ducey MJ, Fraver S, Gough CM, Hollinger DY, Koch G, Kolb T, Munger JW, Novick KA, Ollinger SV, Ouimette AP, Pederson N, Ricciuto DM, Seyednasrollah B, Vogel CS, Richardson AD. 2022. Coupling of Tree Growth and Photosynthetic Carbon Uptake Across Six North American Forests. J Geophys Res Biogeosciences 127:1–20.

Thornthwaite CW. 1948. An Approach toward a Rational Classification of Climate. Geogr Rev 38:55.

Tumajer J, Scharnweber T, Smiljanic M, Wilmking M. 2022. Limitation by vapour pressure deficit shapes different intra-annual growth patterns of diffuse- and ring-porous temperate broadleaves. New Phytol 233:2429–2441.

Vicente-Serrano SM, Lasanta T, Romo A. 2004. Analysis of spatial and temporal evolution of vegetation cover in the Spanish central pyrenees: Role of human management. Environ Manage 34:802–818.

Vicente-Serrano SM, Beguería S, López-Moreno JI. 2010. A multiscalar drought index sensitive to global warming: The standardized precipitation evapotranspiration index. J Clim 23:1696–1718.

Vicente-Serrano SM, Gouveia C, Camarero JJ, Beguería S, Trigo R, López-Moreno JI, Azorín-Molina C, Pasho E, Lorenzo-Lacruz J, Revuelto J, Morán-Tejeda E, Sanchez-Lorenzo A. 2012. Response of vegetation to drought time-scales across global land biomes. Proc Natl Acad Sci U S A 110:52–57.

Vicente-Serrano SM, Camarero JJ, Olano JM, Martín-Hernández N, Peña-Gallardo M, Tomás-Burguera M, Gazol A, Azorin-Molina C, Bhuyan U, El Kenawy A. 2016. Diverse relationships between forest growth and the Normalized Difference Vegetation Index at a global scale. Remote Sens Environ 187:14–29. https://doi.org/10.1016/j.rse.2016.10.001.

Vicente-Serrano SM, Martín-Hernández N, Camarero JJ, Gazol A, Sánchez-Salguero R, Peña-Gallardo M, El Kenawy A, Domínguez-Castro F, Tomas-Burguera M, Gutiérrez E, de Luis M, Sangüesa-Barreda G, Novak K, Rozas V, Tíscar PA, Linares JC, del Castillo EM, Ribas M, García-González I, Silla F, Camisón A, Génova M, Olano JM, Longares LA, Hevia A, Diego Galván J. 2020. Linking tree-ring growth and satellite-derived gross primary growth in multiple forest biomes. Temporal-scale matters. Ecol Indic 108:105753. https://doi.org/10.1016/j.ecolind.2019.105753

Wang J, Rich PM, Price KP, Kettle WD. 2004. Relations between NDVI and tree productivity in the central Great Plains. Int J Remote Sens 25:3127–3138.

Wang Z, Lyu L, Liu W, Liang H, Huang J, Zhang Q Bin. 2021. Topographic patterns of forest decline as detected from tree rings and NDVI. Catena 198:105011. https://doi.org/10.1016/j.catena.2020.105011

Weigel R, Henry HAL, Beil I, Gebauer G, Jurasinski G, Klisz M, van der Maaten E, Muffler L, Kreyling J. 2021. Ecosystem Processes Show Uniform Sensitivity to Winter Soil Temperature Change Across a Gradient from Central to Cold Marginal Stands of a Major Temperate Forest Tree. Ecosystems 24:1545–1560. https://doi.org/10.1007/s10021-021-00600-4.

Wong CYS, Young DJN, Latimer AM, Buckley TN, Magney TS. 2021. Importance of the legacy effect for assessing spatiotemporal correspondence between interannual tree-ring width and remote sensing products in the Sierra Nevada. Remote Sens Environ 265:112635. https://doi.org/10.1016/j.rse.2021.112635

Wu X, Liu H, Li X, Ciais P, Babst F, Guo W, Zhang C, Magliulo V, Pavelka M, Liu S, Huang Y, Wang P, Shi C, Ma Y. 2017. Differentiating drought legacy effects on vegetation growth over the temperate Northern Hemisphere. Glob Chang Biol 24:504–516.

Xu P, Fang W, Zhou T, Zhao X, Luo H, Hendrey G, Yi C. 2019. Spatial upscaling of tree-ring-based forest response to drought with satellite data. Remote Sens 11:16–18.

Zang C, Biondi F. 2015. Treeclim: An R package for the numerical calibration of proxy-climate relationships. Ecography (cop) 38:431–436.

Zhan Z-Z, Liu H-B, Li H-M, Wu W, Zhong B. 2012. The Relationship between NDVI and Terrain Factors –A Case Study of Chongqing. Procedia Environ Sci 12:765–771. https://doi.org/10.1016/j.proenv.2012.01.347.

Zhang H, Wang K, Xu X, Song T, Xu Y, Zeng F. 2015. Biogeographical patterns of biomass allocation in leaves, stems, and roots in Chinas forests. Sci Rep 5:1–12.

Zhang T, Zhang R, Lu B, Mambetov BT, Kelgenbayev N, Dosmanbetov D, Maisupova B, Chen F, Yu S, Shang H, Huang L. 2018. *Picea schrenkiana* tree-ring chronologies development and vegetation index reconstruction for the Alatau Mountains, Central Asia. Geochronometria 45:107–118.

Zhu Z, Wang S, Woodcock CE. 2015. Improvement and expansion of the Fmask algorithm: Cloud, cloud shadow, and snow detection for Landsats 4–7, 8, and Sentinel 2 images. Remote Sens Environ 159:269–277. https://doi.org/10.1016/j.rse.2014.12.014.

Responses of stem growth and canopy greenness of temperate conifers to dry spells

Jiří Mašek [a*], Isabel Dorado-Liñán[b], Václav Treml [a]

[a] *Department of Physical Geography and Geoecology, Faculty of Science, Charles University, Albertov 6, 128 43 Prague, Czech Republic*

[b] *Dpto. de Sistemas y Recursos Naturales, Universidad Politécnica de Madrid, Madrid, Spain.*

[*] *Corresponding author: jiri.masek@natur.cuni.cz (Jiří Mašek)*

ORCID:

JM: 0000-0002-3494-9113

IDL: 0000-0002-8913-0420

VT: 0000-0002-3494-9113

Abstract

Dry spells strongly influence biomass production in forest ecosystems. Their effects may last several years following a drought event, prolonging growth reduction and therefore carbon sequestration. Yet, the understanding of the impact of dry spells on the vitality of trees' above-ground biomass components (e.g., stems and leaves) at a landscape level remains limited. We analyzed the responses of *Pinus sylvestris* and *Picea abies* to the four most severe drought years in topographically complex sites. To represent stem growth and canopy greenness, we used chronologies of tree rings and time series of the Normalized Difference Vegetation Index (NDVI). We analyzed the responses of tree rings and NDVI to dry spells using superposed epoch analysis and further explored this relationship using mixed-effect models. Our results show a stronger and more persistent response of radial growth to dry spells compared to canopy greenness but faster recovery of canopy greenness. Canopy greenness started to recover the year after the dry spell, whereas radial tree growth remained reduced for the two subsequent years and did not recover the pre-drought level until the fourth year after the event. Stem growth and canopy greenness were influenced by climatic conditions during and after drought events, while the effect of topography was irrelevant. The opposite responses of stem growth

and canopy greenness following drought events suggest a differential impact of droughts on trees´ sink and source compartments. These results underscore the crucial importance of understanding the complexities of tree growth as a major sink of atmospheric carbon.

Keywords: tree rings, NDVI, dry spells, biomass allocation, growth response, topography

Statements and Declaration

Competing Interests:

The author declares no conflict of interest.

Acknowledgment

We appreciate the permission and help of the administrators of the protected areas Kokořínsko hills and Šumava Mts. to carry out our research. We are grateful to the Charles University Grant Agency (GAUK 548120) for the financial support.

Funding

The study was funded by the Charles University Grant Agency (GAUK 548120) and the European Union program ERASMUS+ study visit in Madrid (3023230).

IDL acknowledges funding from Proyectos de Generación de Conocimiento, Ministerio de Ciencia e Innovación (#PID2021-128759OA-I00), and Fondos de Investigación Beatriz Galindo UPM-CAM (#M190020074A)

Credit authorship contribution statement

All authors contributed to the conceptualization and methodology of the paper. Sample collection, measurements, and analysis were performed by [Jiří Mašek]. The first draft of the manuscript was written by [Jiří Mašek] and all authors commented on and adjusted the following versions of the manuscript. All authors read and approved the final manuscript.

1. Introduction

An increasing number of extreme climatic events, mainly droughts and heat waves, significantly impact terrestrial ecosystems and their biomass production (Allen et al. 2010). Understanding trees' responses to single or compound dry spells is crucial for estimating terrestrial carbon sequestration and carbon pools (Bonan 2008, Kannenberg et al. 2020). Carbon sequestration into forest biomass remains one of the most uncertain aspects of climate change projections simulated by Earth System Models (Friend et al. 2019), partly due to the absence of the explicit representation of growth processes within the land surface component (Zuidema et al. 2018). While plant growth in global models is computed as the difference between photosynthesis and plant respiration, direct environmental constraints on stem growth may be stronger than those on photosynthesis (Dorado-Liñán et al. 2022, Fatichi et al. 2014). As a result, the above-ground tree biomass compartments might respond to drought differently in terms of the magnitude and duration of the response. Especially at a landscape scale, where also topography matters, the coherence in responses of stems and leaves to drought spells is poorly understood.

A significant proportion of carbon is stored in aboveground compartments of trees, including the stem (35–60 % of annually formed biomass) and leaves (7–16 %) (Bernoulli and Körner 1999, DeLucia et al. 2000). Annual increments of stem biomass can be represented by tree-ring widths (Babst et al. 2017, Girardin et al. 2016). The greenness of leaf biomass (amount and photosynthetic activity) can be represented by vegetation indices derived from remote sensing data, such as NDVI (Vicente-Serrano et al. 2020, Song 2012) which correlates with leaf area index (Eklundh et al. 2001) and photosynthetic activity (Zarco-Tejada et al. 2019). While time series of tree rings and NDVI tend to be correlated at large spatial scales (Babst et al. 2017, Vicente-Serrano et al. 2016), they differ in their climatic drivers (Seftigen et al. 2018) and may, therefore, exhibit different responses to extreme events such as dry spells (Wu et al. 2017).

The impacts of drought on tree growth are recorded not only in the year of the event (Dorado-Liñán et al. 2019, Gazol et al. 2018) but also in the following four years (legacy effects; Anderegg et al. 2015, Szejner et al. 2020). However, different tree compartments may respond differently to dry spells due to changes in biomass allocation (Zhang et al. 2015, Sevanto and Dickman 2015). The xylem, for example,

depletes reserves to recover from hydraulic damage, which can suppress stem growth for several years (Trugman et al. 2018, Wu et al. 2017). In contrast, carbon investment in leaves and root formation may remain relatively unchanged during and after drought (Anderegg et al. 2015). Furthermore, different temperature thresholds are required for photosynthesis (active above 0 °C) and wood formation (active above 4–5 °C) resulting in different seasonal windows of climate sensitivity for leaf and stem biomass within a year (Fatichi et al. 2014).

In addition to the variability of responses to dry spells among biomass compartments, there might be spatial variability in the impact of drought due to microclimatic conditions connected with topographic variability (Wong et al. 2021). The curvature of the terrain, slope inclination, and orientation can affect water retention and exposure to solar radiation which may modulate the response of trees to dry spells (Rabbel et al. 2018, Mašek et al. 2023). However, whether site topographic conditions can influence the responses of the main above-ground tree vegetative organs to dry spells at the landscape level remains unanswered.

The aim of this study is to compare the responses of wood biomass (represented by tree ring widths) and canopy greenness (represented by the NDVI) to dry spells while accounting for the effect of topographic variability. We selected 20 plots for each of the two main coniferous tree species in Central Europe: *Picea abies* and *Pinus sylvestris* in both mountain and lowland sites with complex topography. We hypothesize that (1) the response of tree ring widths and NDVI to dry spells will differ in terms of magnitude and duration and (2) the recovery of stem growth and canopy greenness will depend on the severity of the drought and the climatic conditions that follow, modulated by site topography.

2. Methods

2.1 Study sites and selected tree species

Coniferous forests in Central Europe primarily consist of *Picea abies* and *Pinus sylvestris* (PCAB and PISY, respectively) comprising approximately 60 % of total forest coverage (Spiecker 2000). PCAB is a semi-shade tolerant, shallow-rooted tree species that typically grows in mountainous areas, forming

dense closed canopies. On the other hand, PISY is a light-demanding deep-rooted species that occupies less productive sites such as sandstone and rocky slopes, where it grows in open canopies (Durrant et al. 2016).

We selected two study sites in the Czech Republic: Šumava Mts. and Kokořínsko hills which are dominated almost exclusively by PCAB and PISY, respectively (Fig. 1A). The Šumava Mts. is an old metamorphic mountain range with gentle slopes and an average elevation of 1000 m a. s. l. The Kokořínsko hills are a sandstone platform with an elevation of approximately 400 m a. s. l. divided by deep narrow valleys where the highest peaks are formed by volcanic intrusions (Fig. 1B). The Šumava Mts. site is classified as having a wet temperate climate, with annual precipitation totals of about 1040 mm and a mean annual temperature of 5 °C. Kokořínsko hills are located in a mild temperate climate, with annual total precipitation of about 650 mm and an average annual temperature of 8 °C (period 1985–2017, Fig. 1C). In both sites, soils are generally nutrient-poor podzols, leptosols, and cambisols (Ložek et al. 2005, Albrecht et al. 2003).

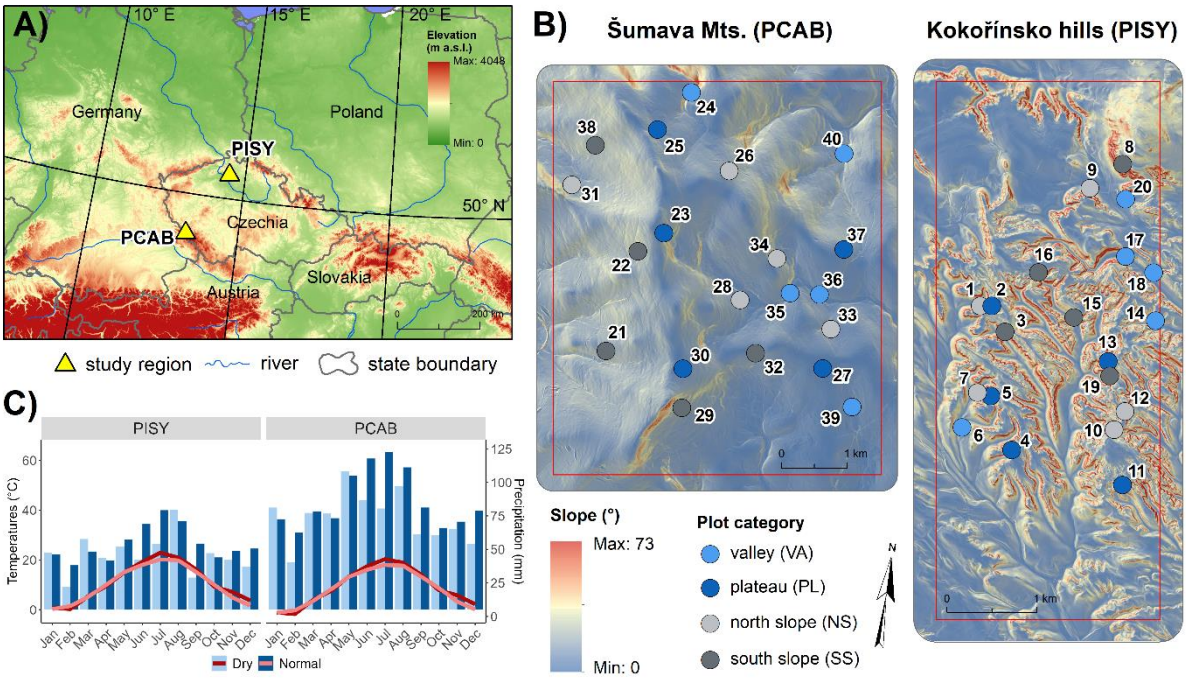

Figure 1: Location of two study sites dominated by Picea abies and Pinus sylvestris (PCAB and PISY respectively, panel A). Location and classification in plot categories, and plot numbers correspond to

those in Table S2 (panel B). Composite climate diagrams for the selected drought years: 1994, 2003, 2006, and 2015 with respect to average climate conditions (1985–2017) derived from ERA5 climatic reanalysis data (panel C).

2.2 Sample collection and processing

We collected samples from twenty plots across each sampling site, taking into account the topographic variability and associated plot characteristics such as sunlight exposure, runoff, and water retention. This involved selecting five plots for each of the following plot categories: south-facing slope (plots with high insolation), north-facing slope (plots with low insolation), plateau (plots with low water availability), and valley bottom (plots with higher water availability; Table S1, Fig. S1). Each plot was circular, with a radius of 16 m, which is approximately equivalent to the resolution of Landsat scenes (30 m per pixel). At each plot, we sampled at least 26 mature canopy-level trees without visible damage, using a Pressler's increment borer. Sampling was done in the years 2020–2021 and in total our dataset contains 1147 trees, 508 for PCAB and 639 for PISY (Table S2).

We used standard dendrochronological methods to process the tree cores (Stokes and Smiley 1998). Samples were scanned with a resolution of 1200 dpi and tree-ring widths were measured using WinDENDRO (Regent Instruments 2011). Cross-dating of the tree-ring series was done in PAST 4 (Knibbe 2004) by visual verification and statistical t-test. To focus on high-frequency variability, we detrended the individual series using a 30-year-long cubic smoothing spline with a 50 % frequency cut-off to remove low to medium-frequency trends including the age trend. Tree-ring indices (TRI) were calculated as ratios between observed and modelled growth (Cook and Peters 1981). We calculated plot TRI chronologies for both species by averaging plot tree-ring series using Tukey's biweight robust mean (R package dplR 1.7.2; Bunn 2008).

2.3 NDVI data

The time series of the NDVI were calculated using Landsat (high-quality T1_SR) scenes since it provides the longest available dataset of multispectral satellite images with high resolution (30 m per pixel). Each Landsat mission covers a different time window and uses a different sensor, TM (Thematic Mapper), ETM+ (Enhanced Thematic Mapper Plus), and OLI (Operational Land Imager) for Landsat 5, 7, and 8, respectively. Google Earth Engine (Gorelick et al. 2017) was used to recalculate datasets of Landsat 5 and 7 by regression to be comparable with Landsat 8 (Roy et al. 2016). Clouds and their shadows were erased from all images to avoid distortion of spectral data (Zhu et al. 2015).

Next, we subset all available images for the growing season period. The beginning of the growing season was defined as the first day when the mean temperature of the preceding five days exceeded 12 °C and 9 °C for PISY and PCAB plots, respectively. These temperatures are reported to trigger bud bursts for the species under study in similar elevations (Hájková et al. 2012). Although the increment of leaf biomass is usually completed in July (Kraus et al. 2016, Fajstavr et al. 2019) the end of the growing season was set to 30th September (DOY 274) when trees in lowlands and highlands of Central Europe usually stop cell division and the tree ring is complete (Etzold et al. 2021, Tumajer et al. 2022). This approach was selected from three variants of NDVI calculations with different seasonal windows because it captures both leaf and wood phenology. Moreover, the NDVI time series did not differ considerably between different variants of calculation (Fig. S2). NDVI was calculated as follows:

$$NDVI = \frac{NIR - Red}{NIR + Red}$$

where 'Red' stands for reflectance in the red spectrum and 'NIR' indicates the reflectance in the near-infrared spectrum (NASA 2022). The median of all scenes within individual years was computed and the time series of NDVI for our plots were extracted. The resulting values of the time series were calculated as the mean of pixels weighted by the proportion of the sampling plot area located inside a specific grid cell.

Time series of vegetation indices tend to be affected by numerous factors such as forest densification as trees are getting older and larger (Vicente-Serrano et al. 2004), and increasing tree and leaf size due to

CO_2 fertilization reflected also in a gradual increase in NDVI values (Donohue et al. 2013). To remove those long-term trends, we fitted a linear regression to individual NDVI series over time, and residuals from this trend line were used for calculating a mean NDVI series per plot.

NDVI tends to saturate during the growing season, particularly in evergreen conifer forests. However, in our case, the values of NDVI are slowly increasing each year and never reach full saturation (Fig. S3). We are aware, that although we tried to carefully select monospecific undisturbed plots, our NDVI data might be affected by distortion of spectral data due to admixed vegetation, and in the case of open PISY canopies, there might be also a signal of understory and soil. However, the adjacent pixels of Landsat scenes returned almost identical time series, so the signal of understory vegetation is probably of limited significance.

2.4 Climate data

We used ERA5 climatic reanalysis data (Hersbach et al. 2020, 2023) with a spatial resolution of 0.25° per pixel. Monthly data on temperature (T), precipitation (P), downward surface solar radiation (SR), and soil moisture in 10 cm (SM) were obtained from Climate Earth Explorer. Based on T and P we also calculated the Standardised Precipitation-Evapotranspiration Index (SPEI, Vicente-Serrano et al. 2010) using the Thornthwaite method (Thornthwaite 1948). We considered various durations of the preceding period spanning from 1 to 12 months for the calculation of SPEI (R package SPEI 1.7, Beguería and Vicente-Serrano 2017). Since there were negligible differences in correlations between TRI or NDVI with different SPEI versions, we selected SPEI with four preceding months. It represents a balance in terms of differences in rooting strategies and depth of water uptake. While deeply rooting species (PISY) can use water retained in the soil most of the year, shallow rooting species (PCAB) reach subsurface layers of soil with a fast turnover of infiltrating precipitation (Sprenger et al. 2019).

We computed the mean climatic series for summer (June, July, August; JJA) and the growing season (May through September; GS). Since the results for JJA and GS showed little differences, only JJA results are shown in the main body of the text.

2.5 Statistical analysis

We selected the time window of 1985–2017, which was covered by both TRI and NDVI time series as the common period for analyses. All analyses were performed using R software (R 4.2.0; R Core Team 2022).

To identify the main climatic drivers, we calculated Pearson's correlations between TRI, NDVI chronologies, and climatic variables in the current and previous year. Since SR and SM showed the highest correlations with TRI and NDVI, the most severe non-consecutive drought years were selected based on the lowest (SM) and the highest (SR) values. Three of the four resulting drought years overlapped for both SM and SR. For simplicity, we decided to use those derived from SR because they were identical for both tree species. Non-consecutive drought years were selected to avoid the potential cumulative effect of successive drought years on tree growth (Anderegg et al. 2020, Gessler et al. 2020).

To explore the response of stem (TRI) and canopy greenness (NDVI) to dry spells, we employed superposed epoch analysis (SEA; Chree 1913) which calculates the significance of the deviation from the mean of a given year and several lagged years. We used the 'sea' function in R package dplR (1.7.2; Bunn 2008) and considered a four-year lag before and after the dry spell (Anderegg et al. 2015, Wu et al. 2017).

Additionally, we developed linear mixed-effect models (R package lme4 1.1-30; Bates et al. 2015) with TRI and scaled NDVI in a given drought year and the four following years as the dependent variables. Explanatory variables were the severity of solar radiation in the drought year (anomaly from average SR; SEV0), the solar radiation severity in each of the four years following the dry spell (anomaly from average SR; SEV), while the plot category was treated as a random effect. For each variable in all models, we calculated the variance inflation factor (VIF; R package 'car'; 3.1-1; Fox and Weisberg 2019). We created three variants of models: a full model with all predictors and two models always with a single predictor omitted (successively: SEV0, SEV). We assessed the performance of each model using the Akaike information criterion (AIC), marginal and conditional R^2 (R package MuMIn 1.47.1; Barton 2022), pseudo-R^2, t values, and p-values of all predictors. The significance of the random effect

(plot category) was calculated by the function 'ranova' from R package lmerTest (3.1-3; Kuznetsova et al. 201,7). Finally, we checked the normal distribution of residuals using qqplots.

3. Results

3.1 Climatic signal

Both species and biomass compartments showed negative correlations with seasonal temperatures and surface solar radiation while precipitation, soil moisture, and SPEI had a positive influence on productivity (Fig S4). PCAB TRI primarily reflected the influence of the previous year's climate, whereas NDVI appeared to be minimally affected by climate. There was no difference between plot categories. PISY NDVI showed the strongest climate signal, displaying significant correlations with all climatic variables, especially with SM and SR, with no differences between plot categories. PISY TRI exhibited the most significant correlations in plots located on plateaus, whereas correlations in other plot categories were less or non-significant (Fig. S4).

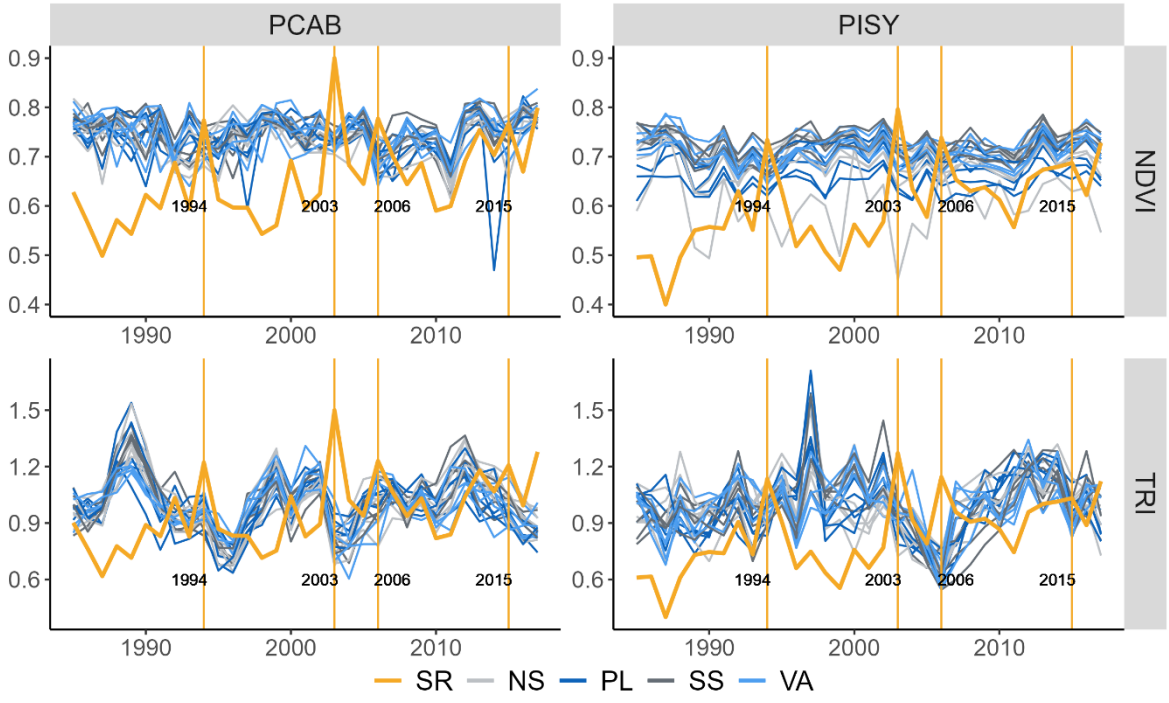

Figure 2: Time series of normalized difference vegetation index (NDVI; upper panel) and tree-ring indices (TRI; lower panel) for each plot and tree species: Picea abies (PCAB; left panel), and Pinus sylvestris (PISY; right panel). Colors indicate the plot categories (SS-South slops, NS-North slope, PL-Plateau, VA-Valley). The orange line corresponds to the surface solar radiation time series (SR) and vertical lines highlight the selected drought years.

3.2 Responses to dry spells

In both plots, the identified driest years were 1994, 2003, 2006, and 2015 (Fig. 2). The response of PCAB TRI to these dry spells exhibited large variability among individual plots (Fig. 3). However, a synchronized and significant decrease in tree growth lasting the following two years affected almost all plots irrespective of the plot category. The recovery of tree growth is visible from the third post-drought year onwards when trees reached pre-drought levels of growth (Fig. 3). PISY TRI significantly dropped in the year of the drought event at most of the plots. The growth reduction lasted for the next two years, but only significantly for the slope plots (i.e., north and south slope plots; Fig. 3). At some PISY plots, trees did not recover to the pre-drought radial growth level four years after the dry spell.

For both tree species, we observed a significant reduction in NDVI during drought events. In PCAB, this reduction was followed by a significant increase in NDVI two years after the dry spell, achieving even higher levels of greenness than before the drought event (Fig. 3). However, three years after the dry spell, the NDVI dropped, and this change was significant for most PCAB plots. Conversely, PISY did not recover pre-drought NDVI levels four years after the drought event. Overall, there were no differences in the response between plot categories, irrespective of species or TRI and NDVI.

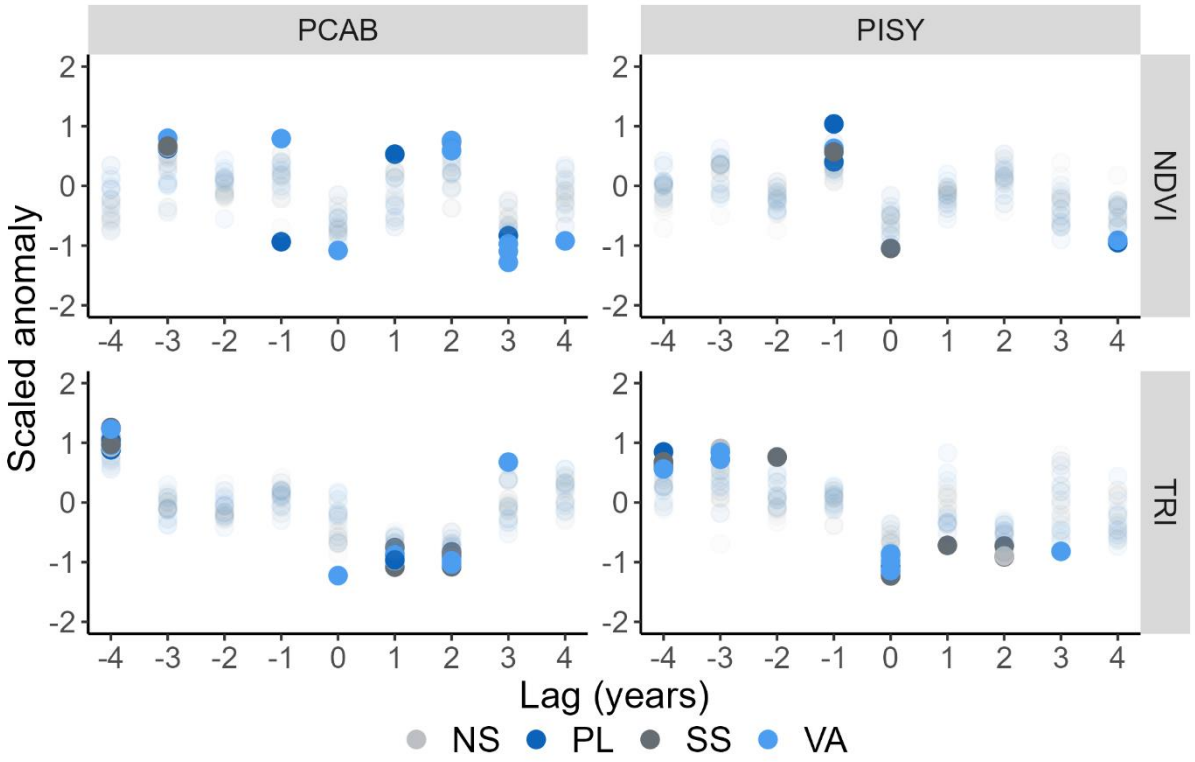

Figure 3: Responses of normalized difference vegetation index (NDVI; upper panel) and tree-ring indices (TRI; lower panel) to drought years for Picea abies (PCAB; left panel) and Pinus sylvestris (PISY; right panel) as indicated by superposed epoch analysis. Solid dots denote statistically significant change ($p<0.05$) and color indicates the plot category (SS-South slope, NS-North slope, PL-Plateau, VA-Valley).

3.3 Factors affecting the responses of TRI and NDVI

The models for PISY TRI explained approximately 24 % of the variability in the data, with the climate severity in the year of the event (Severity0) and the years following the drought event (Severity) emerging as significant predictors (Table 1). In turn, the models for PCAB TRI captured approximately 12 % of data variability with no significant influence of any predictor. Models for PISY NDVI accounted for 28 % of the variability with both climate severities (Severity0 and Severity) demonstrating significant effects. In the case of PCAB NDVI, approximately 21% of the variability was explained, with both climate severities being statistically significant. In all cases, the explained variability of the models decreased when Severity0 was omitted. Models without the Severity variable also exhibited

lower explained variance compared to full models (except the model for PCAB TRI) but the decrease was substantially smaller compared to models without Severity0 (Table 1). All predictors in all models had VIF below 2 and a distribution of residuals close to normal.

SPECIES	VAR	Model	AIC	R2 marginal	R2 conditional	pseudo R2	Severity0	Severity	Plot category
PISY	TRI	**Full model**	-251.647	0.289	0.311	0.315	**-7.253**	**-3.261**	0.998
		without SEV0	-215.165	0.111	0.114	0.115	NA	**-5.975**	0.993
		without SEV	-258.734	0.266	0.287	0.291	**-7.377**	NA	0.973
	NDVI	**Full model**	720.300	0.435	0.466	0.469	**-9.338**	**-10.365**	0.883
		without SEV0	841.901	0.142	0.142	0.143	NA	**-7.722**	1.000
		without SEV	827.109	0.218	0.241	0.243	**-9.313**	NA	0.936
PCAB	TRI	**Full model**	-469.296	0.159	0.207	0.209	1.535	-0.894	0.910
		without SEV0	-447.903	0.000	0.000	0.000	NA	-0.004	1.000
		without SEV	-487.156	0.157	0.199	0.201	1.505	NA	0.699
	NDVI	**Full model**	860.422	0.356	0.356	0.358	**-9.563**	**-8.411**	1.000
		without SEV0	959.970	0.054	0.054	0.054	NA	**-4.520**	1.000
		without SEV	908.825	0.229	0.229	0.230	**-9.232**	NA	1.000

Table 1: Results of linear mixed-effect models explaining normalized difference vegetation index (NDVI) and tree-ring indices (TRI) for Pinus sylvestris (PISY) and Picea abies (PCAB). The columns indicate the Akaike information criterion (AIC), R^2 marginal, R^2 conditional, pseudo-R^2, and t-values of predictors (Severity0 and Severity). Bold numbers indicate significant p values ($p<0.05$) of predictors and the random variable (plot category).

4. Discussion

We combined the analysis of TRI (a proxy for stem growth dynamics) and NDVI (a proxy for canopy greenness) for two conifer species (*Pinus sylvestris* and *Picea abies*) in Central Europe growing under different microenvironments to comprehensively characterize their response to drought. Our results suggest that following dry spells, conifers undergo a systematic shift in physiological activity between stem and leaf. The growth of trees during the drought year and the three following years is influenced by climatic conditions while the effect of topography is marginal.

4.1 Differential response of TRI and NDVI to dry spells

Our sampling sites are landscapes characterized by complex topography, associated with high spatial variability in solar radiation and water availability. The PISY site, located in Kokořínsko hills, experiences warm and dry conditions leading to pronounced drought effects on both stem growth and leaf greenness in trees. In contrast, the PCAB site in the Šumava Mountains encounters climate conditions that closely align with the PCAB climatic optimum, resulting in a weaker influence of climate on both analyzed proxies, TRI and NDVI, is relatively subdued.

Consistent with previous studies, the impact of a dry spell in both TRI and NDVI persisted for three years following the event in both tree species (Wu et al. 2017, Szejner et al. 2020, Janecka et al. 2022). The impact of the drought event on PISY TRI was more pronounced than on PCAB TRI, which can be explained by the higher moisture limitation of the PISY site compared to the PCAB site (Fig. S4). The response of PCAB TRI in the years after the dry spell was similar to that of PISY, though the reduction was more significant and persistent for most of the PCAB plots (Marchand et al. 2021, Zlobin 2022). This might be due to the different rooting strategies of both species (Durrant et al. 2016). Shallow-rooting species such as PCAB are assumed to be more sensitive to dry spells than deep-rooting PISY, which buffers against drought effects by accessing groundwater in deeper soil layers (Kannenberg et al. 2020, Mackay et al. 2019). Differences may also be related to the higher isohydricity of PISY compared to relatively more anisohydric PCAB (Marchand et al. 2021, Li et al. 2020). Furthermore, PCAB TRI growth is negatively influenced by the temperature of the preceding summer and positively impacted

during the winter (Fig. S4, Mašek et al. 2023). Winter conditions may interact with the preceding summer and late autumn weather, leading to the observed strong negative growth responses over two consecutive years (Harvey et al. 2020).

After dry spells, stem growth (i.e., TRI) was reduced and this reduction persisted for two years, whereas NDVI, which is a proxy integrating photosynthetic activity and leaf biomass, increased for both species during the same period (Fig. 3). This suggests a stem-leaf biomass trade-off. According to our results, trees changed their allocation strategy in the years following dry spells, probably in order to invest more carbon into the leaf biomass to enhance photosynthesis (replenish sugar pools) and therefore restore canopy damage (Kannenberg et al. 2019a, Anderegg et al. 2013). Such an NDVI enhancement was more significant for PCAB which might be connected to a stronger reduction of TRI observed for this species. Increases in forest ecosystems' NDVI in years following a dry spell were also observed and reported by other studies (Rita et al. 2019, Dong et al. 2022, Gazol et al. 2022), evidencing that responses of stem growth and leaf biomass greenness to dry spells are uncoupled (Gazol et al. 2020, Moreno-Fernández et al. 2022).

The larger reduction of stem growth compared to canopy greenness during drought events (Fig. S3) has been previously reported by other studies using canopy vigor proxies derived from remotely-sensed vegetation indices or eddy covariance data (Kannenberg et al. 2020, Moreno-Fernández et al. 2022, Kannenberg et al. 2019a). All these findings reveal that stem growth during a dry spell is more limited by climate conditions than canopy greenness (Cabon et al. 2022, Dow et al. 2022). Wood formation stops at higher plant water potential than photosynthesis (vegetation greenness) since radial tree growth is limited by a low turgor in cambial cells (Cabon et al. 2020). Low water potential also reduces the ability to transport assimilated carbon (Fatichi et al. 2014), leading to the accumulation of non-structural carbohydrates in trees that might be invested in other tree organs than stems such as roots (Teets et al. 2022, Lapenis et al. 2013), respired or stored in carbon pools. In the end, all these factors might contribute to an overall more pronounced response of stem compared to canopy greenness in the drought year.

In the two years following the dry spell, the canopy greenness is restored probably at the expense of stem growth (Anderegg et al. 2013). Only in the third year after the dry spell, does the stem growth return to a normal level (Martínez-Sancho et al. 2022, Anderson-Teixeira and Kannenberg 2022) assuring sufficient conductive capacity for leaves (Kröber et al. 2014), with some indications that this is accompanied by a simultaneous decrease of NDVI values. We can speculate that stem growth is enhanced at the expense of leaf biomass in the third year after a dry spell, however, our data doesn't provide direct evidence. In the fourth year, both biomass compartments recovered back to the pre-drought values of TRI and NDVI (Klesse et al. 2022, Szejner et al. 2020, Leifsson et al. 2023). Detected differences between tree rings and NDVI in this study imply partial decoupling of stem and leaf biomass responses and probably also varying carbon allocation strategies after dry spells.

All selected dry spells (1994, 2003, 2006, 2015) are well-known to have affected plant growth in Central Europe (Spinoi et al. 2015, Moravec et al. 2021), but they differ in their meteorological characteristics. The variability in drought severity, duration, and timing leads to significant differences in the response of both stem growth and canopy greenness to individual dry years (Gao et al. 2018, Huang et al. 2018, Kannenberg et al. 2019b, Wu et al. 2022) and hence, in trees' resilience, resistance and recovery (Text S1, Table S3, Fig. S5).

4.2 Factors shaping the responses to drought

We hypothesized that drought severity and topography modulate the response of trees to dry spells. Our results suggest that drought severity is a very important factor, while the topography has a limited effect in our dataset.

The severity of the dry spell and the climatic severity during the following years were highly significant predictors of stem growth and canopy greenness for both studied species, corroborating the results of other studies for conifers and broadleaf species from the temperate biome (Brun et al. 2020, Song et al. 2022, Castellaneta et al. 2022, Meng et al. 2015). Differences in the response to dry spells might be partly caused by different rooting strategies of species under study, since root properties such as root length, fine root diameter, and root density may significantly influence drought tolerance (Chen et al.

2022). Deep-rooting has been observed as a mitigation strategy in response to drought (Mohammadi Alagoz et al. 2022, Chitra-Tarak et al. 2021).

Overall the influence of topography was rather marginal (Schmied et al. 2023, Table 1). Likely, drought severity outperforms the potential effect of topography. Alternatively, the impact of dry spells was so severe that even the conditions in valleys (water accumulation) were not favorable enough to provide a sufficient amount of soil moisture. This means that during mild droughts, the topography may play a role as demonstrated by trees growing in topographically distinct conditions (Strum et al. 2022, Rabbel et al. 2018). The highly variable response of PISY TRI in SEA (Fig. 3) might be a result of complex topographic conditions in Kokořínsko hills (Fig. 1). However, considering resilience metrics, there was no difference between the plot categories for any species or biomass compartment (Fig. S5).

5. Conclusions

Forest responses to drought are complex with potential differences among tree species and tree biomass compartments, and across topographically complex landscapes. We focused on the responses of stem growth (represented by tree-ring widths) and canopy greenness (represented by NDVI) to a drought of two important coniferous tree species (*Pinus sylvestris* and *Picea abies*) in Central Europe. Our findings reveal a decoupled response of stem growth and canopy greenness in the period following dry spells. During the drought year, both TRI and NDVI experienced significant declines. In the two following years, canopy greenness rebounded, whereas stem growth remained suppressed. The magnitude of the response to drought spells was also species-specific: stem growth reduction and NDVI increase of deep-rooting *Pinus sylvestris* were not as conspicuous as those of the shallow-rooting *Picea abies*. Furthermore, drought severity appears to outweigh any potential variations in response linked to topography, as the influence of landscape features was marginal. We demonstrated the decisive role of drought severity in the response of above-ground tree compartments, which, in turn, exhibit systematic differences in the recovery period. Understanding the carbon allocation strategies triggered by dry spells is crucial for forecasting changes in ecosystems and improving our knowledge of forest responses to extreme droughts.

Data availability

Tree-ring width data have been uploaded to the International Tree-Ring Data Bank (ITRDB). Codes for NDVI time-series calculation in Google Earth Engine are provided here:

PCAB: https://code.earthengine.google.com/ddb1fc420d3be0f01719effb1facfa2b

PISY: https://code.earthengine.google.com/8a54269c4279d7795aeec9cc5873d109

All used data (climate, ring width, and NDVI) are available for download on GitHub (https://github.com/JirkaSkaut/Responses-to-dry-spells) including the R script for all calculations and figures.

References

Albrecht J. (ed) (2003) Českobudějovicko, Šumava. In: Chráněná území ČR. p 624

Allen CD, Macalady AK, Chenchouni H, et al (2010) A global overview of drought and heat-induced tree mortality reveals emerging climate change risks for forests To cite this version: A global overview of drought and heat-induced tree mortality reveals emerging climate change risks for forests. https://doi.org/10.1016/j.foreco.2009.09.001ï

Anderegg WRL, Plavcová L, Anderegg LDL, et al (2013) Drought's legacy: Multiyear hydraulic deterioration underlies widespread aspen forest die-off and portends increased future risk. Glob Chang Biol 19:1188–1196. https://doi.org/10.1111/gcb.12100

Anderegg WRL, Schwalm C, Biondi F, et al (2015) Pervasive drought legacies in forest ecosystems and their implications for carbon cycle models. Science (80-) 349:528–528. https://doi.org/10.1126/science.aab4097

Anderegg WRL, Trugman AT, Badgley G, et al (2020) Divergent forest sensitivity to repeated extreme droughts. Nat Clim Chang 10:1091–1095. https://doi.org/10.1038/s41558-020-00919-1

427 Anderson-Teixeira, Kristina J, Kannenberg SA (2022) What drives forest carbon storage? The
428 ramifications of source–sink decoupling. New Phytol 236:5–8

429 Babst F, Poulter B, Bodesheim P, et al (2017) Improved tree-ring archives will support earth-system
430 science. Nat Ecol Evol 1:1–2. https://doi.org/10.1038/s41559-016-0008

431 Babst F, Bodesheim P, Charney N, et al (2018) When tree rings go global: Challenges and
432 opportunities for retro- and prospective insight. Quat. Sci. Rev. 197:1–20

433 Bartoń K (2022) _MuMIn: Multi-Model Inference_. R package version 1.47.1, <https://CRAN.R-
434 project.org/package=MuMIn>

435 Bates D, Mächler M, Bolker BM, Walker SC (2015) Fitting linear mixed-effects models using lme4. J
436 Stat Softw 67:. https://doi.org/10.18637/jss.v067.i01

437 Beguería S, Vicente-Serrano SM (2017) SPEI: Calculation of the Standardised Precipitation-
438 Evapotranspiration Index. R package version 1.7. https://CRAN.R-project.org/package=SPEI

439 Bennett AC, Mcdowell NG, Allen CD, Anderson-Teixeira KJ (2015) Larger trees suffer most during
440 drought in forests worldwide. Nat Plants 1:. https://doi.org/10.1038/nplants.2015.139

441 Bernoulli M, Körner C (1999) Dry Matter Allocation in Treeline Trees. Ann Rei Bot 39:7–12

442 Bonan, B G (2008) Forests and Climate Change: Forcings, Feedbacks, and the Climate Benefits of
443 Forests. Science (80-) 320:1444–1449. https://doi.org/10.1126/science.1155121

444 Brun P, Psomas A, Ginzler C, et al (2020) Large-scale early-wilting response of Central European
445 forests to the 2018 extreme drought. Glob Chang Biol 26:7021–7035.
446 https://doi.org/10.1111/gcb.15360

447 Bunn AG (2008) A dendrochronology program library in R (dplR). Dendrochronologia 26:115–124.
448 https://doi.org/10.1016/j.dendro.2008.01.002

449 Cabon A, Peters RL, Fonti P, et al (2020) Temperature and water potential co-limit stem cambial
450 activity along a steep elevational gradient. New Phytol 226:1325–1340.
451 https://doi.org/10.1111/nph.16456

Cabon A, Kannenberg SA, Arain A, et al (2022) Cross-biome synthesis of source versus sink limits to tree growth. Science (80-) 758–761

Carrer M, Urbinati C (2004) Age-Dependent Tree-Ring Growth Responses to Climate in Larix decidua and Pinus cembra Author (s): Marco Carrer and Carlo Urbinati Published by : Wiley Stable URL : http://www.jstor.org/stable/3450399 REFERENCES Linked references are available on JSTOR f. Ecology 85:730–740

Castellaneta M, Rita A, Camarero JJ, et al (2022) Declines in canopy greenness and tree growth are caused by combined climate extremes during drought-induced dieback. Sci Total Environ 813:. https://doi.org/10.1016/j.scitotenv.2021.152666

Cook ER, Peters K (1981) The Smoothing Spline: A New Approach to Standardizing Forest Interior Tree-Ring Width Series for Dendroclimatic Studies Item type Article

DeLucia EH, Maherali H, Carey E V. (2000) Climate-driven changes in biomass allocation in pines. Glob Chang Biol 6:587–593. https://doi.org/10.1046/j.1365-2486.2000.00338.x

Dong B, Yu Y, Pereira P (2022) Non-growing season drought legacy effects on vegetation growth in southwestern China. Sci Total Environ 846:. https://doi.org/10.1016/j.scitotenv.2022.157334

Donohue RJ, Roderick ML, McVicar TR, Farquhar GD (2013) Impact of CO2 fertilization on maximum foliage cover across the globe's warm, arid environments. Geophys Res Lett 40:3031–3035. https://doi.org/10.1002/grl.50563

Dorado-Liñán I, Piovesan G, Martínez-Sancho E, et al (2019) Geographical adaptation prevails over species-specific determinism in trees' vulnerability to climate change at Mediterranean rear-edge forests. Glob Chang Biol 25:1296–1314. https://doi.org/10.1111/gcb.14544

Dorado-Liñán I, Ayarzagüena B, Babst F, et al (2022) Jet stream position explains regional anomalies in European beech forest productivity and tree growth. Nat Commun 13:. https://doi.org/10.1038/s41467-022-29615-8

476 Dow C, Kim AY, D'Orangeville L, et al (2022) Warm springs alter timing but not total growth of
477 temperate deciduous trees. Nature 608:552–557. https://doi.org/10.1038/s41586-022-05092-3

478 Durrant T (2016) Pinus sylvestris in Europe: distribution, habitat, usage and threats. In: San-Miguel-
479 Ayanz J, de Rigo D, Caudullo G, et al. (eds) European Atlas of Forest Tree Species. p 202

480 Eklundh L, Harrie L, Kuusk A (2001) Investigating relationships between landsat ETM+ sensor data
481 and leaf area index in a boreal conifer forest. Remote Sens Environ 78:239–251.
482 https://doi.org/10.1016/S0034-4257(01)00222-X

483 Etzold S, Sterck F, Bose AK, et al (2022) Number of growth days and not length of the growth period
484 determines radial stem growth of temperate trees. Ecol Lett 25:427–439.
485 https://doi.org/10.1111/ele.13933

486 Fajstavr M, Bednářová E, Nezval O, et al (2019) How needle phenology indicates the changes of
487 xylem cell formation during drought stress in Pinus sylvestris L. Dendrochronologia 56:.
488 https://doi.org/10.1016/j.dendro.2019.05.004

489 Fatichi S, Leuzinger S, Körner C (2014) Moving beyond photosynthesis: from carbon source to sink-
490 driven vegetation modeling. New Phytol 201:1086–1095

491 Fox J, Weisberg S (2019) An {R} Companion to Applied Regression, Third Edition. Thousand Oaks
492 CA: Sage. URL: https://socialsciences.mcmaster.ca/jfox/Books/Companion/

493 Friend AD, Eckes-Shephard AH, Fonti P, et al (2019) On the need to consider wood formation
494 processes in global vegetation models and a suggested approach. Ann For Sci 76:.
495 https://doi.org/10.1007/s13595-019-0819-x

496 Gao S, Liu R, Zhou T, et al (2018) Dynamic responses of tree-ring growth to multiple dimensions of
497 drought. Glob Chang Biol 24:5380–5390. https://doi.org/10.1111/gcb.14367

498 Gazol A, Camarero JJ, Sangüesa-Barreda G, Vicente-Serrano SM (2018) Post-drought resilience after
499 forest die-off: Shifts in regeneration, composition, growth and productivity. Front Plant Sci 871:.
500 https://doi.org/10.3389/fpls.2018.01546

Gazol A, Camarero JJ, Sánchez-Salguero R, et al (2020) Drought legacies are short, prevail in dry conifer forests and depend on growth variability. J Ecol 108:2473–2484. https://doi.org/10.1111/1365-2745.13435

Gazol A, Rozas V, Cuende Arribas S, et al (2022) Stand characteristics modulate secondary growth responses to drought and gross primary production in Pinus halepensis afforestation. Eur J For Res. https://doi.org/10.1007/s10342-022-01526-9

Gessler A, Bottero A, Marshall J, Arend M (2020) The way back: recovery of trees from drought and its implication for acclimation. New Phytol. 228:1704–1709

Girardin MP, Bouriaud O, Hogg EH, et al (2016) No growth stimulation of Canada's boreal forest under half-century of combined warming and CO2 fertilization. Proc Natl Acad Sci U S A 113:E8406–E8414. https://doi.org/10.1073/pnas.1610156113

Gorelick N, Hancher M, Dixon M, et al (2017) Google Earth Engine: Planetary-scale geospatial analysis for everyone. Remote Sens Environ 202:18–27. https://doi.org/10.1016/j.rse.2017.06.031

Hájková L (ed) (2012) Atlas fenologických poměrů Česka. Praha: Český hydrometeorologický ústav; Olomouc, 2012. ISBN 978– 80–86690–98–8.

Harvey JE, Smiljanić M, Scharnweber T, et al (2020) Tree growth influenced by warming winter climate and summer moisture availability in northern temperate forests. Glob Chang Biol 26:2505–2518. https://doi.org/10.1111/gcb.14966

Hersbach H, Bell B, Berrisford P, et al (2020) The ERA5 global reanalysis. Q J R Meteorol Soc 146:1999–2049. https://doi.org/10.1002/qj.3803

Huang M, Wang X, Keenan TF, Piao S (2018) Drought timing influences the legacy of tree growth recovery. Glob Chang Biol 24:3546–3559. https://doi.org/10.1111/gcb.14294

Chen Z, Li S, Wan X, Liu S (2022) Strategies of tree species to adapt to drought from leaf stomatal regulation and stem embolism resistance to root properties. Front Plant Sci 13:1–18. https://doi.org/10.3389/fpls.2022.926535

526 Chitra-Tarak R, Xu C, Aguilar S, et al (2021) Hydraulically-vulnerable trees survive on deep-water
527 access during droughts in a tropical forest. New Phytol 231:1798–1813.
528 https://doi.org/10.1111/nph.17464

529 Chree C (1913) Some Phenomena of Sunspots and of Terrestrial Magnetism at Kew Observatory

530 Janecka K, Metslaid S, Metslaid M, et al (2022) Short-Term Effects of Droughts and Cold Winters on
531 the Growth of Scots Pine at Coastal Sand Dunes around the South Baltic Sea. Forests 13:.
532 https://doi.org/10.3390/f13030477

533 Kannenberg SA, Novick KA, Alexander MR, et al (2019a) Linking drought legacy effects across
534 scales: From leaves to tree rings to ecosystems. Glob Chang Biol 25:2978–2992.
535 https://doi.org/10.1111/gcb.14710

536 Kannenberg SA, Maxwell JT, Pederson N, et al (2019b) Drought legacies are dependent on water
537 table depth, wood anatomy and drought timing across the eastern US. Ecol. Lett. 22:119–127

538 Kannenberg SA, Schwalm CR, Anderegg WRL (2020) Ghosts of the past: how drought legacy effects
539 shape forest functioning and carbon cycling. Ecol. Lett. 23:891–901

540 Klesse S, Babst F, Evans MEK, et al (2022) Legacy effects in radial tree growth are rarely significant
541 after accounting for biological memory. J Ecol. https://doi.org/10.1111/1365-2745.14045

542 Knibbe B (2004) Personal Analysis System for Tree-ring Research 4 - Instruction Manual. Vienna:
543 SCIEM

544 Kraus C, Zang C, Menzel A (2016) Elevational response in leaf and xylem phenology reveals different
545 prolongation of growing period of common beech and Norway spruce under warming conditions in
546 the Bavarian Alps. Eur J For Res 135:1011–1023. https://doi.org/10.1007/s10342-016-0990-7

547 Kröber W, Zhang S, Ehmig M, Bruelheide H (2014) Linking xylem hydraulic conductivity and
548 vulnerability to the leaf economics spectrum - A cross-species study of 39 evergreen and deciduous
549 broadleaved subtropical tree species. PLoS One 9:1–24.
550 https://doi.org/10.1371/journal.pone.0109211

Kuznetsova A, Brockhoff PB, Christensen RHB (2017) lmerTest Package: Tests in Linear Mixed Effects Models. J Stat Softw 82:1–26. https://doi.org/10.18637/JSS.V082.I13

Lapenis AG, Lawrence GB, Heim A, et al (2013) Climate warming shifts carbon allocation from stemwood to roots in calcium-depleted spruce forests. Global Biogeochem Cycles 27:101–107. https://doi.org/10.1029/2011GB004268

Ložek V (ed) (2005) Střední Čechy, Kokořínsko. In: Chráněná území ČR. AO, p 699

Mackay DS, Savoy PR, Grossiord C, et al (2020) Conifers depend on established roots during drought: results from a coupled model of carbon allocation and hydraulics. New Phytol 225:679–692. https://doi.org/10.1111/nph.16043

Marchand W, Girardin MP, Hartmann H, et al (2021) Contrasting life-history traits of black spruce and jack pine influence their physiological response to drought and growth recovery in northeastern boreal Canada. Sci Total Environ 794:. https://doi.org/10.1016/j.scitotenv.2021.148514

Martínez-Sancho E, Treydte K, Lehmann MM, et al (2022) Drought impacts on tree carbon sequestration and water use – evidence from intra-annual tree-ring characteristics. New Phytol 236:58–70. https://doi.org/10.1111/nph.18224

Martínez-Vilalta J, Poyatos R, Aguadé D, et al (2014) A new look at water transport regulation in plants. New Phytol 204:105–115. https://doi.org/10.1111/nph.12912

Mašek J, Tumajer J, Lange J, et al (2023) Variability in Tree-ring Width and NDVI Responses to Climate at a Landscape Level. Ecosystems. https://doi.org/10.1007/s10021-023-00822-8

Meng R, Dennison PE, Huang C, et al (2015) Effects of fire severity and post-fire climate on short-term vegetation recovery of mixed-conifer and red fir forests in the Sierra Nevada Mountains of California. Remote Sens Environ 171:311–325. https://doi.org/10.1016/j.rse.2015.10.024

Mérian P, Lebourgeois F (2011) Size-mediated climate-growth relationships in temperate forests: A multi-species analysis. For Ecol Manage 261:1382–1391. https://doi.org/10.1016/j.foreco.2011.01.019

Mohammadi Alagoz S, Zahra N, Hajiaghaei Kamrani M, et al (2022) Role of Root Hydraulics in Plant Drought Tolerance. J Plant Growth Regul. https://doi.org/10.1007/s00344-022-10807-x

Moravec V, Markonis Y, Rakovec O, et al (2021) Europe under multi-year droughts: How severe was the 2014–2018 drought period? Environ Res Lett 16:. https://doi.org/10.1088/1748-9326/abe828

Moreno-Fernández D, Julio Camarero J, García M, et al (2022) The Interplay of the Tree and Stand-Level Processes Mediate Drought-Induced Forest Dieback: Evidence from Complementary Remote Sensing and Tree-Ring Approaches. Ecosystems 25:1738–1753. https://doi.org/10.1007/s10021-022-0079

NASA (National Aeronautics and Space Administration) (2022) Measuring vegetation NDVI and EVI. Normalized Difference Vegetation Index (NDVI) https://earthobservatory.nasa.gov/features/MeasuringVegetation/measuring_vegetation_2.php [27.6.2023]

R Core Team (2022) R: A language and environment for statistical computing. R Foundation for Statistical Computing, Vienna, Austria. URL https://www.R-project.org/

Rabbel I, Neuwirth B, Bogena H, Diekkrüger B (2018) Exploring the growth response of Norway spruce (Picea abies) along a small-scale gradient of soil water supply. Dendrochronologia 52:123–130. https://doi.org/10.1016/j.dendro.2018.10.007

Regent Instruments (2011) WinDendro Image Analysis System. Regent Instruments Inc., Quebec

Riihimäki H, Heiskanen J, Luoto M (2017) The effect of topography on arctic-alpine aboveground biomass and NDVI patterns. Int J Appl Earth Obs Geoinf 56:44–53. https://doi.org/10.1016/j.jag.2016.11.005

Rita A, Camarero JJ, Nolè A, et al (2020) The impact of drought spells on forests depends on site conditions: The case of 2017 summer heat wave in southern Europe. Glob Chang Biol 26:851–863. https://doi.org/10.1111/gcb.14825

Roy DP, Kovalskyy V, Zhang HK, et al (2016) Characterization of Landsat-7 to Landsat-8 reflective wavelength and normalized difference vegetation index continuity. Remote Sens Environ 185:57–70. https://doi.org/10.1016/j.rse.2015.12.024

Seftigen K, Frank DC, Björklund J, et al (2018) The climatic drivers of normalized difference vegetation index and tree-ring-based estimates of forest productivity are spatially coherent but temporally decoupled in Northern Hemispheric forests. Glob Ecol Biogeogr 27:1352–1365. https://doi.org/10.1111/geb.12802

Sevanto S, Dickman LT (2015) Where does the carbon go?-Plant carbon allocation under climate change. Tree Physiol. 35:581–584

Schlerf M, Verhoef W, Buddenbaum H, et al (2007) Comparing three canopy reflectance models with hyperspectral multi-angular satellite data. In: Schaepman M, Liang S, Groot N, Kneubühler M (eds) 10th ISPMSRS. Davos, Switzerland: Intl. Archives of the Photogrammetry, Remote Sensing and Spatial Information Science. pp 404–407

Song C (2012) Optical remote sensing of forest leaf area index and biomass. Prog Phys Geogr 37:98–113. https://doi.org/10.1177/0309133312471367

Song Y, Sterck F, Sass-Klaassen U, et al (2022) Growth resilience of conifer species decreases with early, long-lasting and intense droughts but cannot be explained by hydraulic traits. J Ecol 110:2088–2104. https://doi.org/10.1111/1365-2745.13931

Spiecker H (2000) Spruce Monocultures in Central Europe – Problems and Prospects. European Forest Institute

Spinoni J, Naumann G, Vogt J V., Barbosa P (2015) The biggest drought events in Europe from 1950 to 2012. J Hydrol Reg Stud 3:509–524. https://doi.org/10.1016/j.ejrh.2015.01.001

Sprenger M, Stumpp C, Weiler M, et al (2019) The Demographics of Water: A Review of Water Ages in the Critical Zone. Rev Geophys 57:800–834. https://doi.org/10.1029/2018RG000633

Stokes MA, Smiley LT (1981) An introduction to tree-ring dating. The University of Chicago Press

Sturm J, Santos MJ, Schmid B, Damm A (2022) Satellite data reveal differential responses of Swiss forests to unprecedented 2018 drought. Glob Chang Biol 28:2956–2978. https://doi.org/10.1111/gcb.16136

Szejner P, Belmecheri S, Ehleringer JR, Monson RK (2020) Recent increases in drought frequency cause observed multi-year drought legacies in the tree rings of semi-arid forests. Oecologia 192:241–259. https://doi.org/10.1007/s00442-019-04550-6

Teets A, Moore DJP, Alexander MR, et al (2022) Coupling of Tree Growth and Photosynthetic Carbon Uptake Across Six North American Forests. J Geophys Res Biogeosciences 127:. https://doi.org/10.1029/2021JG006690

Thornthwaite CW (1948) An Approach toward a Rational Classification of Climate. Geogr Rev 38:55. https://doi.org/10.2307/210739

Trouillier M, van der Maaten-Theunissen M, Scharnweber T, et al (2019) Size matters—a comparison of three methods to assess age- and size-dependent climate sensitivity of trees. Trees - Struct Funct 33:183–192. https://doi.org/10.1007/s00468-018-1767-z

Trugman AT, Detto M, Bartlett MK, et al (2018) Tree carbon allocation explains forest drought-kill and recovery patterns. Ecol. Lett. 21:1552–1560

Tumajer J, Scharnweber T, Smiljanic M, Wilmking M (2022) Limitation by vapour pressure deficit shapes different intra-annual growth patterns of diffuse- and ring-porous temperate broadleaves. New Phytol 233:2429–2441. https://doi.org/10.1111/nph.17952

Vicente-Serrano SM, Lasanta T, Romo A (2004) Analysis of spatial and temporal evolution of vegetation cover in the Spanish central pyrenees: Role of human management. Environ Manage 34:802–818. https://doi.org/10.1007/s00267-003-0022-5

Vicente-Serrano SM, Beguería S, López-Moreno JI (2010) A multiscalar drought index sensitive to global warming: The standardized precipitation evapotranspiration index. J Clim 23:1696–1718. https://doi.org/10.1175/2009JCLI2909.1

650 Vicente-Serrano SM, Gouveia C, Camarero JJ, et al (2012) Response of vegetation to drought time-
651 scales across global land biomes. Proc Natl Acad Sci U S A 110:52–57.
652 https://doi.org/10.1073/pnas.1207068110

653 Vicente-Serrano SM, Camarero JJ, Olano JM, et al (2016) Diverse relationships between forest growth
654 and the Normalized Difference Vegetation Index at a global scale. Remote Sens Environ 187:14–
655 29. https://doi.org/10.1016/j.rse.2016.10.001

656 Vicente-Serrano SM, Martín-Hernández N, Camarero JJ, et al (2020) Linking tree-ring growth and
657 satellite-derived gross primary growth in multiple forest biomes. Temporal-scale matters. Ecol
658 Indic 108:. https://doi.org/10.1016/j.ecolind.2019.105753

659 Wong CYS, Young DJN, Latimer AM, et al (2021) Importance of the legacy effect for assessing
660 spatiotemporal correspondence between interannual tree-ring width and remote sensing products in
661 the Sierra Nevada. Remote Sens Environ 265:. https://doi.org/10.1016/j.rse.2021.112635

662 Wu X, Liu H, Li X, et al (2017) Differentiating drought legacy effects on vegetation growth over the
663 temperate Northern Hemisphere. Glob Chang Biol 24:504–516. https://doi.org/10.1111/gcb.13920

664 Wu X, Liu H, Hartmann H, et al (2022) Timing and Order of Extreme Drought and Wetness
665 Determine Bioclimatic Sensitivity of Tree Growth. Earth's Futur 10:.
666 https://doi.org/10.1029/2021EF002530

667 Zarco-Tejada PJ, Hornero A, Beck PSA, et al (2019) Chlorophyll content estimation in an open-
668 canopy conifer forest with Sentinel-2A and hyperspectral imagery in the context of forest decline.
669 Remote Sens Environ 223:320–335. https://doi.org/10.1016/j.rse.2019.01.031

670 Zhang H, Wang K, Xu X, et al (2015) Biogeographical patterns of biomass allocation in leaves, stems,
671 and roots in Chinas forests. Sci Rep 5:. https://doi.org/10.1038/srep15997

672 Zhu Z, Wang S, Woodcock CE (2015) Improvement and expansion of the Fmask algorithm: Cloud,
673 cloud shadow, and snow detection for Landsats 4-7, 8, and Sentinel 2 images. Remote Sens
674 Environ 159:269–277. https://doi.org/10.1016/j.rse.2014.12.014

675 Zlobin IE (2022) Linking the growth patterns of coniferous species with their performance under
676 climate aridization. Sci. Total Environ. 831

677 Zuidema PA, Poulter B, Frank DC (2018) A Wood Biology Agenda to Support Global Vegetation
678 Modelling. Trends Plant Sci. 23:1006–1015

Responses of stem growth and canopy greenness of temperate conifers to dry spells

Jiří Mašek[a*], Isabel Dorado-Liñán[b], Václav Treml[a]

[a] Department of Physical Geography and Geoecology, Faculty of Science, Charles University, Albertov 6, 128 43 Prague, Czech Republic

[b] Dpto. de Sistemas y Recursos Naturales, Universidad Politécnica de Madrid, Madrid, Spain.

[*] Corresponding author: jiri.masek@natur.cuni.cz (Jiří Mašek)

Supplementary material

Fig S1: Topographic characteristics (ALT-Altitude, HLI-Heath load index, NOR_DEV-Deviation from north, SLOPE-Slope, TWI-Topographic wetness index) of plot categories (SS-South slope, NS-North slope, PL-Plateau, VA-Valley) for *Pinus sylvestris* (PISY) and *Picea abies* (PCAB). For specifications of HLI, NOR_DEV, and TWI please see Table S1.

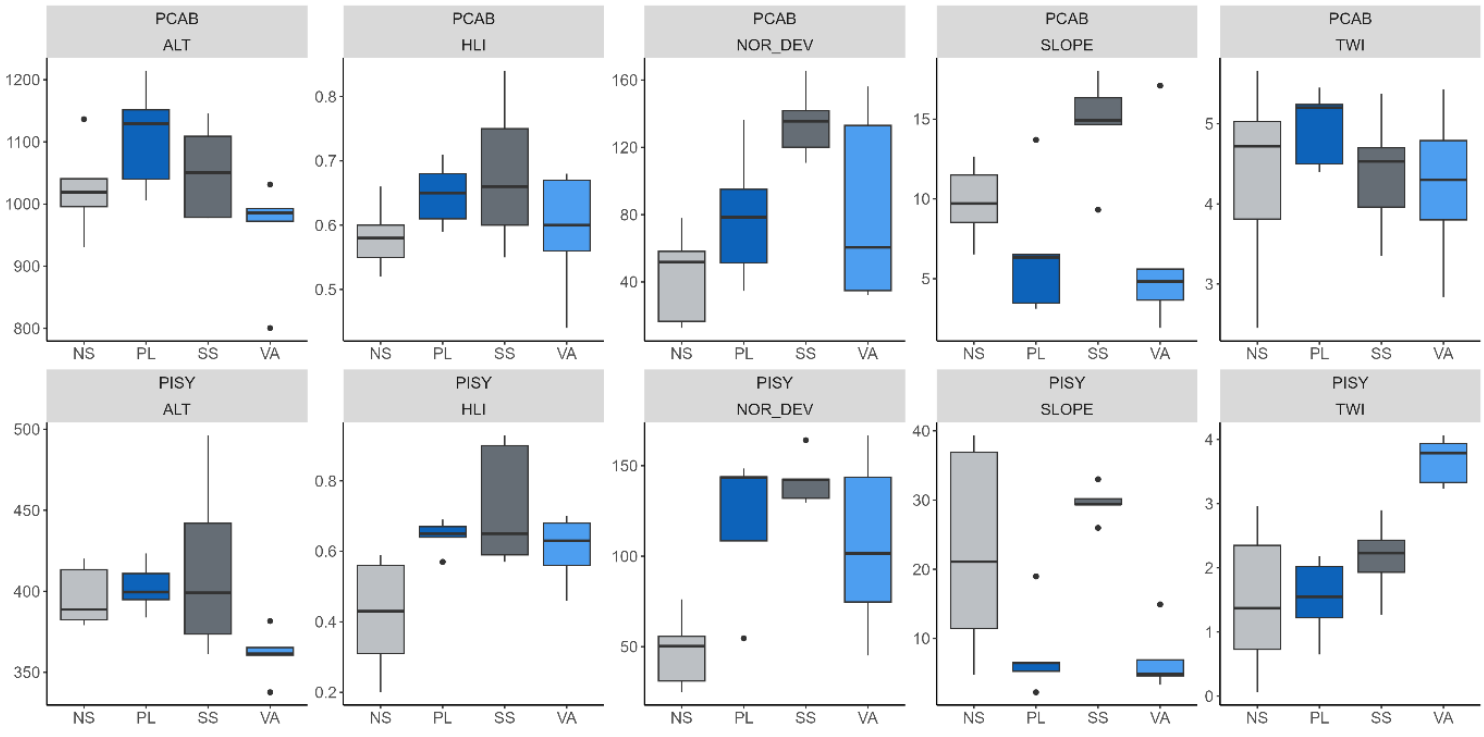

Table S1: Topographic characteristics (Heath load index-HLI; North deviation-NOR_DEV; Topographic wetness index-TWI) specifications and equations. Calculations were performed on LIDAR-based surface topography models with a regular grid of 5 x 5 m (DMR 4G; ČÚZK 2013) using ArcMap 10.7.1 (ESRI 2020).

Variable	Description	Equation	Reference
Heath load index (HLI)	HLI represents the capacity of a given place for heating (high values) or cooling (low values) due to favorable slope, orientation, and latitude	HLI=EXP[-1.467+1582*(cos(L)*cos(S))-1.5*(cos(A)* sin(S)* sin (L))-0.262*(sin(L)* sin(S))+0.607*(sin(A) * sin(S))] L=latitude (rad) S=slope (rad) A=180-|ASP-180| (rad) ASP = aspect of slope (deg)	McCune and Keon (2002)
North deviation (NOR_DEV)	NOR_DEV represents the insolation of a given place due to orientation to the north (low values) or to the south (high values)	NOR_DEV = ((ASP<180)*ASP)+|(ASP>180)*(APS-360)| ASP = aspect of slope (deg)	
Topographic wetness index (TWI)	TWI represents a topographically induced predisposition of a given place for moisture accumulation (high values)	TWI = ln(α/tan(β)) α = flow accumulation β = surface slope (rad)	Beven and Kirkby (1979)

Table S2: General plot characteristics of *Pinus sylvestris* (PISY) and *Picea abies* (PCAB). Study plots, ordered according to species and plot category.

Plot no.	Species	Plot category	Coordinates (Lat; Long)	Elevation (m a. s. l.)	No. of trees	Mean age (± SD)	Mean DBH ± SD (cm)
1	PISY	North slope	50.583; 14.432	388.79	26	66 ± 41	33 ± 7
7	PISY	North slope	50.574; 14.433	379.11	26	118 ± 20	35 ± 7
9	PISY	North slope	50.596; 14.447	382.54	26	78 ± 34	37 ± 6
10	PISY	North slope	50.572; 14.455	420.16	65	122 ± 88	34 ± 6
12	PISY	North slope	50.574; 14.457	413.36	26	149 ± 11	36 ± 7
2	PISY	Plateau	50.583; 14.434	411.01	27	128 ± 42	38 ± 4
4	PISY	Plateau	50.569; 14.440	383.86	26	128 ± 36	31 ± 5
5	PISY	Plateau	50.574; 14.436	394.91	26	148 ± 19	25 ± 5
11	PISY	Plateau	50.567; 14.458	399.54	59	158 ± 80	35 ± 8
13	PISY	Plateau	50.579; 14.453	423.42	25	138 ± 9	23 ± 10
3	PISY	South slope	50.580; 14.436	373.56	26	78 ± 31	22 ± 9

8	PISY	South slope	50.599; 14.451	496.45	64	125 ± 11	37 ± 7
15	PISY	South slope	50.583; 14.447	361.25	26	94 ± 45	34 ± 5
16	PISY	South slope	50.587; 14.440	442.00	26	143 ± 16	46 ± 8
19	PISY	South slope	50.577; 14.454	399.07	26	144 ± 12	39 ± 7
6	PISY	Valley	50.570; 14.432	337.70	26	73 ± 17	42 ± 6
14	PISY	Valley	50.584; 14.460	360.62	35	119 ± 8	42 ± 5
17	PISY	Valley	50.590; 14.454	365.34	26	110 ± 17	43 ± 4
18	PISY	Valley	50.588; 14.458	361.48	26	61 ± 5	36 ± 4
20	PISY	Valley	50.595; 14.452	381.66	26	94 ± 21	42 ± 6
26	PCAB	North slope	49.211; 13.260	1136.41	26	160 ± 9	47 ± 8
28	PCAB	North slope	49.193; 13.266	1018.92	26	101 ± 3	54 ± 8
31	PCAB	North slope	49.206; 13.227	930.87	23	99 ± 17	44 ± 10
33	PCAB	North slope	49.191; 13.286	995.72	25	123 ± 30	47 ± 7
34	PCAB	North slope	49.200; 13.272	1040.71	26	94 ± 19	38 ± 7
23	PCAB	Plateau	49.201; 13.248	1214.19	25	93 ± 21	40 ± 8
25	PCAB	Plateau	49.215; 13.243	1129.26	26	101 ± 13	47 ± 8
27	PCAB	Plateau	49.186; 13.285	1039.89	26	117 ± 10	40 ± 7
30	PCAB	Plateau	49.183; 13.256	1151.50	25	113 ± 12	47 ± 9
37	PCAB	Plateau	49.203; 13.286	1005.97	26	87 ± 5	35 ± 7
21	PCAB	South slope	49.184; 13.240	977.47	26	111 ± 10	52 ± 10
22	PCAB	South slope	49.198; 13.243	1145.46	26	123 ± 16	44 ± 9
29	PCAB	South slope	49.178; 13.257	1108.93	26	118 ± 13	45 ± 9
32	PCAB	South slope	49.187; 13.271	1050.51	24	108 ± 10	51 ± 10
38	PCAB	South slope	49.211; 13.231	978.54	25	132 ± 17	36 ± 9
24	PCAB	Valley	49.221; 13.249	1031.37	25	179 ± 27	42 ± 11
35	PCAB	Valley	49.195; 13.276	985.95	25	150 ± 30	40 ± 7
36	PCAB	Valley	49.196; 13.282	972.35	26	103 ± 29	55 ± 12
39	PCAB	Valley	49.181; 13.292	992.90	25	100 ± 12	38 ± 14
40	PCAB	Valley	49.216; 13.283	800.47	26	66 ± 6	44 ± 8

Figure S2: Correlations between normalized difference vegetation index (NDVI) for the individual plots of *Pinus sylvestris* (PISY) and *Picea abies* (PCAB). Colors denote pairs of settings of the growing season: May–September (MS), Jun–August (JA), and the variable start of the growing season for each year based on daily climate data to September (DOY 274, series presented in this paper).

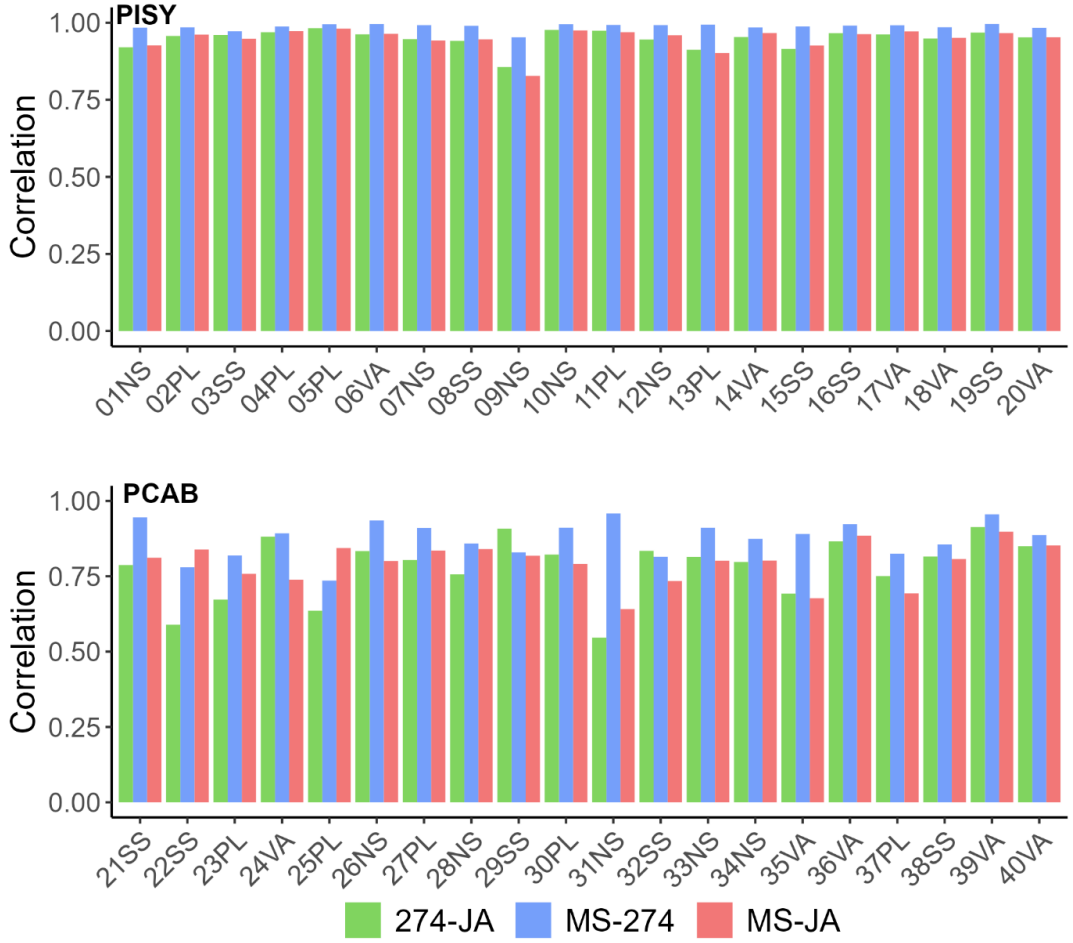

Figure S3: NDVI values of individual Landsat scenes during the vegetation period (from the day of bud burst to 30th September) for random points within studied sites for *Pinus sylvestris* (PISY) and *Picea abies* (PCAB). Colors denote individual years.

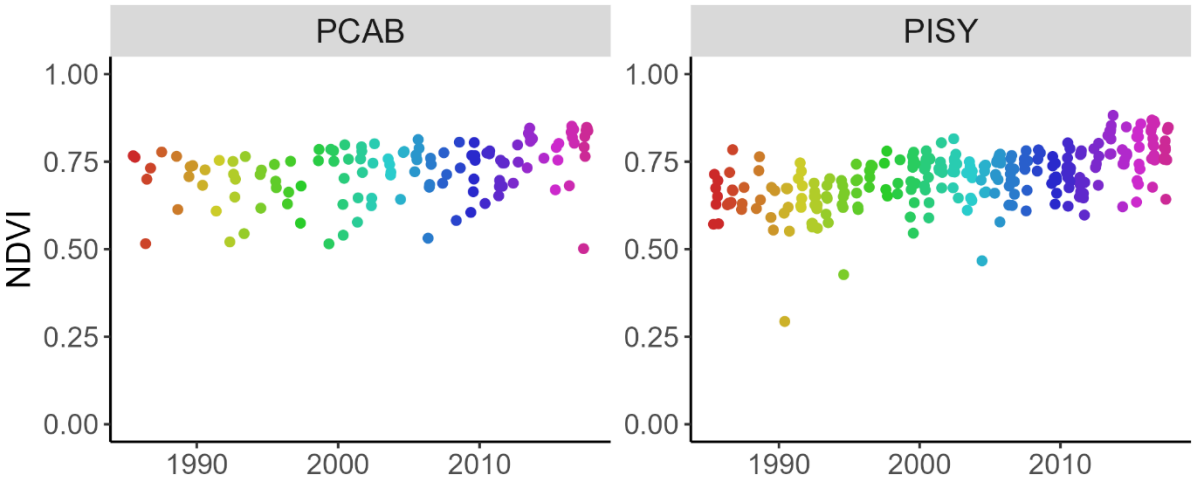

Figure S4: Mean correlation (bars) and standard deviations (error bars) of normalized difference vegetation index (NDVI; upper panel) and tree-ring width (TRI; lower panel) for *Picea abies* (PCAB; left panel) and Pin*us sylvestris* (PISY; right panel) with climatic variables (colors; P-Precipitation, SM-Soil moisture, SPEI- Standardised precipitation-evapotranspiration index, SP-Solar radiation, T-Temperature) for plot categories (SS-South slope, NS-North slope, PL-Plateau, VA-Valley) for previous and current year (transparent and solid color, respectively). Dashed lines indicate statistical significance ($p<0.05$).

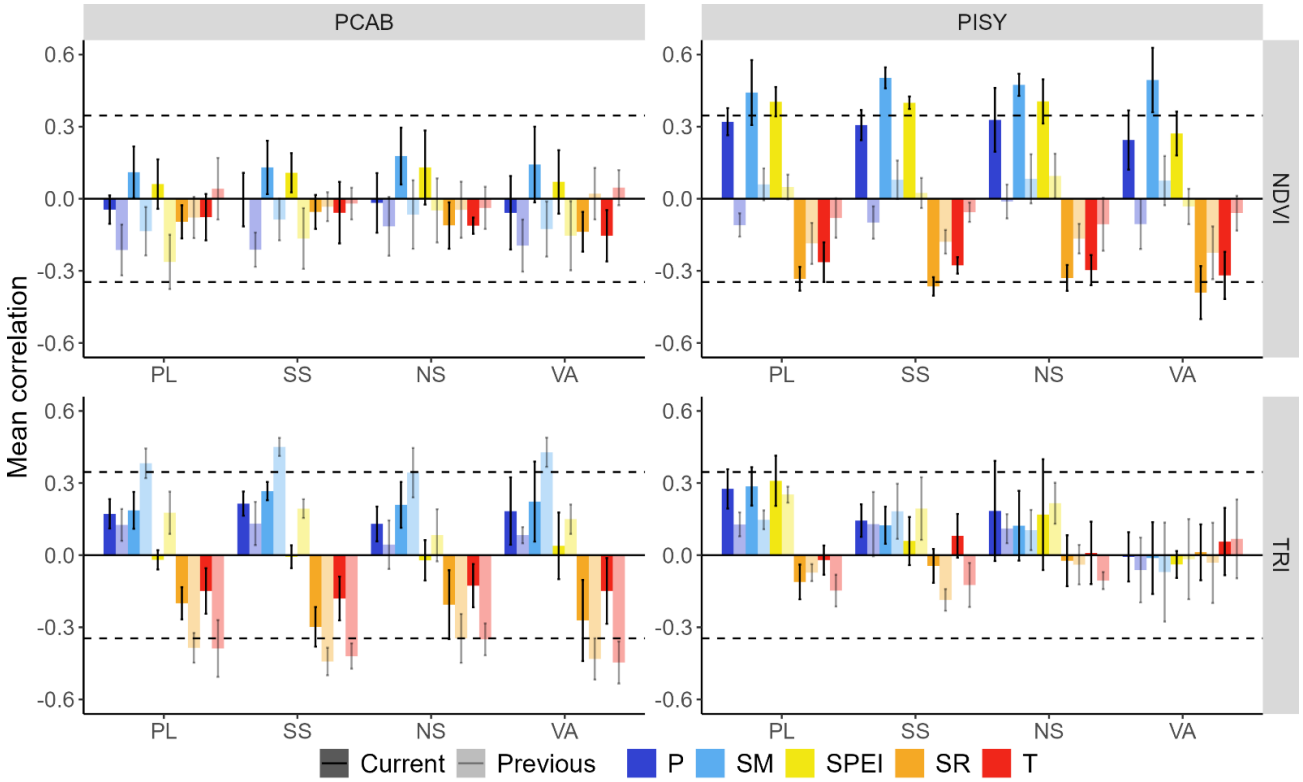

Text S1: To quantify the resiliency of the biomass compartments in response to dry spells, we calculated three resilience indices following Lloret et al. (2011): resilience (RS = post-drought growth/pre-drought growth), resistance (RT = growth in drought year/pre-drought growth), and recovery (RC = growth in drought year/post-drought growth). We considered four years pre- and post-drought, and we used for the calculations the R package pointRes 2.0.1 (van der Maaten-Theunissen et al. 2015). The RS indicates the capacity to achieve the pre-drought level of growth, the RT represents the ability to retain normal growth rates during drought and RC denotes post-drought growth relative to the growth depression during the drought event (Lloret et al. 2011). We applied the Wilcox pairwise test to determine differences in resilience components between drought years (Fig. S5, Table S2).

Table S3: Differences in resilience indices: resilience (RS), resistance (RT), and recovery (RC) of normalized difference vegetation index (NDVI) and tree-ring width (TRI) among individual drought years for *Pinus sylvestris* (PISY) and *Picea abies* (PCAB) and their plot categories (SS-South slope, NS-North slope, PL-Plateau, VA-Valley) indicated by the Wilcox pairwise post hoc test. Red font denotes statistical significance ($p<0.05$).

			RS				RT				RC			
SPECIES	**VAR**	**YEAR**	**NS**	**PL**	**SS**	**VA**	**NS**	**PL**	**SS**	**VA**	**NS**	**PL**	**SS**	**VA**
PISY	**TRI**	**1994-2003**	0.024	0.024	0.024	0.048	0.222	0.032	0.024	0.095	0.095	0.024	0.024	0.032
		1994-2006	0.841	0.032	0.310	0.548	0.048	0.024	0.032	0.024	0.024	0.151	0.024	0.024
		2003-2006	0.024	0.024	0.111	0.048	0.111	0.095	0.151	0.024	0.024	0.024	0.024	0.024
	NDVI	**1994-2003**	0.024	0.024	0.024	0.024	0.167	0.286	1.000	1.000	1.000	0.024	0.024	0.286
		1994-2006	0.310	0.024	0.024	0.024	0.619	0.444	1.000	1.000	1.000	0.151	0.190	0.286
		2003-2006	0.024	0.024	0.024	0.095	0.619	0.444	1.000	1.000	1.000	0.063	0.190	1.000
PCAB	**TRI**	**1994-2003**	0.421	0.095	0.310	0.095	0.024	0.024	0.024	0.024	0.024	0.024	0.024	0.048
		1994-2006	0.024	0.024	0.024	0.032	0.095	0.024	0.024	0.222	0.095	0.222	0.095	0.841
		2003-2006	0.032	0.024	0.024	0.024	0.024	0.024	0.024	0.032	0.063	0.024	0.032	0.444
	NDVI	**1994-2003**	0.024	0.095	0.095	0.095	0.310	0.421	0.032	0.421	0.024	0.619	0.690	0.444
		1994-2006	0.024	0.302	0.190	0.111	0.048	0.167	0.024	0.048	1.000	0.619	0.032	0.444
		2003-2006	0.421	0.548	1.000	1.000	0.063	0.302	0.032	0.111	0.111	0.452	0.024	0.286

Figure S5: Boxplots of resilience indices: resilience (RS), resistance (RT), and recovery (RC) of normalized difference vegetation index (NDVI; upper panel) and tree-ring width (TRI; lower panel) in individual dry years between plot categories (color; SS-South slope, NS-north slope, PL-Plateau, VA-Valley) for *Pinus sylvestris* (PISY; right panel) and *Picea abies* (PCAB; left panel).

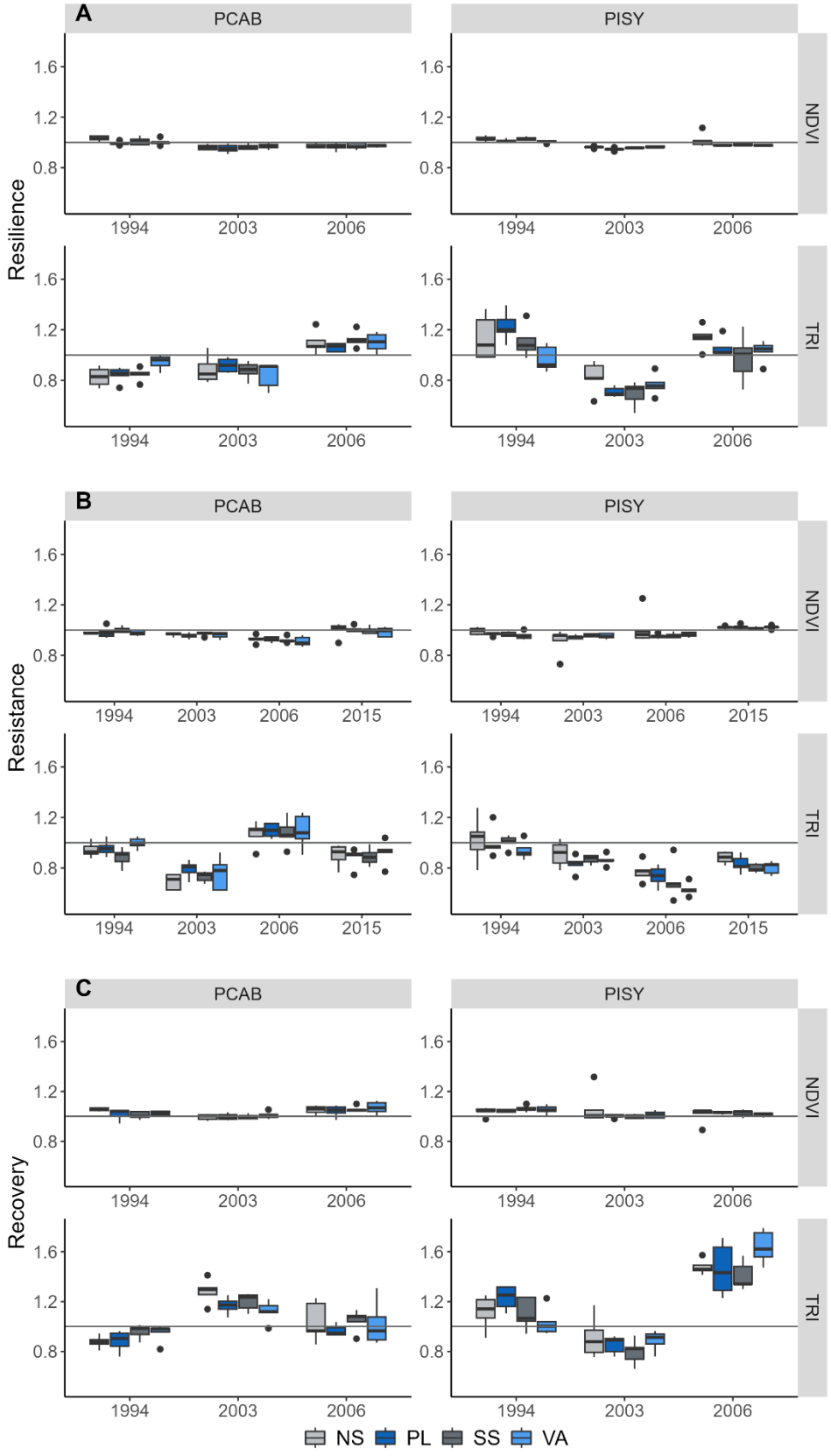

Science of the Total Environment 908 (2024) 168275

Contents lists available at ScienceDirect

Science of the Total Environment

journal homepage: www.elsevier.com/locate/scitotenv

Shifting climatic responses of tree rings and NDVI along environmental gradients

Jiří Mašek [a,*], Jan Tumajer [a], Jelena Lange [a], Monika Vejpustková [b], Jakub Kašpar [c], Pavel Šamonil [c], Tomáš Chuman [a], Tomáš Kolář [d,e], Michal Rybníček [d,e], Michal Jeníček [a], Ivana Vašíčková [c], Vojtěch Čada [f], Ryszard Kaczka [a], Miloš Rydval [f], Miroslav Svoboda [f], Ondřej Nedělčev [a], Martin Hais [g], Václav Treml [a]

[a] Department of Physical Geography and Geoecology, Faculty of Science, Charles University, Albertov 6, 128 43 Prague, Czech Republic
[b] Forestry and Game Management Research Institute, Strnady 136, 252 02 Jíloviště, Czech Republic
[c] Department of Forest Ecology, The Silva Tarouca Research Institute, Lidická 971/25, 602 Brno, Czech Republic
[d] Department of Wood Science and Technology, Faculty of Forestry and Wood Technology, Mendel University in Brno, Lesnická 3, 613 00 Brno, Czech Republic
[e] Global Change Research Institute of the Czech Academy of Sciences, Bělidla 986/4a, 603 00 Brno, Czech Republic
[f] Department of Forest Ecology, Faculty of Forestry and Wood Science, Czech University of Life Science, Kamýcká 129, 165 00 Prague, Czech Republic
[g] Department of Ecosystem Biology, Faculty of Science, University of South Bohemia, Branišovská 1760, 370 05 České Budějovice, Czech Republic

HIGHLIGHTS

- Coherence of climatic responses of tree rings (TRI) and NDVI was studied.
- TRI and NDVI relationship was explained by climate, topography and soil category.
- Decoupling of TRI and NDVI climatic responses across environmental gradients.
- Agreement between TRI and NDVI at warm/dry part of Picea species range.
- TRI sensitive to climate and stand age, NDVI reflects climate, topography and soils.

GRAPHICAL ABSTRACT

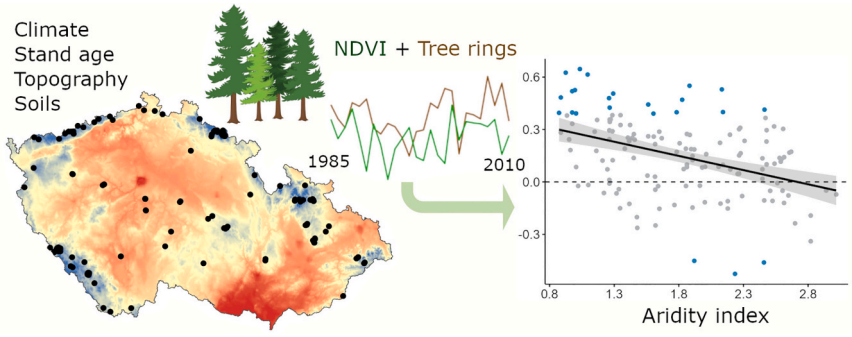

ARTICLE INFO

Editor: Elena Paoletti

Keywords:
Picea abies
Climate-growth relationship
Biomass compartments
Tree-ring width
Canopy vigor
Remote sensing

ABSTRACT

Variations in the growth of aboveground biomass compartments such as tree stem and foliage significantly influence the carbon cycle of forest ecosystems. Yet the patterns of climate-driven responses of stem and foliage and their modulating factors remain poorly understood. In this study, we investigate the climatic response of Norway spruce (*Picea abies*) at 138 sites covering wide spatial and site fertility gradients in temperate forests in Central Europe. To characterize the annual growth rate of stem biomass and seasonal canopy vigor, we used tree-ring chronologies and time-series of NDVI derived from Landsat imagery. We calculated correlations of tree-ring width and NDVI with mean growing season temperature and standardized precipitation evapotranspiration index (SPEI). We evaluated how these climate responses varied with aridity index, soil category, stand age, and topographical factors. The results show that the climate-growth responses of tree rings shift from positive to

* Corresponding author.
E-mail address: jiri.masek@natur.cuni.cz (J. Mašek).

https://doi.org/10.1016/j.scitotenv.2023.168275
Received 23 July 2023; Received in revised form 30 October 2023; Accepted 31 October 2023
Available online 3 November 2023

negative for SPEI and from negative to positive for temperature from dry (warm) to wet (cold) areas. By contrast, NDVI revealed a negative response to temperature across the entire climatic gradient. The negative response of NDVI to temperature likely results from drought effects in warm areas and supporting effects of cloudy conditions on foliage greenness in wet areas. Contrary to NDVI, climate responses of tree rings differed according to stand age and were unaffected by local topographical features and soil conditions. Our findings demonstrate that the decoupling of stem and foliage climatic responses may result from their different climatic limitation along environmental gradients. These results imply that in temperate forest ecosystems, the canopy vigor may show different trends compared to stem growth under ongoing climate change.

1. Introduction

Aboveground biomass growth in forest ecosystems represents a large atmospheric carbon sink (Bonan, 2008). The intensity of carbon sequestration is modulated by climatic factors such as soil moisture, evaporative demand, and air temperature (Anderegg et al., 2013a; Allen et al., 2010). After the assimilation of the carbon into carbohydrates, it gets allocated to the various tree compartments with stem, foliage, and roots contributing the most to the process of biomass formation and long-term carbon sequestration (Bernoulli and Körner, 1999; Schiestl-Aalto et al., 2019). However, each of these compartments might show significantly different climatic responses (Babst et al., 2018; Seftigen et al., 2018). Considering aboveground parts of a tree, tree-ring width chronologies can be used as a proxy for annual radial increment of stem biomass (Girardin et al., 2016; Fritts, 1976). Moreover, time-series of vegetation indices derived from remote sensing data, such as the normalized difference vegetation index (NDVI), represent year-to-year variability in leaf greenness indicative of canopy vigor (Vicente-Serrano et al., 2016; Song, 2012). Both proxies are accessible from databases that cover wide environmental gradients at high spatial and temporal resolution (Babst et al., 2017, 2018; Pearl et al., 2020). This represents a unique potential for studying the overall responses of carbon pools in forest biomes to ongoing climate warming.

Despite the obvious correlation between tree-ring chronologies and NDVI (Babst et al., 2018; Vicente-Serrano et al., 2020), there is increasing evidence for partial decoupling of the climatic responses of both aboveground biomass compartments (Seftigen et al., 2018; Beck et al., 2013; Brehaut and Danby, 2018). Differences between tree rings and NDVI might be caused by different climatic conditions driving the formation and functioning of the xylem and leaves. Whereas photosynthesis (hence one component of foliage greenness through chlorophyll content; Toomey et al., 2015) is active at temperatures close to 0 °C, wood formation is usually not sustained under temperatures below 5 °C (Fatichi et al., 2014; Rossi et al., 2007). Moreover, stem growth stops at a higher plant water potential than photosynthesis because cell division depends on high turgor pressure in cambial cells (Cabon et al., 2020). The relatively strong sink limitation of carbon deposition during the wood formation process might explain stronger climate-growth relationships of tree rings compared to vegetation indices indicative of canopy vigor or primary production derived from eddy covariance data (Kannenberg et al., 2020; Gazol et al., 2018; Schwalm et al., 2017; Moreno-Fernández et al., 2022). Differences in climatic limitation between stems and leaves also lead to shifted time windows of sensitivity within the year for both tree rings and NDVI (Seftigen et al., 2018).

The connection between tree rings and NDVI and their climatic responses has been reported to vary through bioclimatic zones. The responses of NDVI tend to be positive for temperature and negative for moisture in cold areas, while in drier zones, this response is reversed (Peng et al., 2012; Vicente-Serrano et al., 2012). Strong climatic forcing (in very cold or dry regions) was shown to increase the correlation between tree rings and NDVI (Bhuyan et al., 2017; Kaufmann et al., 2008) while these two variables might be decoupled in moderate environments (Bhuyan et al., 2017). Accordingly, where both tree rings and NDVI are limited by low temperature (Wang et al., 2011; Piedallu et al., 2019; Huang et al., 2020), their correlations are high (Huang et al., 2015; Vicente-Serrano et al., 2016). Despite these seemingly systematic patterns of tree rings and NDVI, many contrasting results have been reported and the influence of various non-climatic effects remains largely unknown because of a lack of systematic testing. For example, the high correlation between tree rings and NDVI in climatically-limiting environments is not a general pattern since a mismatch between tree rings and NDVI was observed in cold areas like Alaska and in dry lowlands of Central Europe (Beck et al., 2013; D'Andrea et al., 2022).

Climate responses of both tree rings and NDVI can also be influenced by tree species (Vicente-Serrano et al., 2020; Mašek et al., 2023), and internal tree characteristics such as age and size (Carrer and Urbinati, 2004; Trouillier et al., 2019; Stephenson et al., 2014). Among external factors affecting the climatic response of tree rings and NDVI, one should also consider local topography influencing moisture and solar irradiation (Del-Toro-Guerrero et al., 2019; Vicente-Serrano et al., 2020; Wang et al., 2021). The soil properties might modulate the climate limitation of trees since they influence available moisture (Schmied et al., 2023; Piedallu et al., 2019). Moreover, the level of decoupling between series of radial growth and leaf greenness can be unstable over time. For instance, it was observed that after extreme droughts, trees tend to allocate more carbon into leaves than to the stem in order to retain the assimilation rate and hence reduce stem growth for up to two years following the drought (Anderegg et al., 2013a, 2013b; Kannenberg et al., 2019). These examples show very clearly that there is still a large knowledge gap regarding many direct and combined effects of drivers potentially affecting the climatic responses of tree rings and NDVI along environmental gradients in temperate forest ecosystems. Moreover, the majority of studies used NDVI data derived from medium to low resolution imagery such as MODIS or AVHRR (e.g. Vicente-Serrano et al., 2016; Bhuyan et al., 2017; Seftigen et al., 2018), while the relationship between tree rings and high resolution satellite data has been substantially less studied.

In this study, we examined the effects of environmental gradients represented by site climatic conditions, soil properties, local topography, and of tree age on climate responses of tree rings (a proxy for stem biomass) and NDVI (a proxy for canopy vigor). We focused on 138 monospecific *Picea abies* sites covering a wide environmental gradient of Central European temperate forests with respect to the above-mentioned factors. We calculated the correlation of tree-ring indices and NDVI with summer temperature and SPEI for each site. These correlations were then used as a response variable in spatial regression models with various explanatory environmental variables. We hypothesized that (i) the direction and strength of climate responses of tree rings and NDVI differ and that (ii) climate responses are modulated by regional to local site factors such as climate, soil properties, topography, and stand age. With our results, we aim to contribute to a better understanding of the carbon storage process in wood and leaves under differing environmental conditions.

2. Methods

2.1. Study species and tree-ring data

Coniferous forest ecosystems in Central Europe are dominated by *Picea abies* (PCAB; Fig. 1A), representing about 30 % of the forest stock

(Spiecker, 2000). The species naturally grows mainly in uplands and mountains above 900 m a.s.l., and at moist sites in lower elevations or in valleys with thermal inversion. However, it was also commonly planted outside its ecological and growth optima including warm and dry locations in lowlands (Spiecker, 2000; Fig. 1A). Since it is adapted to cold environments, it is highly vulnerable to drought near the low-elevation margins of its range (Lévesque et al., 2013; Treml et al., 2022).

We used tree-ring data from the new TreeDataClim database (https://treedataclim.cz/databaze/), which contains tree-ring width measurements of the main tree species in the Czech Republic. We selected monospecific PCAB stands where mainly dominant canopy-level trees were sampled with the last tree ring dated to 2010 or later. Sites located in open-canopy stands were not considered since their spectral signal can be distorted by understory vegetation. The resulting dataset contained 138 sites (Table S1) covering a large altitudinal (200–1300 m a.s.l.; Fig. 1B) and climatic gradient (2.5–9 °C mean annual temperature, 500–1400 mm of annual precipitation totals; Fig. 1C).

To remove the age trend from the tree-ring series, we used a 30-year-long cubic smoothing spline with a 50 % frequency cut-off as an adaptive function predicting radial growth and then we calculated tree-ring

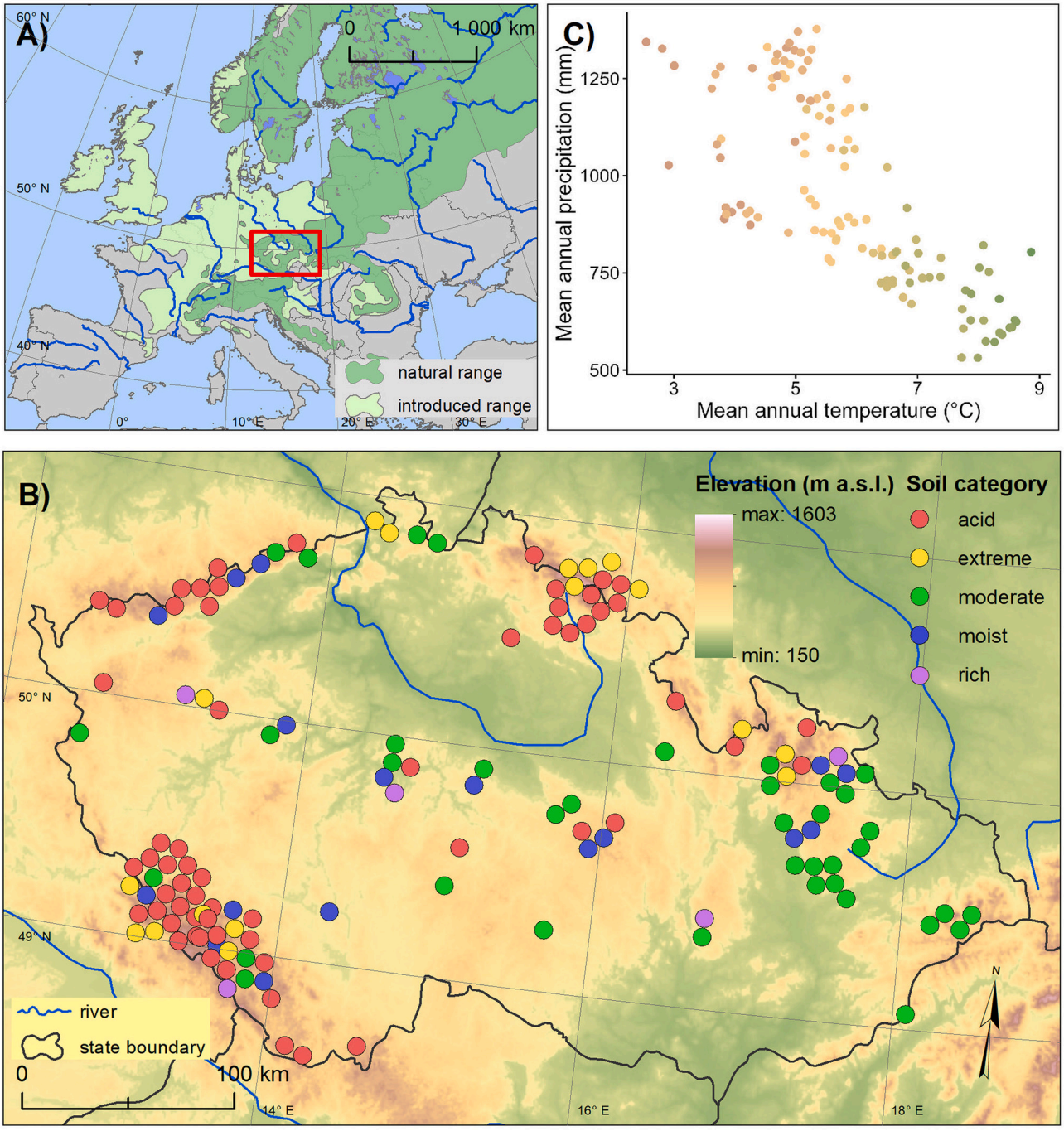

Fig. 1. Location of the study region (red rectangle) and distribution range of *Picea abies* (green areas; Caudullo et al., 2017; panel A). Study sites and their soil category indicated by color (red-acid, yellow-extreme, green-moderate, blue-moist, purple-rich; Viewegh et al., 2003). The position of sites in areas with high site density (mainly mountain areas) was cartographically offset to enhance their visibility on the map, thus some sites seem to lie outside the territory of the Czech Republic (panel B). Climatic characteristics: mean annual temperature and mean precipitation totals for 1985–2010 per site. Colors from green to brown refer to elevation from low to high according to the legend in panel B, respectively (panel C).

indices (TRI; Fig. S1) as ratios between observed and modeled growth (Cook and Peters, 1981). Our detrending approach preserved mainly the high-frequency variability of the tree-ring series. One standard chronology for each site was created using averaging of all series by Tukey's bi-weight robust mean (R package dplR 1.7.4; Bunn et al., 2022). We also determined the mean tree age for each site because it is known to influence climate sensitivity (Carrer and Urbinati, 2004). We approximated the tree age by the number of tree rings measured on the increment core. Therefore, our age variable represents a minimal estimate since we neglected missing rings close to the pith (in the case of off-pith cores) and below the sampling position.

2.2. NDVI data

The longest available and homogenous time-series of high-resolution (30 m per pixel since 1984) multispectral images are provided by Landsat satellite missions. We used high-quality T1_SR scenes to calculate the NDVI time-series. In Google Earth Engine (Gorelick et al., 2017), we first linearly recalculated images of Landsat 5 and 7 to be comparable because each of them uses a different sensor (Roy et al., 2016). According to Zhu et al. (2015), we erased clouds and their shadows to avoid their influence on the spectral signal. Since PCAB usually completes the growth of annual shoots approximately at the end of June (Kraus et al., 2016), we selected scenes from 1st July to 30th September (day of year 182–273). Therefore, there should be no influence of varying leaf phenology between years on the NDVI series since our data reflects the peak growing season at most sites. Next, the NDVI was computed using the formula (Tucker, 1979):

$$NDVI = \frac{NIR - Red}{NIR + Red}$$

where 'NIR' denotes spectral response in the near-infrared part of the spectrum and 'Red' stands for the reflectance in the red part of the spectrum (NASA, 2022). For each pixel, we calculated the median from all scenes of the defined growing season (Jul-Sep) within one year. Final values for individual sites were calculated as an average of pixels weighted by the proportion of the sampled site located inside the given pixel. We considered the shape of all sites to be a circle with a diameter of about 30 m which corresponds to the average plot size in the Tree-DataClim database. We additionally tested larger polygon sizes to compute NDVI (50 m, 100 m). The results, however, did not significantly differ from the original 30 m plots. Moreover, we preferred a 30 m circle since this area definitely overlaps all sampled plots in the database (including the smallest), which might not be the case for larger polygons.

Various factors such as increasing forest density and canopy closure as trees are getting larger (Vicente-Serrano et al., 2004) and increasing CO_2 fertilization (Donohue et al., 2013) lead to positive trends in the time-series of vegetation indices. Therefore, we linearly detrended the individual time-series of NDVI (Fig. S1), and residuals from this trend line were used for all subsequent analyses. By removing trend from NDVI we make this time series comparable with TRI detrended also by removal of low-frequency component of variability.

2.3. Climate data

For the individual study sites, monthly time-series (1985–2010) of mean air temperature and precipitation totals were produced by means of spatial interpolation from a network of station data into climate grids with a resolution of 1 km × 1 km. The grids were calculated using all available meteorological stations for the Czech Republic operated by the Czech Hydrometeorological Institute (719 stations for precipitation, and 296 stations for air temperature in 2020; ČHMÚ, 2023). The number of stations used for interpolation varied during the study period, reflecting the continuous development of the monitoring network and the station density. Kriging was used to interpolate precipitation. A generalized additive model was applied to air temperature to include its change with elevation based on the digital terrain model with the same spatial resolution as the climate grid. The R packages 'gstat' (2.0–8; Pebesma, 2004) and 'mgcv' (1.8–38; Wood, 2011) were used for the climate grids calculations.

Time series of temperature and precipitation for each site were extracted from climate grids using R packages 'ncdf4' (1.21; Pierce, 2023), 'raster' (3.6–14; Hijmans, 2023), and 'rgdal' (Bivand et al., 2023). Monthly climatic data were used to calculate the standardized precipitation evapotranspiration index (SPEI; Vicente-Serrano et al., 2010). To estimate evapotranspiration, the Thornthwaite method was used (Thornthwaite, 1948). PCAB as a shallow-rooting species can reach the soil layers with water turnover of about several weeks (Sprenger et al., 2019), therefore two previous months were considered in the calculation of the ratio between rainfall and evapotranspiration (R package 'SPEI' 1.8; Beguería and Vicente-Serrano, 2023).

For the subsequent analyses, the seasonal mean temperature and SPEI were calculated for the period between June and August of the current year (Fig. S1) which is the part of the growing season with the highest correlations of tree-ring width (Treml et al., 2022; Tumajer et al., 2017) and NDVI in the Czech Republic (Mašek et al., 2023; Fig. S2). In both tree rings and NDVI, we also found a climatic signal of the previous year's summer (Fig. S2). Since a relatively small amount of conifer growth is influenced by the previous year's conditions (initial phases of wood formation and the effect of the size of shoots from previous years; Vaganov et al., 2006, Simard et al., 2013), the signal of the previous year is unclear (Fig. S6).

To characterize local climate, we calculated for each site the UNEP aridity index (AI; UNEP, 1993) according to the formula:

$$AI = \frac{TAP}{PET}$$

where TAP is total annual precipitation in mm and PET is potential evapotranspiration in mm. High AI values are indicative for cold and wet sites whereas low AI values represent warm and dry sites.

2.4. Topographic and soil data

To characterize the surface topography of each site, we used a Lidar-based digital elevation model of the Czech Republic with a resolution of 5 m per pixel (DMR 4G; ČÚZK, 2013). We then calculated three metrics: mean slope inclination (SLP), topographic wetness index (TWI), and heat load index (HLI). TWI represents a topographically induced predisposition of a given place for moisture accumulation (high values) or, conversely, fast runoff due to a steep slope (low values) and is defined as follows:

$$TWI = ln\left(\frac{\alpha}{tan\beta}\right)$$

In this formula, α stands for flow accumulation and β indicates the slope of the surface in radians (Beven and Kirkby, 1979). HLI represents the capacity of a given place for heating (high values) or cooling (low values) due to favorable slope, orientation, and latitude and is calculated according to the formula:

$$HLI = EXP[-1.467 + 1582*(cos(L)*cos(S)) - 1.5*(cos(A)*sin(S)*sin(L)) - 0.262*(sin(L)*sin(S)) + 0.607*(sin(A)*sin(S))]$$

$$A = 180 - abs(Aspect - 180)$$

where L stands for latitude, S indicates slope and A is folded aspect, all in radians (McCune and Keon, 2002). The abovementioned topographic factors for each site were calculated as a mean value of a circle with 30 m in diameter to be consistent with the site size used in the calculation of NDVI (see Section 2.2). All topographic calculations were performed in ArcMap 10.7.1 (ESRI, 2020).

For each site, we also determined soil category in terms of fertility and moisture availability derived from the national forest ecosystem classification (Viewegh et al., 2003, Fig. 1B). For a description of those categories, see Table 1.

2.5. Statistical analysis

All statistical analyses were carried out using R 4.2.0 (R Core Team, 2022) for the period 1985 (the first feasible Landsat scenes) and 2010 balancing the availability of tree-ring width series from the TreeData-Clim database and a reasonable timespan.

To determine the climatic response of both biomass compartments at each site, we calculated Pearson's correlations of TRI and NDVI with mean temperature and SPEI for the June–August growing season using the 'treeclim'2.0.6.0 package (Zang and Biondi, 2015). To identify factors driving the climate response, these correlation coefficients were used as response variables in spatial regressions (Dormann et al., 2007), where AI, TWI, SLP, HLI, stand age (AGE), and soil category (SOIL) were explanatory variables.

First, we calculated the ordinary least square regression model using the formula:

$$COR_{biomass\ vs.climate} = AI + TWI + SLP + HLI + AGE + SOIL$$

We then tested for the spatial autocorrelation attributed to spatial dependence of covariates and spatial dependence of error terms of the model using Moran's I and Lagrange multiplier test statistics (Anselin, 1988). Lagrange statistics was used to decide which type of simultaneous autoregressive models (spatial error or spatial lag models) should be used (Anselin, 1988; Kissling and Carl, 2008). While the spatial error model was applied when the Lagrange multiplier test for error dependence was significant, the spatial lag model was used in case the Lagrange multiplier test for a missing spatially lagged dependent variable was significant (Anselin et al., 1996). "Spatialreg" 1.2–9 and "spdep" 1.2–8 packages were employed to compute the spatial autoregressive models (Pebesma and Bivand, 2023). Correlations and the variance inflation factor (R package 'car'3.1–1; Fox and Weisberg, 2019) were calculated to inspect the collinearity among explanatory variables. We did not consider interactions between explanatory variables because they were very weakly correlated (Fig. S3). The importance of individual variables was then evaluated by means of their standardized regression estimates and their significance.

We also correlated TRI and NDVI in order to quantify the level of their coherence. Next, to explain any variation in this coherence, we again calculated autocorrelation measures and constructed a spatial regression model with the same predictors as above (AI, TWI, SLP, HLI, AGE, and SOIL).

3. Results

The temperature signal of TRI significantly changed with the aridity index, declining from 0.47 in cold/wet areas to −0.58 in warm/dry areas (Fig. 2A). Correlations were significant for 19 % of the sites. Correlations between TRI and SPEI showed the opposite pattern, they increased from −0.39 in cold/wet areas to 0.70 in warm/dry areas (Fig. 2A). 24 % of the correlations were significant. By contrast, responses of NDVI to temperature were generally negative (mean −0.29, 37 % significant) with no significant change along the gradient of AI. Accordingly, correlations between NDVI and SPEI were prevailingly positive (mean 0.16, 12 % significant) with a negative slope along the AI gradient (Figs. 2, 3). Spatially, most of the significant climate-growth responses can be found in the central lowlands for TRI (negative to temperature and positive to SPEI), while the strongest responses of NDVI (negative to temperature and positive to SPEI) can be found in mountain areas in the north-east and south-west of the study area (Fig. 2B).

Based on Lagrange multiplier statistics (Table S2) we applied spatial error models to the following response variables: correlations of TRI-Temperature, TRI-SPEI, and NDVI-SPEI. The spatial lag model was used to explain the NDVI-Temperature correlation.

The spatial error model for the TRI-Temperature correlation was highly significant (Table S2). The most important explanatory variables were AI (highest positive correlations at cold and wet sites, Fig. 3) and stand age (TRI of old stands tended to have higher positive correlations with temperature compared to young stands). The model explaining TRI and SPEI correlations was also highly significant and similar to TRI-Temperature, however, with opposite effect signs for statistically significant predictors (AI, Age, Fig. 3). Correlations were highest at sites with lowest AI (driest sites) and vice versa and were higher for juvenile stands than for mature stands.

The spatial lag model explaining the NDVI-Temperature correlation was statistically significant (Table S2). Variables significantly influencing the correlation values were topographic wetness index (TWI) and site slope inclination (SLP) (Fig. 3). Their effect was negative meaning that higher NDVI-Temperature correlations were observed at well-drained sites and preferably on gentle slopes. Furthermore, moist soils exhibited significantly lower correlations than the most frequent category of acid soils (Fig. 3). The spatial error model for NDVI-SPEI correlations revealed significant effects of AI (negative, highest correlations at wettest/coldest sites), and site slope inclination (positive, higher correlations at steeper slopes). Correlations were further significantly higher at sites with moist soils compared to the prevailing category of acid soils (Fig. 3).

Correlation coefficients between TRI and NDVI followed a trend from positive at dry/warm sites to negative at wet/cold sites and were significant at 17 % of sites (20 positives, 3 negatives, Fig. 4). The spatial

Table 1
Soil categories from the national forest typology (Viewegh et al., 2003).

Soil category	Description
Acid	Soils without significant water influence, mostly well-drained nutrient-poor to very nutrient-poor acidic soils, often on slopes with high skeletal content. Soils show a rather poor decomposition and low cation exchange capacity. Dominant soils are Dystric Cambisols and Cambic Podzols.
Extreme	Soils without significant water influence, highly water deficient, shallow soils with high skeletal content, predominantly on silicate rocks, mostly oligotrophic. Dominant soils are Leptosols, frequently Skeletic Leptosols. This category, however, also comprises highly water-deficient, shallow soils with high skeletal content on base cation-rich bedrocks, but these sites are rare.
Moderate	Soils without significant water influence, nutrient availability is medium to rich, mostly deep soils on silicate rocks, also comprises sites on limestone, loess loam, or basalts. Dominant soils are Cambisols, Luvisols.
Moist	Soils with significant water influence, nutrient availability is medium to rich, mostly deep soils often on alluvial sediments with an abundance of nitrophilous species, but could also include nutrient-poor Gleysols. Soils often show hydromorphic signs of water stagnation.
Rich	Soils enriched in humus, deep eutrophic soils with an abundance of nitrophilous species often on colluvial deposits with favorable moisture regimes.

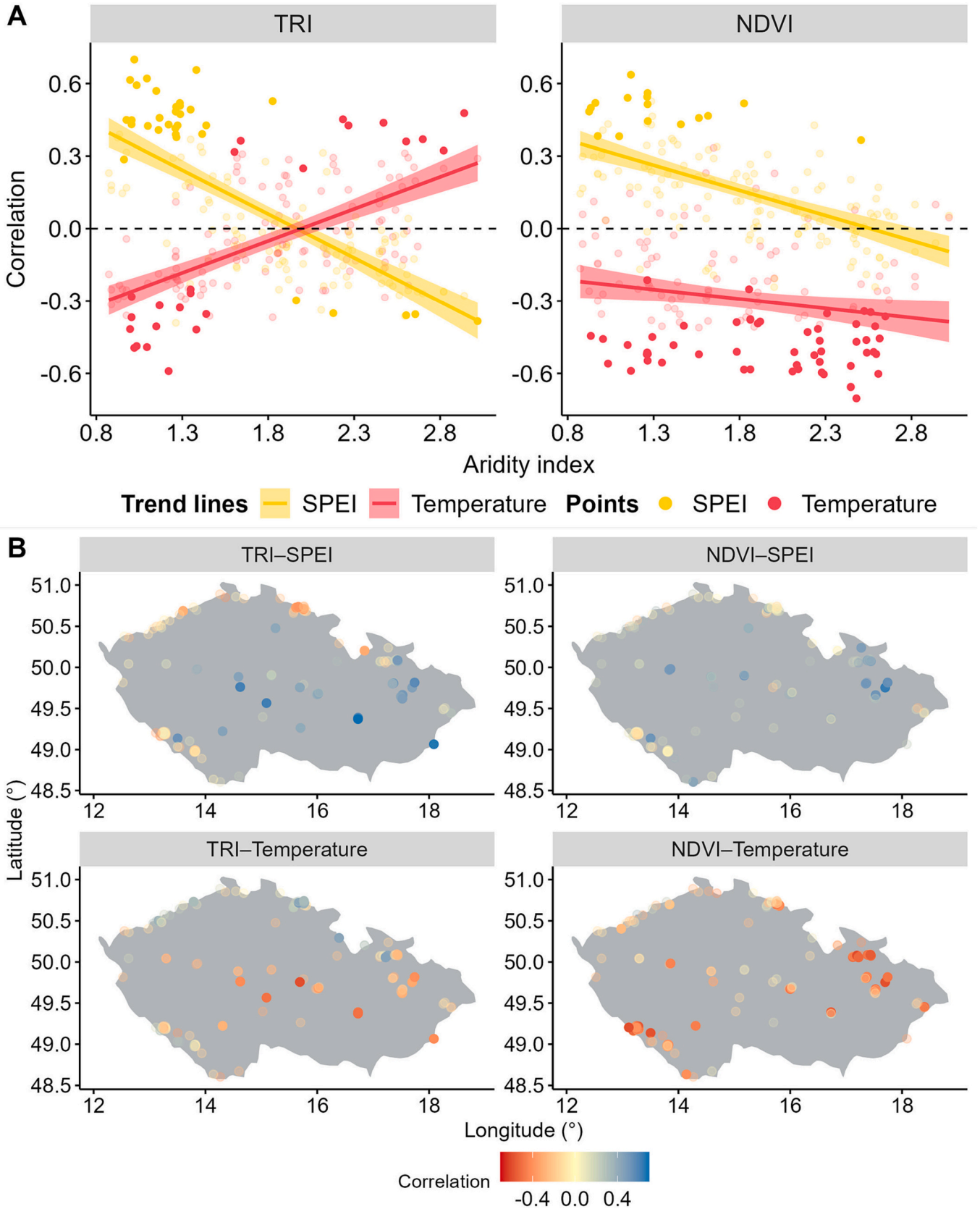

Fig. 2. Panel A shows correlations of tree-ring indices (TRI) and the normalized difference vegetation index (NDVI) with temperature (red color) and the standardized precipitation evapotranspiration index (SPEI; yellow color) for each site and their dependence on the aridity index. Solid dots denote sites with statistically significant correlations ($p < 0.05$). Regression lines and shaded areas indicate a linear model and its confidence interval (95 %) between climate-growth correlations and the aridity index. Panel B shows the location of study sites and the correlation of their TRI or NDVI with temperature and SPEI.

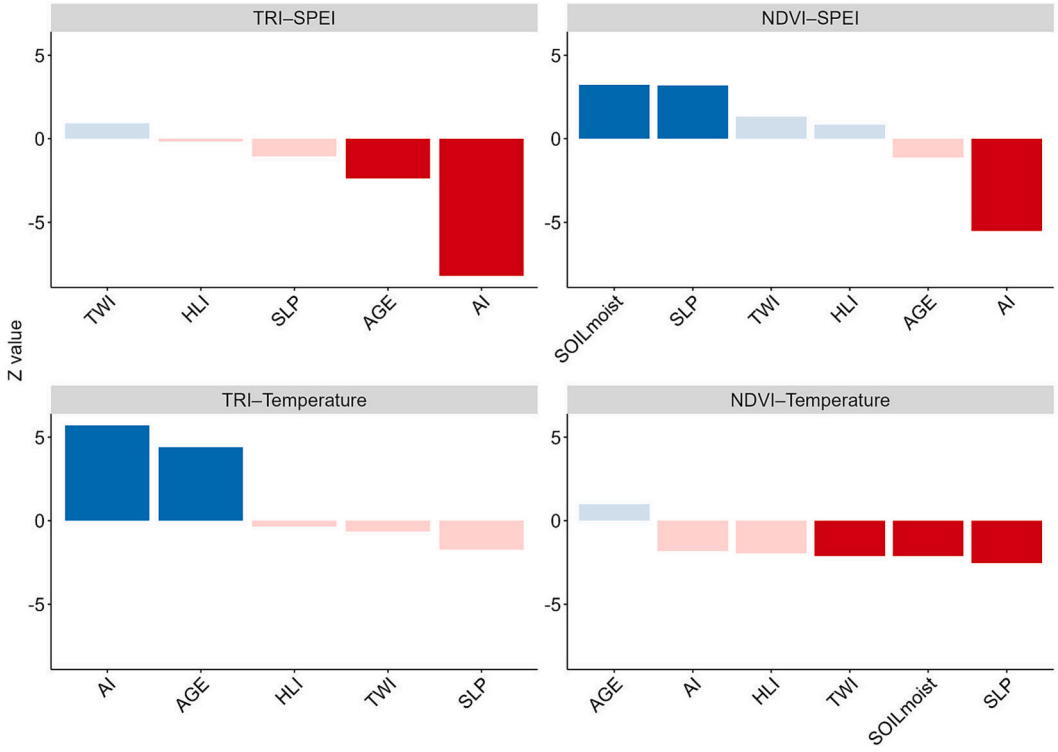

Fig. 3. Relative significance of predictors in spatial regressions as indicated by z-values (estimate divided by standard error). The blue and red color indicates positive and negative effects, respectively. The solid bars were used for statistically significant variables in the model ($p < 0.05$), transparent bars indicate non-significant effects. Only soil categories with significant effects are shown.

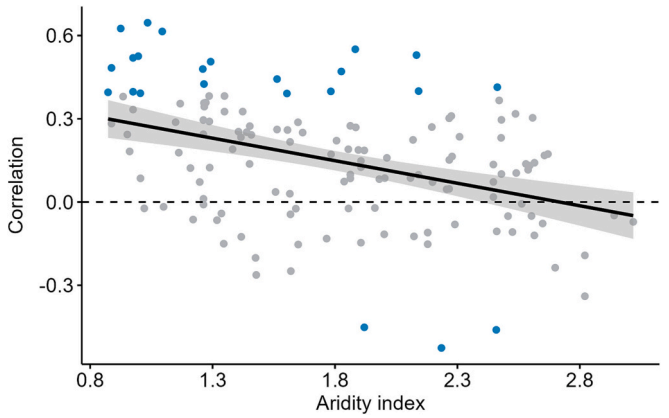

Fig. 4. The correlations between tree-ring indices (TRI) and normalized difference vegetation index (NDVI) and their dependence on the aridity index from dry/warm (low values) to wet/cold (high values). Blue color refers to statistically significant correlations ($p < 0.05$), which are more common under drier and warmer conditions (mostly lower elevation).

error model was statistically significant (Table S2). Predictors with significant effects included the aridity index (negative effect) and soil category, namely extreme soils where correlations between TRI and NDVI were lower (Fig. S5B). Other variables had statistically nonsignificant effects (Table S2).

4. Discussion

We combined analyses of tree-ring width (a proxy for stem biomass) and NDVI (a proxy for canopy vigor) series of *Picea abies* to examine the effects of site properties on the climate response of both biomass compartments in temperate forests. Our results highlight that while the climatic signal of tree rings systematically changed with the aridity index, in line with principles of growth-limiting factors (climate-growth correlations increased for SPEI but decreased for temperature from wet to dry areas), the responses of NDVI to temperature were consistently negative throughout the whole investigated climatic gradient.

4.1. Climatic response of TRI and NDVI

Related to our first hypothesis, we expected weaker climate-growth correlations for NDVI compared to TRI since the greenness of the canopy, reflecting chlorophyll content or the dynamics of needle formation, is less climatically constrained compared to cambial activity (Kannenberg et al., 2020; Moreno-Fernández et al., 2022; Schwalm et al., 2017). Second, we assumed the climatic signal of both TRI and NDVI to change along environmental gradients, because both stem and leaf biomass formation depend on local climatic conditions (Babst et al., 2013). While we found support for the first hypothesis, the second has been challenged by the diverging trends in correlations of both biomass compartments with temperature along the climatic gradient.

Our research corroborates existing patterns of TRI response of PCAB to climate along a climatic gradient, as shown in studies that have focused on either lowland or mountain areas in temperate parts of Europe, as well as along elevational gradients (Leal et al., 2007; Hartl-Meier et al., 2014). In line with these studies, we found a strong positive temperature-growth correlation in cold/wet mountains (Babst et al., 2013; Ponocná et al., 2016; Rybníček et al., 2010) and a strong negative correlation to temperature in warm/dry lowlands (Rybníček et al., 2012; Babst et al., 2013). In warm and dry conditions of the lowlands, trees are limited by available moisture (SPEI), and high temperatures amplify drought stress by increasing potential water loss through evapotranspiration (Condon et al., 2020). By contrast, in cold, moist, and cloudy conditions in the mountains, stem growth is limited by low temperatures and short growing seasons making radial growth of trees highly sensitive to variations in summer temperature (Treml et al., 2015, 2012). The

optimal growth conditions of moisture-demanding and drought-sensitive PCAB in Central Europe are located around 1000 m a.s.l. (Mäkinen et al., 2002; Šagát et al., 2021; Tumajer et al., 2017). This is consistent with our nonsignificant correlations of TRI with both temperature and SPEI, i.e., with a weak climatic limitation of wood formation, at sites with an aridity index of around 1.8 roughly corresponding to elevations of 1000 m a.s.l. (Fig. 2).

In contrast, we observed a steady negative response of NDVI to June–August temperature throughout the entire climatic gradient. In warm and dry areas, the negative correlations of NDVI with temperature and the positive ones with SPEI are in line with low moisture availability, hence a drought limitation. This moisture signal of NDVI in dry areas is consistent with that of TRI, as also supported by the strong coherence of NDVI and TRI in drier areas (Fig. 4). The prevailingly positive response of NDVI to moisture availability across the drier part of the climatic gradient, as found in our study, is consistent with previously reported findings mainly from semi-arid regions worldwide (Pompa-García et al., 2021; Karnieli et al., 2010; Herrmann et al., 2016; Coulthard et al., 2017), from the temperate zone (Zhu et al., 2021; Babst et al., 2013; Pompa-García et al., 2022), but also from some boreal and subalpine regions (Beck et al., 2011; Liang et al., 2005, 2009; Tang et al., 2017; Zheng et al., 2021).

On the other hand, our finding of negative and insignificant responses of NDVI to temperature and SPEI in wet and cold areas (high mountains) is surprising because it contrasts with previous findings of a positive effect of temperature on NDVI in the coldest mountain forests (Huang et al., 2020; Li et al., 2015; Piedallu et al., 2019; Wang et al., 2011). There are studies that have reported negative correlations of NDVI with temperature even in cold environments for sites with shallow soils and a shallow root system, making trees sensitive to drought stress (Verbyla, 2015). However, this is less likely in our dataset as we did not find any significant drought signal in our tree-ring chronologies in cold/wet areas. Low growing season temperatures in the mountains of Central Europe are associated with cloudy conditions and hence a higher amount of diffuse radiation. Diffuse radiation is usually more effective in penetrating into the canopy compared to direct radiation (Urban et al., 2007, 2012). Consequently, light use efficiency and net ecosystem productivity, which are connected with NDVI (Wu and Niu, 2012; Yuan et al., 2007; Chai et al., 2019), were proven to increase in cloudy conditions with a high share of diffuse radiation (Dengel and Grace, 2010; Knohl and Baldocchi, 2008; Mercado et al., 2009; Schwalm et al., 2006; Zhang et al., 2010). Additionally, there is a decrease in photosynthetic rate (low chlorophyll content) because of reduced stomatal conductance during days with direct sunlight and high temperature (Urban et al., 2012). Besides chlorophyll content associated with clear-sky days, also active chlorophyll destruction due to tropospheric ozone production during hot summer days might contribute to negative NDVI correlations with temperature (Ainsworth et al., 2012; Anav et al., 2011, 2019) since Central Europe belongs to areas with high ozone loads in high elevations (Hůnová and Bäumelt, 2018; Chevalier et al., 2007). Additionally, there is a stronger dependence of the NDVI response to previous year's temperature at wet and cold sites (mainly June and July; Fig. S2). Trees in harsh environments tend to be influenced by conditions of the previous year (Treml et al., 2012; Correa-Díaz et al., 2019), so the negative response of NDVI to temperature in the current year might to some extent result from stronger lagged effects masking the influence of the current-year weather. We cannot decide which of the above-mentioned explanations is the most probable, however, we assume that each of them – a higher amount of direct radiation, low stomatal conductance, and increased tropospheric ozone concentrations during warm and sunny days – probably interact and jointly lead to the prevailing negative effect of temperature on NDVI values in cold/wet areas.

With respect to the methodological approach used in this study, there could be an influence of the chosen time window of the vegetation period for NDVI calculation (Vicente-Serrano et al., 2016), which might differ between sites. However, results for a longer or shifted time window of NDVI calculation (DOY 91–304) did not differ considerably. Similarly, Mašek et al. (2023) found for mountain spruce a weak negative climatic signal for the current growing season temperature, even though they applied flexible window for NDVI calculation starting at the bud burst date. Climatic signals in the NDVI series from mountain regions might have been distorted by historical crown defoliation because of intense nitrogen and sulfur deposition in the Czech Republic (Lomský et al., 2012). However, correlations of NDVI and TRI with defoliation inventory data for a subset of mountain sites in the northern Czech Republic did not reveal any systematic pattern (not shown), suggesting that both biomass compartments are not primarily sensitive to defoliation but rather respond to climatic variation. In addition, we believe that by detrending the time-series of NDVI, we eliminated the potential influence of defoliation.

Similar climate-growth correlations of both compartments in dry/warm areas but different climatic sensitivity at wet/cold sites explain decreasing correlations between TRI and NDVI with the aridity index. In addition, a portion of non-significant correlations between TRI and NDVI recorded at dry and intermediate locations could be ascribed to lagged effects of extreme droughts (Kannenberg et al., 2019). They are manifested differently in both biomass compartments due to different carbon allocation strategies. The high temperature associated with drought is known to reduce NDVI in a drought year (Brun et al., 2020; Rita et al., 2020), but this decrease might be followed by an increase of NDVI in order to gain more assimilates and restore the canopy damage (Anderegg et al., 2013b). Contrary to NDVI, tree-ring formation might be suppressed for up to four years after the dry spell (Wu et al., 2017). The length and magnitude of these legacy effects (Anderegg et al., 2015) could thus contribute to the decoupling of TRI and NDVI. Moreover, extreme drought resulting in forest defoliation may lead to higher NDVI values due to understory plant vegetation, which has a higher NDVI than the conifer canopy (Schlerf et al., 2007). On the other hand, high temperatures and drought turned out to be the strongest common growth-limiting factors for both biomass compartments in this study, leading to a synchronous, immediate growth response of both biomass compartments (negative to temperature, positive to SPEI). This highlights the high susceptibility of *Picea abies* growing in Central European temperate forests to drought.

Summarized, we here demonstrated diverging climatic drivers of TRI and NDVI and shifting correlations between stem biomass and canopy vigor along environmental (climatic) gradients, with drought being the strongest common growth-limiting factor. This complicates spatial upscaling of biomass trends of *Picea abies* forests observed from TRI by using NDVI derived from high-resolution satellite imagery, mainly in areas with climatically optimal growing conditions and towards the colder part of *Picea abies* species' range (Xu et al., 2019).

4.2. Effect of environmental conditions on climatic sensitivity of TRI and NDVI

The main predictor of the climatic signal of both TRI and NDVI was the aridity index, which reflects either limitation through low temperature (cold and wet areas) or through drought (dry and warm areas), as discussed in Section 4.1.

Besides the aridity index, one of the main significant predictors of the climate response of TRI was the stand age. Older stands exhibited higher sensitivity to low temperatures, whereas juvenile stands were more sensitive to drought. Both effects might be related to the fact that older, large trees are more exposed to ambient conditions (mainly temperature) while young, small trees grow in a more sheltered environment, however they also experience greater drought stress under competition pressure of larger trees with more developed root system (Zang et al., 2012; Kloeppel et al., 1993). We are aware that the age/size effects on the temperature signal strength also depend on the frequency component of the tree-ring time series and on the evaluated age ranges (Mašek et al., 2021; Konter et al., 2016).

The climatic response of NDVI was more influenced by topographical and soil variables compared to TRI which corroborates outcomes of other studies showing that inclusion of topographical variables increases robustness of models predicting NDVI (Misra et al., 2018; Lubenow and Reinhardt, 2020; Rita et al., 2020). Slope inclination was positively related to the correlation of NDVI and SPEI (high correlations at steep slopes) and negatively to the correlation of NDVI and temperature (low correlations at gentle slopes). At well drained steep slopes, the NDVI tends to decrease and be more sensitive to available moisture ((Del-Toro-Guerrero et al., 2019). Low values of topographic wetness index (low water accumulation) led to higher correlations between NDVI and temperature, at the same time the effect of topographic wetness index on correlations between NDVI and SPEI was insignificant. This pattern might be attributed to the position of the highest elevated stands usually located on well drained cold summit sites where biomass production is positively associated with temperature (Wang et al., 2021).

For our soil categories, we found significant effects on climate responses of NDVI mainly for extreme and moist soil categories as also shown by differences in slopes and intercepts of linear fits between climate-growth responses of NDVI and aridity index (Fig. S4), and between TRI and NDVI themselves (Fig. S5B). Sites located on extreme and moist soil categories revealed higher negative correlations of NDVI to temperature and lower correlations to SPEI, and also less pronounced trends in temperature-NDVI correlation along aridity gradient. Moist soils probably significantly decrease drought stress recorded in foliage greenness (Piedallu et al., 2019). Extreme soils are shallow and nutrient poor often with more open tree canopies compared to other soil categories. The lower correlations of NDVI to TRI and to climate might be there attributed either to additional limiting factors (e.g. nutrients, Jian-Sheng et al., 2018) or to higher noise associated with dynamic of ground vegetation (Wang et al., 2022).

5. Conclusions

We demonstrated that climatic constraints of tree-ring widths (a proxy for stem biomass) and NDVI (a proxy for canopy vigor) of *Picea abies* are decoupled across environmental gradients. While tree-ring width followed the expected pattern with drought limitation in warm/dry areas and temperature limitation in cold/wet areas, the responses of NDVI were negative to temperature throughout the entire climatic gradient. Within the climatic gradient covered in our study, tree rings tend to agree with NDVI at its warm and dry edges, i.e., in the lowlands. This emphasizes the strong susceptibility of *P. abies* to drought, as under warm/dry conditions, both tested compartments respond synchronously negative. The response of NDVI is probably influenced by joint effects of direct radiation and tropospheric ozone which all negatively affect leaf greenness during warm and sunny days in mountains and counteract the positive effect of temperature on leaf formation and photosynthesis. The pattern of climate-growth correlations of both tree rings and NDVI is mainly explained by site climatic conditions (aridity index). The responses of tree rings were then influenced by stand age while NDVI revealed the influence of local topography and soil conditions. Our results advocate against the upscaling of *Picea abies* tree rings by Landsat-derived NDVI to assess forest growth trends and vigor outside of warm/dry part of *Picea abies* distribution. Further research is needed to assess the responses of other species and larger spatial scales under ongoing global change.

Funding

The study was funded by the Centre for Landscape and Biodiversity DivLand (Technology Agency of Czech Republic [SS02030018]). J.T. was supported by Charles University [UNCE/HUM 018]. M.Ryb. and T. K. were supported by Czech Science Foundation [23-07583S]. J.L. received personal support from an Alexander von Humboldt Foundation fellowship for Postdoctoral researchers (Feodor Lynen Fellowship). M.V. acknowledges funding by the Ministry of Agriculture of the Czech Republic, institutional support [MZE-RO0123].

CRediT authorship contribution statement

JM: Conceptualization, Methodology, Formal analysis, Software.
VT: Conceptualization, Methodology, Formal analysis, Supervision.
JT: Methodology.
MJ, ON: Data curation (climatic data).
TCH: Data curation (categories data).
JM, VT, JT, MS, VČ, MV, PŠ, IV, MRyd, JK, RK, TK, MRyb: Data curation (tree ring data).
JM, VT, JT, JL, JK, TK, MRyb, PŠ, IV, MV, MJ, TCh, MH: Writing - original draft.

Declaration of competing interest

The author declares no conflict of interest.

Data availability

Tree ring data are accessible through the TreeDataClim database (www.treedataclim.cz).

Climatic grids and shapefile of soil categories will be provided on request.

The GEE script for the calculation of the NDVI time-series is accessible here: https://code.earthengine.google.com/a04787fa38c83987be3cdee48192301e

R script with all calculations and figure drawings is available here: https://github.com/JirkaSkaut/PCAB_clima_responses

Acknowledgment

We are grateful to the Centre for Landscape and Biodiversity DivLand (TAČR SS02030018) for financial support. We appreciate the permission and help of protected areas authorities and forest managers. Thanks to all people who helped with collecting data in the field.

Appendix A. Supplementary data

Supplementary data to this article can be found online at https://doi.org/10.1016/j.scitotenv.2023.168275.

References

Ainsworth, E.A., Yendrek, C.R., Sitch, S., Collins, W.J., Emberson, L.D., 2012. The effects of tropospheric ozone on net primary productivity and implications for climate change. Annu. Rev. Plant Biol. 63, 637–661. https://doi.org/10.1146/annurev-arplant-042110-103829.

Allen, C.D., Macalady, A.K., Chenchouni, H., Bachelet, D., McDowell, N., Vennetier, M., Kitzberger, T., Rigling, A., Breshears, D.D., Hogg, E.H., Gonzalez, P., Fensham, R., Zhang, Z., Castro, J., Demidova, N., Lim, J.H., Allard, G., Running, S.W., Semerci, A., Cobb, N., 2010. A global overview of drought and heat-induced tree mortality reveals emerging climate change risks for forests. For. Ecol. Manage. 259, 660–684. https://doi.org/10.1016/j.foreco.2009.09.001.

Anav, A., Menut, L., Khvorostyanov, D., Viovy, N., 2011. Impact of tropospheric ozone on the Euro-Mediterranean vegetation. Glob. Chang. Biol. 17, 2342–2359. https://doi.org/10.1111/j.1365-2486.2010.02387.x.

Anav, A., De Marco, A., Friedlingstein, P., Savi, F., Sicard, P., Sitch, S., Vitale, M., Paoletti, E., 2019. Growing season extension affects ozone uptake by European forests. Sci. Total Environ. 669, 1043–1052. https://doi.org/10.1016/j.scitotenv.2019.03.020.

Anderegg, W.R.L., Kane, J.M., Anderegg, L.D.L., 2013a. Consequences of widespread tree mortality triggered by drought and temperature stress. Nat. Clim. Chang. 3, 30–36. https://doi.org/10.1038/nclimate1635.

Anderegg, W.R.L., Plavcová, L., Anderegg, L.D.L., Hacke, U.G., Berry, J.A., Field, C.B., 2013b. Drought's legacy: multiyear hydraulic deterioration underlies widespread aspen forest die-off and portends increased future risk. Glob. Chang. Biol. 19, 1188–1196. https://doi.org/10.1111/gcb.12100.

Anderegg, W.R.L., Schwalm, C., Biondi, F., Camarero, J.J., Koch, G., Litvak, M., Ogle, K., Shaw, J.D., Shevliakova, E., Williams, A.P., Wolf, A., Ziaco, E., Pacala, S., 2015. Pervasive drought legacies in forest ecosystems and their implications for carbon

cycle models. Science (80-.) 349, 528–532. https://doi.org/10.1126/science.aab1833.
Anselin, L., 1988. Spatial Econometrics: Methods and Models. Springer.
Anselin, L., Bera, A.K., Florax, R., Yoon, M.J., 1996. Simple diagnostic tests for spatial dependence. Reg. Sci. Urban Econ. 26, 77–104. https://doi.org/10.1016/0166-0462(95)02111-6.
Babst, F., Poulter, B., Trouet, V., Tan, K., Neuwirth, B., Wilson, R., Carrer, M., Grabner, M., Tegel, W., Levanic, T., Panayotov, M., Urbinati, C., Bouriaud, O., Ciais, P., Frank, D., 2013. Site- and species-specific responses of forest growth to climate across the European continent. Glob. Ecol. Biogeogr. 22, 706–717. https://doi.org/10.1111/geb.12023.
Babst, F., Poulter, B., Bodesheim, P., Mahecha, M.D., Frank, D.C., 2017. Improved tree-ring archives will support earth-system science. Nat. Ecol. Evol. 1, 1–2. https://doi.org/10.1038/s41559-016-0008.
Babst, F., Bodesheim, P., Charney, N., Friend, A.D., Girardin, M.P., Klesse, S., Moore, D.J. P., Seftigen, K., Björklund, J., Bouriaud, O., Dawson, A., DeRose, R.J., Dietze, M.C., Eckes, A.H., Enquist, B., Frank, D.C., Mahecha, M.D., Poulter, B., Record, S., Trouet, V., Turton, R.H., Zhang, Z., Evans, M.E.K., 2018. When tree rings go global: challenges and opportunities for retro- and prospective insight. Quat. Sci. Rev. https://doi.org/10.1016/j.quascirev.2018.07.009.
Beck, P.S.A., Juday, G.P., Alix, C., Barber, V.A., Winslow, S.E., Sousa, E.E., Heiser, P., Herriges, J.D., Goetz, S.J., 2011. Changes in forest productivity across Alaska consistent with biome shift. Ecol. Lett. 14, 373–379. https://doi.org/10.1111/j.1461-0248.2011.01598.x.
Beck, P.S.A., Andreu-Hayles, L., D'Arrigo, R., Anchukaitis, K.J., Tucker, C.J., Pinzón, J.E., Goetz, S.J., 2013. A large-scale coherent signal of canopy status in maximum latewood density of tree rings at arctic treeline in North America. Glob. Planet. Chang. 100, 109–118. https://doi.org/10.1016/j.gloplacha.2012.10.005.
Beguería, S., Vicente-Serrano, S.M., 2023. SPEI: calculation of the standardized precipitation-evapotranspiration index. R package version 1.8.0. https://CRAN.R-project.org/package=SPEI.
Bernoulli, M., Körner, C., 1999. Dry matter allocation in treeline trees. Ann. Rei Bot. 39, 7–12.
Beven, K.J., Kirkby, M.J., 1979. A physically based, variable contributing area model of basin hydrology. Hydrol. Sci. Bull. 24, 43–69. https://doi.org/10.1080/02626667909491834.
Bhuyan, U., Zang, C., Vicente-Serrano, S.M., Menzel, A., 2017. Exploring relationships among tree-ring growth, climate variability, and seasonal leaf activity on varying timescales and spatial resolutions. Remote Sens. (Basel) 9. https://doi.org/10.3390/rs9060526.
Bivand, R., Keitt, T., Rowlingson, B., 2023. rgdal: bindings for the 'Geospatial' data abstraction library. R package version 1.6-4. https://CRAN.R-project.org/package=rgdal.
Bonan, B.G., 2008. Forests and climate change: forcings, feedbacks, and the climate benefits of forests. Science (80-.) 320, 1444–1449. https://doi.org/10.1126/science.1155121.
Brehaut, L., Danby, R.K., 2018. Inconsistent relationships between annual tree ring-widths and satellite-measured NDVI in a mountainous subarctic environment. Ecol. Indic. 91, 698–711. https://doi.org/10.1016/j.ecolind.2018.04.052.
Brun, P., Psomas, A., Ginzler, C., Thuiller, W., Zappa, M., Zimmermann, N.E., 2020. Large-scale early-wilting response of central European forests to the 2018 extreme drought. Glob. Chang. Biol. 26, 7021–7035. https://doi.org/10.1111/gcb.15360.
Bunn, A., Korpela, M., Biondi, F., Campelo, F., Mérian, P., Qeadan, F., Zang, C., 2022. dplR: dendrochronology program library in R. R package version 1.7.4. https://CRAN.R-project.org/package=dplR.
Cabon, A., Peters, R.L., Fonti, P., Martínez-Vilalta, J., De Cáceres, M., 2020. Temperature and water potential co-limit stem cambial activity along a steep elevational gradient. New Phytol. 226, 1325–1340. https://doi.org/10.1111/nph.16456.
Carrer, M., Urbinati, C., 2004. Age-dependent tree-ring growth responses to climate in Larix decidua and Pinus cembra. Ecology 85, 730–740.
Caudullo, G., Welk, E., San-Miguel-Ayanz, J., 2017. Chorological maps for the main European woody species. Data Brief 12, 662–666. https://doi.org/10.1016/j.dib.2017.05.007.
Chai, X., Shi, P., Song, M., Zong, N., He, Y., Zhao, G., Zhang, X., 2019. Carbon flux phenology and net ecosystem productivity simulated by a bioclimatic index in an alpine steppe-meadow on the Tibetan Plateau. Ecol. Model. 394, 66–75. https://doi.org/10.1016/j.ecolmodel.2018.12.024.
Chevalier, A., Gheusi, F., Delmas, R., Ordóñez, C., Sarrat, C., Zbinden, R., Thouret, V., Athier, G., Cousin, J.-M., 2007. Atmospheric chemistry and physics influence of altitude on ozone levels and variability in the lower troposphere: a ground-based study for western Europe over the period 2001-2004. Atmos. Chem. Phys. 7, 4311–4326.
ČHMÚ (Czech Hydrometeorological Institute), 2023. https://www.chmi.cz/ [13.7.2023].
Condon, L.E., Atchley, A.L., Maxwell, R.M., 2020. Evapotranspiration depletes groundwater under warming over the contiguous United States. Nat. Commun. 11 https://doi.org/10.1038/s41467-020-14688-0.
Cook, R.E., Peters, K., 1981. The smoothing spline: a new approach to standardizing forest interior tree-ring width series for dendroclimatic studies. Tree-Ring Bull. 41, 45–53.
Correa-Díaz, A., Silva, L.C.R., Horwath, W.R., Gómez-Guerrero, A., Vargas-Hernández, J., Villanueva-Díaz, J., 2019. Linking remote sensing and dendrochronology to quantify climate-induced shifts in high-elevation forests over space and time. Eur. J. Vasc. Endovasc. Surg. 124, 166–183. https://doi.org/10.1029/2018JG004687.
Coulthard, B.L., Touchan, R., Anchukaitis, K.J., Meko, D.M., Sivrikaya, F., 2017. Tree growth and vegetation activity at the ecosystem-scale in the eastern Mediterranean. Environ. Res. Lett. 12 https://doi.org/10.1088/1748-9326/aa7b26.
ČÚZK (Czech Office for Surveying, Mapping and Cadastre), 2013. Digital Model of Relief of Czech Republic, 4th Generation.
D'Andrea, G., Šimůnek, V., Castellaneta, M., Vacek, Z., Vacek, S., Pericolo, O., Zito, R.G., Ripullone, F., 2022. Mismatch between annual tree-ring width growth and NDVI index in Norway spruce stands of Central Europe. Forests 13, 1–16. https://doi.org/10.3390/f13091417.
Del-Toro-Guerrero, F.J., Kretzschmar, T., Bullock, S.H., 2019. Precipitation and topography modulate vegetation greenness in the mountains of Baja California, México. Int. J. Biometeorol. 63, 1425–1435. https://doi.org/10.1007/s00484-019-01763-5.
Dengel, S., Grace, J., 2010. Carbon dioxide exchange and canopy conductance of two coniferous forests under various sky conditions. Oecologia 164, 797–808. https://doi.org/10.1007/s00442-010-1687-0.
Donohue, R.J., Roderick, M.L., McVicar, T.R., Farquhar, G.D., 2013. Impact of CO2 fertilization on maximum foliage cover across the globe's warm, arid environments. Geophys. Res. Lett. 40, 3031–3035. https://doi.org/10.1002/grl.50563.
Dormann, F.C., McPherson, J.M., Araújo, M.B., Bivand, R., Bolliger, J., Carl, G., Davies, R.G., Hirzel, A., Jetz, W., Daniel Kissling, W., Kühn, I., Ohlemüller, R., Peres-Neto, P.R., Reineking, B., Schröder, B., Schurr, F.M., Wilson, R., 2007. Methods to account for spatial autocorrelation in the analysis of species distributional data: a review. Ecography 30, 609–628. https://doi.org/10.1111/j.2007.0906-7590.05171.x.
ESRI (Environmental Systems Research Institute), 2020. ArgcGIS Desktop 10.7.1. Redlands, CA.
Fatichi, S., Leuzinger, S., Körner, C., 2014. Moving beyond photosynthesis: from carbon source to sink-driven vegetation modeling. New Phytol. 201, 1086–1095.
Fox, J., Weisberg, S., 2019. An R Companion to Applied Regression. SAGE Publications Ltd.
Fritts, H.C., 1976. Tree Rings and Climate. Academic Press. https://doi.org/10.1016/b978-0-12-268450-0.x5001-0.
Gazol, A., Camarero, J.J., Vicente-Serrano, S.M., Sánchez-Salguero, R., Gutiérrez, E., de Luis, M., Sangüesa-Barreda, G., Novak, K., Rozas, V., Tíscar, P.A., Linares, J.C., Martín-Hernández, N., Martínez del Castillo, E., Ribas, M., García-González, I., Silla, F., Camisón, A., Génova, M., Olano, J.M., Longares, L.A., Hevia, A., Tomás-Burguera, M., Galván, J.D., 2018. Forest resilience to drought varies across biomes. Glob. Chang. Biol. 24, 2143–2158. https://doi.org/10.1111/gcb.14082.
Girardin, M.P., Bouriaud, O., Hogg, E.H., Kurz, W., Zimmermann, N.E., Metsaranta, J.M., De Jong, R., Frank, D.C., Esper, J., Büntgen, U., Guo, X.J., Bhatti, J., 2016. No growth stimulation of Canada's boreal forest under half-century of combined warming and CO2 fertilization. Proc. Natl. Acad. Sci. U. S. A. 113, E8406–E8414. https://doi.org/10.1073/pnas.1610156113.
Gorelick, N., Hancher, M., Dixon, M., Ilyushchenko, S., Thau, D., Moore, R., 2017. Google earth engine: planetary-scale geospatial analysis for everyone. Remote Sens. Environ. 202, 18–27. https://doi.org/10.1016/j.rse.2017.06.031.
Hartl-Meier, C., Zang, C., Dittmar, C., Esper, J., Göttlein, A., Rothe, A., 2014. Vulnerability of Norway spruce to climate change in mountain forests of the European Alps. Climate Res. 60, 119–132. https://doi.org/10.3354/cr01226.
Herrmann, S.M., Didan, K., Barreto-Munoz, A., Crimmins, M.A., 2016. Divergent responses of vegetation cover in Southwestern US ecosystems to dry and wet years at different elevations. Environ. Res. Lett. 11 https://doi.org/10.1088/1748-9326/11/12/124005.
Hijmans, R., 2023. raster: geographic data analysis and modeling. R package version 3.6-14. https://CRAN.R-project.org/package=raster.
Huang, K., Yi, C., Wu, D., Zhou, T., Zhao, X., Blanford, W.J., Wei, S., Wu, H., Ling, D., Li, Z., 2015. Tipping point of a conifer forest ecosystem under severe drought. Environ. Res. Lett. 10 https://doi.org/10.1088/1748-9326/10/2/024011.
Huang, C., Yang, Q., Guo, Y., Zhang, Y., Guo, L., 2020. The pattern, change and driven factors of vegetation cover in the Qin Mountains region. Sci. Rep. 10, 1–11. https://doi.org/10.1038/s41598-020-75845-5.
Hůnová, I., Bäumelt, V., 2018. Observation-based trends in ambient ozone in the Czech Republic over the past two decades. Atmos. Environ. 172, 157–167. https://doi.org/10.1016/j.atmosenv.2017.10.039.
Jian-Sheng, Y., Jiu-Ying, P., Chan, F., 2018. Under which climate and soil conditions the plant productivity–precipitation relationship is linear or nonlinear? Sci. Total Environ. 616–617, 1174–1180. https://doi.org/10.1016/j.scitotenv.2017.10.203.
Kannenberg, S.A., Novick, K.A., Alexander, M.R., Maxwell, J.T., Moore, D.J.P., Phillips, R.P., Anderegg, W.R.L., 2019. Linking drought legacy effects across scales: from leaves to tree rings to ecosystems. Glob. Chang. Biol. 25, 2978–2992. https://doi.org/10.1111/gcb.14710.
Kannenberg, S.A., Schwalm, C.R., Anderegg, W.R.L., 2020. Ghosts of the past: how drought legacy effects shape forest functioning and carbon cycling. Ecol. Lett. https://doi.org/10.1111/ele.13485.
Karnieli, A., Agam, N., Pinker, R.T., Anderson, M., Imhoff, M.L., Gutman, G.G., Panov, N., Goldberg, A., 2010. Use of NDVI and land surface temperature for drought assessment: merits and limitations. J. Climate 23, 618–633. https://doi.org/10.1175/2009JCLI2900.1.
Kaufmann, R.K., D'Arrigo, R.D., Paletta, L.F., Tian, H.Q., Jolly, W.M., Myneni, R.B., 2008. Identifying climatic controls on ring width: the timing of correlations between tree rings and NDVI. Earth Interact. 12, 1–14. https://doi.org/10.1175/2008EI263.1.
Kissling, W.D., Carl, G., 2008. Spatial autocorrelation and the selection of simultaneous autoregressive models. Glob. Ecol. Biogeogr. 17, 59–71. https://doi.org/10.1111/j.1466-8238.2007.00334.x.

Kloeppel, B.D., Abrams, M.D., Kubiske, M.E., 1993. Seasonal ecophysiology and leaf morphology of four successional Pennsylvania barrens species in open versus understory environments. Can. J. For. Res. 23, 181–189. https://doi.org/10.1139/x93-025.

Knohl, A., Baldocchi, D.D., 2008. Effects of diffuse radiation on canopy gas exchange processes in a forest ecosystem. J. Geophys. Res. Biogeo. 113 https://doi.org/10.1029/2007JG000663.

Konter, O., Büntgen, U., Carrer, M., Timonen, M., Esper, J., 2016. Climate signal age effects in boreal tree-rings: lessons to be learned for paleoclimatic reconstructions. Quat. Sci. Rev. 142, 164–172. https://doi.org/10.1016/j.quascirev.2016.04.020.

Kraus, C., Zang, C., Menzel, A., 2016. Elevational response in leaf and xylem phenology reveals different prolongation of growing period of common beech and Norway spruce under warming conditions in the Bavarian Alps. Eur. J. For. Res. 135, 1011–1023. https://doi.org/10.1007/s10342-016-0990-7.

Leal, S., Melvin, T.M., Grabner, M., Wimmer, R., Briffa, K.R., 2007. Tree-ring growth variability in the Austrian Alps: the influence of site, altitude, tree species and climate. Boreas 36, 426–440. https://doi.org/10.1080/03009480701267063.

Lévesque, M., Saurer, M., Siegwolf, R., Eilmann, B., Brang, P., Bugmann, H., Rigling, A., 2013. Drought response of five conifer species under contrasting water availability suggests high vulnerability of Norway spruce and European larch. Glob. Chang. Biol. 19, 3184–3199. https://doi.org/10.1111/gcb.12268.

Li, H., Li, Y., Shen, W., Li, Y., Lin, J., Lu, X., Xu, X., Jiang, J., 2015. Elevation-dependent vegetation greening of the Yarlung Zangbo River basin in the Southern Tibetan Plateau, 1999-2013. Remote Sens. (Basel) 7, 16672–16687. https://doi.org/10.3390/rs71215844.

Liang, E.Y., Shao, X.M., He, J.C., 2005. Relationships between tree growth and NDVI of grassland in the semi-arid grassland of north China. Int. J. Remote Sens. 26, 2901–2908. https://doi.org/10.1080/01431160500056931.

Liang, E., Eckstein, D., Liu, H., 2009. Assessing the recent grassland greening trend in a long-term context based on tree-ring analysis: a case study in North China. Ecol. Indic. 9, 1280–1283. https://doi.org/10.1016/j.ecolind.2009.02.007.

Lomský, B., Šrámek, V., Novotný, R., 2012. Changes in the air pollution load in the Jizera Mts.: effects on the health status and mineral nutrition of the young Norway spruce stands. Eur. J. For. Res. 131, 757–771. https://doi.org/10.1007/s10342-011-0549-6.

Lubenow, D.R., Reinhardt, K., 2020. The environmental drivers of annual variation in forest greenness arevariable in the northern Intermountain West, USA. Ecosphere 11 (8), e03212. https://doi.org/10.1002/ecs2.3212.

Mäkinen, H., Nöjd, P., Kahle, H.-P., Neumann, U., Tveite, B., Mielikäinen, K., Röhle, H., Spiecker, H., 2002. Radial growth variation of Norway spruce (Picea abies (L.) Karst.) across latitudinal and altitudinal gradients in central and northern Europe. For. Ecol. Manage. 171, 243–259.

Mašek, J., Tumajer, J., Rydval, M., Lange, J., Treml, V., 2021. Age and size outperform topographic effects on growth-climate responses of trees in two Central European coniferous forest types. Dendrochronologia 68, 125845. https://doi.org/10.1016/j.dendro.2021.125845.

Mašek, J., Tumajer, J., Lange, J., Kaczka, R., Fišer, P., Treml, V., 2023. Variability in tree-ring width and NDVI responses to climate at a landscape level. Ecosystems. https://doi.org/10.1007/s10021-023-00822-8.

McCune, B., Keon, D., 2002. Equations for potential annual direct incident radiation and heat load-603. J. Veg. Sci. 13, 603–606.

Mercado, L.M., Bellouin, N., Sitch, S., Boucher, O., Huntingford, C., Wild, M., Cox, P.M., 2009. Impact of changes in diffuse radiation on the global land carbon sink. Nature 458, 1014–1017. https://doi.org/10.1038/nature07949.

Misra, G., Buras, A., Heurich, M., Asam, S., Menzel, A., 2018. LiDAR derived topography and forest stand characteristics largely explain the spatial variability observed in MODIS land surface phenology. Remote Sens. Environ. 218, 231–244. https://doi.org/10.1016/j.rse.2018.09.027.

Moreno-Fernández, D., Julio Camarero, J., García, M., Lines, E.R., Sánchez-Dávila, J., Tijerín, J., Valeriano, C., Viana-Soto, A., Ruiz-Benito, P., 2022. The interplay of the tree and stand-level processes mediate drought-induced forest dieback: evidence from complementary remote sensing and tree-ring approaches. Ecosystems 25, 1738–1753. https://doi.org/10.1007/s10021-022-0079.

NASA (National Aeronautics and Space Administration), 2022. Measuring vegetation NDVI and EVI. Normalized Difference Vegetation Index (NDVI). https://earthobservatory.nasa.gov/features/MeasuringVegetation/measuring_vegetation_2.php [27.6.2023].

Pearl, J.K., Keck, J.R., Tintor, W., Siekacz, L., Herrick, H.M., Meko, M.D., Pearson, C.L., 2020. New frontiers in tree-ring research. Holocene 30, 923–941. https://doi.org/10.1177/0959683620902230.

Pebesma, E.J., 2004. Multivariable geostatistics in S: the gstat package. Comput. Geosci. 30, 683–691. https://doi.org/10.1016/j.cageo.2004.03.012.

Pebesma, E., Bivand, R., 2023. Spatial Data Science With Applications in R. Chapman & Hall.

Peng, D., Zhang, B., Liu, L., Fang, H., Chen, D., Hu, Y., Liu, L., 2012. Characteristics and drivers of global NDVI-based FPAR from 1982 to 2006. Global Biogeochem. Cycles 26. https://doi.org/10.1029/2011GB004060.

Piedallu, C., Chéret, V., Denux, J.P., Perez, V., Azcona, J.S., Seynave, I., Gégout, J.C., 2019. Soil and climate differently impact NDVI patterns according to the season and the stand type. Sci. Total Environ. 651, 2874–2885. https://doi.org/10.1016/j.scitotenv.2018.10.052.

Pierce, D., 2023. ncdf4: interface to unidata netCDF (version 4 or earlier) format data files. R package version 1.21. https://CRAN.R-project.org/package=ncdf4.

Pompa-García, M., Camarero, J.J., Colangelo, M., González-Cásares, M., 2021. Inter and intra-annual links between climate, tree growth and NDVI: improving the resolution of drought proxies in conifer forests. Int. J. Biometeorol. 65, 2111–2121. https://doi.org/10.1007/s00484-021-02170-5.

Pompa-García, M., Vivar-Vivar, E.D., Sigala-Rodríguez, J.A., Padilla-Martínez, J.R., 2022. What are contemporary Mexican conifers telling us? A perspective offered from tree rings linked to climate and the NDVI along a spatial gradient. Remote Sens. (Basel) 14. https://doi.org/10.3390/rs14184506.

Ponocná, T., Spyt, B., Kaczka, R., Büntgen, U., Treml, V., 2016. Growth trends and climate responses of Norway spruce along elevational gradients in East-Central Europe. Trees - Struct. Funct. 30, 1633–1646. https://doi.org/10.1007/s00468-016-1396-3.

R Core Team, 2022. R: A Language and Environment for Statistical Computing. R Foundation for Statistical Computing, Vienna, Austria. URL. https://www.R-project.org/.

Rita, A., Camarero, J.J., Nolè, A., Borghetti, M., Brunetti, M., Pergola, N., Serio, C., Vicente-Serrano, S.M., Tramutoli, V., Ripullone, F., 2020. The impact of drought spells on forests depends on site conditions: the case of 2017 summer heat wave in southern Europe. Glob. Chang. Biol. 26, 851–863. https://doi.org/10.1111/gcb.14825.

Rossi, S., Deslauriers, A., Anfodillo, T., Carraro, V., 2007. Evidence of threshold temperatures for xylogenesis in conifers at high altitudes. Oecologia 152, 1–12. https://doi.org/10.1007/s00442-006-0625-7.

Roy, D.P., Kovalskyy, V., Zhang, H.K., Vermote, E.F., Yan, L., Kumar, S.S., Egorov, A., 2016. Characterization of Landsat-7 to Landsat-8 reflective wavelength and normalized difference vegetation index continuity. Remote Sens. Environ. 185, 57–70. https://doi.org/10.1016/j.rse.2015.12.024.

Rybníček, M., Čermák, P., Žid, T., Kolář, T., 2010. Radial growth and health condition of Norway spruce (Picea abies (L.) Karst.) stands in relation to climate (Silesian Beskids, Czech Republic). Geochronometria 36, 9–16. https://doi.org/10.2478/v10003-010-0017-1.

Rybníček, M., Čermák, P., Kolář, T., Žid, T., 2012. Growth responses of Norway spruce (Picea abies (L.) Karst.) to the climate in the South-Eastern part of the ceskomoravská upland (Czech Republic). Geochronometria 39, 149–157. https://doi.org/10.2478/s13386-012-0003-7.

Šagát, V., Ružek, I., Šilhán, K., Beracko, P., 2021. The impact of local climate change on radial Picea abies growth: a case study in natural mountain spruce stand and low-lying spruce monoculture. Forests 12, 1–20. https://doi.org/10.3390/f12081118.

Schiestl-Aalto, P., Ryhti, K., Mäkelä, A., Peltoniemi, M., Bäck, J., Kulmala, L., 2019. Analysis of the NSC storage dynamics in tree organs reveals the allocation to belowground symbionts in the framework of whole tree carbon balance. Front. For. Glob. Chang. 2, 1–14. https://doi.org/10.3389/ffgc.2019.00017.

Schlerf, M., Verhoef, W., Buddenbaum, H., Hill, J., Atzberger, C., Skidmore, A., 2007. Comparing three canopy reflectance models with hyperspectral multi-angular satellite data. In: Schaepman, M., Liang, S., Groot, N., Kneubühler, M. (Eds.), 10th ISPMSRS. Intl. Archives of the Photogrammetry, Remote Sensing and Spatial Information Science, Davos, Switzerland, pp. 404–407.

Schmied, G., Hilmers, T., Mellert, K.H., Uhl, E., Buness, V., Ambs, D., Steckel, M., Biber, P., Šeho, M., Hoffmann, Y.D., Pretzsch, H., 2023. Nutrient regime modulates drought response patterns of three temperate tree species. Sci. Total Environ. 868 https://doi.org/10.1016/j.scitotenv.2023.161601.

Schwalm, C.R., Black, T.A., Amiro, B.D., Arain, M.A., Barr, A.G., Bourque, C.P.A., Dunn, A.L., Flanagan, L.B., Giasson, M.A., Lafleur, P.M., Margolis, H.A., McCaughey, J.H., Orchansky, A.L., Wofsy, S.C., 2006. Photosynthetic light use efficiency of three biomes across an east-west continental-scale transect in Canada. Agric. For. Meteorol. 140, 269–286. https://doi.org/10.1016/j.agrformet.2006.06.010.

Schwalm, C.R., Anderegg, W.R.L., Michalak, A.M., Fisher, J.B., Biondi, F., Koch, G., Litvak, M., Ogle, K., Shaw, J.D., Wolf, A., Huntzinger, D.N., Schaefer, K., Cook, R., Wei, Y., Fang, Y., Hayes, D., Huang, M., Jain, A., Tian, H., 2017. Global patterns of drought recovery. Nature 548, 202–205. https://doi.org/10.1038/nature23021.

Seftigen, K., Frank, D.C., Björklund, J., Babst, F., Poulter, B., 2018. The climatic drivers of normalized difference vegetation index and tree-ring-based estimates of forest productivity are spatially coherent but temporally decoupled in Northern Hemispheric forests. Glob. Ecol. Biogeogr. 27, 1352–1365. https://doi.org/10.1111/geb.12802.

Simard, S., Giovannelli, A., Treydte, K., Traversi, M.L., King, G.M., Frank, D., Fonti, P., 2013. Intra-annual dynamics of non-structural carbohydrates in the cambium of mature conifer trees reflects radial growth demands. Tree Physiol. 33, 913–923. https://doi.org/10.1093/treephys/tpt075.

Song, C., 2012. Optical remote sensing of forest leaf area index and biomass. Prog. Phys. Geogr. 37, 98–113. https://doi.org/10.1177/0309133312471367.

Spiecker, H., 2000. Growth of Norway spruce (Picea abies [L.] karst.) under changing environmental conditions in Europe. In: Klimo, E., Hager, H., Kulhavý, J. (Eds.), Spruce Monocultures in Central Europe – Problems and Prospects. European Forest Institute, p. 208.

Sprenger, M., Stumpp, C., Weiler, M., Aeschbach, W., Allen, S.T., Benettin, P., Dubbert, M., Hartmann, A., Hrachowitz, M., Kirchner, J.W., McDonnell, J.J., Orlowski, N., Penna, D., Pfahl, S., Rinderer, M., Rodriguez, N., Schmidt, M., Werner, C., 2019. The demographics of water: a review of water ages in the critical zone. Rev. Geophys. 57, 800–834. https://doi.org/10.1029/2018RG000633.

Stephenson, N.L., Das, A.J., Condit, R., Russo, S.E., Baker, P.J., Beckman, N.G., Coomes, D.A., Lines, E.R., Morris, W.K., Rüger, N., Álvarez, E., Blundo, C., Bunyavejchewin, S., Chuyong, G., Davies, S.J., Duque, Á., Ewango, C.N., Flores, O., Franklin, J.F., Grau, H.R., Hao, Z., Harmon, M.E., Hubbell, S.P., Kenfack, D., Lin, Y., Makana, J.R., Malizia, A., Malizia, L.R., Pabst, R.J., Pongpattananurak, N., Su, S.H., Sun, I.F., Tan, S., Thomas, D., Van Mantgem, P.J., Wang, X., Wiser, S.K., Zavala, M.

A., 2014. Rate of tree carbon accumulation increases continuously with tree size. Nature 507, 90–93. https://doi.org/10.1038/nature12914.
Tang, Z., Ma, J., Peng, H., Wang, S., Wei, J., 2017. Spatiotemporal changes of vegetation and their responses to temperature and precipitation in upper Shiyang river basin. Adv. Space Res. 60, 969–979. https://doi.org/10.1016/j.asr.2017.05.033.
Thornthwaite, C.W., 1948. An approach toward a rational classification of climate. Geogr. Rev. 38, 55. https://doi.org/10.2307/210739.
Toomey, M., Friedl, M.A., Frolking, S., Hufkens, K., Klosterman, S., Sonnentag, O., Baldocchi, D.D., Bernacchi, C.J., Biraud, S.C., Bohrer, G., Brzostek, E., Burns, S.P., Coursolle, C., Hollinger, D.Y., Margolis, H.A., McCaughey, H., Monson, R.K., Munger, J.W., Pallardy, S., Phillips, R.P., Torn, M.S., Wharton, S., Zeri, M., Richardson, A.D., 2015. Greenness indices from digital cameras predict the timing and seasonal dynamics of canopy-scale photosynthesis. Ecol. Appl. 25, 99–115. https://doi.org/10.1890/14-0005.1.
Treml, V., Ponocná, T., Büntgen, U., 2012. Growth trends and temperature responses of treeline Norway spruce in the Czech-Polish Sudetes Mountains. Climate Res. 55, 91–103. https://doi.org/10.3354/cr01122.
Treml, V., Ponocná, T., King, G.M., Büntgen, U., 2015. A new tree-ring-based summer temperature reconstruction over the last three centuries for east-Central Europe. Int. J. Climatol. 35, 3160–3171. https://doi.org/10.1002/joc.4201.
Treml, V., Mašek, J., Tumajer, J., Rydval, M., Čada, V., Ledvinka, O., Svoboda, M., 2022. Trends in climatically driven extreme growth reductions of Picea abies and Pinus sylvestris in Central Europe. Glob. Chang. Biol. 1–14. https://doi.org/10.1111/gcb.15922.
Trouillier, M., van der Maaten-Theunissen, M., Scharnweber, T., Würth, D., Burger, A., Schnittler, M., Wilmking, M., 2019. Size matters—a comparison of three methods to assess age- and size-dependent climate sensitivity of trees. Trees - Struct. Funct. 33, 183–192. https://doi.org/10.1007/s00468-018-1767-z.
Tucker, C.J., 1979. Red and photographic infrared linear combinations for monitoring vegetation. Remote Sens. Environ. 8, 127–150.
Tumajer, J., Altman, J., Štěpánek, P., Treml, V., Doležal, J., Cienciala, E., 2017. Increasing moisture limitation of Norway spruce in Central Europe revealed by forward modelling of tree growth in tree-ring network. Agric. For. Meteorol. 247, 56–64. https://doi.org/10.1016/j.agrformet.2017.07.015.
UNEP, 1993. World Atlas of Desertification. The United Nations Environment Programme (UNEP), London.
Urban, O., Janouš, D., Acosta, M., Czerný, R., Marková, I., Navrátil, M., Pavelka, M., Pokorný, R., Šprtová, M., Zhang, R., Špunda, V.R., Grace, J., Marek, M.V., 2007. Ecophysiological controls over the net ecosystem exchange of mountain spruce stand. Comparison of the response in direct vs. diffuse solar radiation. Glob. Chang. Biol. 13, 157–168. https://doi.org/10.1111/j.1365-2486.2006.01265.x.
Urban, O., Klem, K., Ač, A., Havránková, K., Holišová, P., Navrátil, M., Zitová, M., Kozlová, K., Pokorný, R., Šprtová, M., Tomášková, I., Špunda, V., Grace, J., 2012. Impact of clear and cloudy sky conditions on the vertical distribution of photosynthetic CO2 uptake within a spruce canopy. Funct. Ecol. 26, 46–55. https://doi.org/10.1111/j.1365-2435.2011.01934.x.
Vaganov, E.A., Hughes, M.K., Shashkin, A.V., 2006. Growth dynamics of conifer tree rings. Taxon. https://doi.org/10.2307/1217399.
Verbyla, D., 2015. Remote sensing of interannual boreal forest NDVI in relation to climatic conditions in interior Alaska. Environ. Res. Lett. 10 https://doi.org/10.1088/1748-9326/10/12/125016.
Vicente-Serrano, S.M., Lasanta, T., Romo, A., 2004. Analysis of spatial and temporal evolution of vegetation cover in the Spanish central pyrenees: role of human management. Environ. Manag. 34, 802–818. https://doi.org/10.1007/s00267-003-0022-5.
Vicente-Serrano, S.M., Beguería, S., López-Moreno, J.I., 2010. A multiscalar drought index sensitive to global warming: the standardized precipitation evapotranspiration index. J. Climate 23, 1696–1718. https://doi.org/10.1175/2009JCLI2909.1.
Vicente-Serrano, S.M., Gouveia, C., Camarero, J.J., Beguería, S., Trigo, R., López-Moreno, J.I., Azorín-Molina, C., Pasho, E., Lorenzo-Lacruz, J., Revuelto, J., Morán-Tejeda, E., Sanchez-Lorenzo, A., 2012. Response of vegetation to drought time-scales across global land biomes. Proc. Natl. Acad. Sci. U. S. A. 110, 52–57. https://doi.org/10.1073/pnas.1207068110.
Vicente-Serrano, S.M., Camarero, J.J., Olano, J.M., Martín-Hernández, N., Peña-Gallardo, M., Tomás-Burguera, M., Gazol, A., Azorin-Molina, C., Bhuyan, U., El Kenawy, A., 2016. Diverse relationships between forest growth and the normalized difference vegetation index at a global scale. Remote Sens. Environ. 187, 14–29. https://doi.org/10.1016/j.rse.2016.10.001.
Vicente-Serrano, S.M., Martín-Hernández, N., Camarero, J.J., Gazol, A., Sánchez-Salguero, R., Peña-Gallardo, M., El Kenawy, A., Domínguez-Castro, F., Tomas-Burguera, M., Gutiérrez, E., de Luis, M., Sangüesa-Barreda, G., Novak, K., Rozas, V., Tíscar, P.A., Linares, J.C., del Castillo, E.M., Ribas, M., García-González, I., Silla, F., Camisón, A., Génova, M., Olano, J.M., Longares, L.A., Hevia, A., Diego Galván, J., 2020. Linking tree-ring growth and satellite-derived gross primary growth in multiple forest biomes. Temporal-scale matters. Ecol. Indic. 108 https://doi.org/10.1016/j.ecolind.2019.105753.
Viewegh, J., Kusbach, A., Mikeska, M., 2003. Czech forest ecosystem classification. J. For. Sci. 49, 74–82. https://doi.org/10.17221/4682-jfs.
Wang, J., Ye, B., Liu, F., Li, J., Yang, G., 2011. Variations of NDVI over elevational zones during the past two decades and climatic controls in the Qilian mountains, northwestern China. Arct. Antarct. Alp. Res. 43, 127–136. https://doi.org/10.1657/1938-4246-43.1.127.
Wang, Z., Lyu, L., Liu, W., Liang, H., Huang, J., Zhang, Q. Bin, 2021. Topographic patterns of forest decline as detected from tree rings and NDVI. Catena 198, 105011. https://doi.org/10.1016/j.catena.2020.105011.
Wang, H., Muller, J.D., Tatarinov, F., Yakir, D., Rotenberg, E., 2022. Disentangling soil, shade, and tree canopy contributions to mixed satellite vegetation indices in a sparse dry forest. Remote Sens. (Basel) 14 (15), 3681. https://doi.org/10.3390/rs14153681.
Wood, S.N., 2011. Fast stable restricted maximum likelihood and marginal likelihood estimation of semiparametric generalized linear models. J. R. Stat. Soc. Ser. B Stat Methodol. 73, 3–36. https://doi.org/10.1111/j.1467-9868.2010.00749.x.
Wu, C., Niu, Z., 2012. Modelling light use efficiency using vegetation index and land surface temperature from MODIS in Harvard Forest. Int. J. Remote Sens. 33, 2261–2276. https://doi.org/10.1080/01431161.2011.608090.
Wu, X., Liu, H., Li, X., Ciais, P., Babst, F., Guo, W., Zhang, C., Magliulo, V., Pavelka, M., Liu, S., Huang, Y., Wang, P., Shi, C., Ma, Y., 2017. Differentiating drought legacy effects on vegetation growth over the temperate Northern Hemisphere. Glob. Chang. Biol. 24, 504–516. https://doi.org/10.1111/gcb.13920.
Xu, P., Fang, W., Zhou, T., Zhao, X., Luo, H., Hendrey, G., Yi, C., 2019. Spatial upscaling of tree-ring-based forest response to drought with satellite data. Remote Sens. (Basel) 11. https://doi.org/10.3390/rs11202344.
Yuan, W., Liu, S., Zhou, G., Zhou, G., Tieszen, L.L., Baldocchi, D., Bernhofer, C., Gholz, H., Goldstein, A.H., Goulden, M.L., Hollinger, D.Y., Hu, Y., Law, B.E., Stoy, P. C., Vesala, T., Wofsy, S.C., 2007. Deriving a light use efficiency model from eddy covariance flux data for predicting daily gross primary production across biomes. Agric. For. Meteorol. 143, 189–207. https://doi.org/10.1016/j.agrformet.2006.12.001.
Zang, C., Biondi, F., 2015. Treeclim: an R package for the numerical calibration of proxy-climate relationships. Ecography (Cop.) 38, 431–436. https://doi.org/10.1111/ecog.01335.
Zang, C., Pretzsch, H., Rothe, A., 2012. Size-dependent responses to summer drought in scots pine, Norway spruce and common oak. Trees - Struct. Funct. 26, 557–569. https://doi.org/10.1007/s00468-011-0617-z.
Zhang, M., Yu, G.R., Zhang, L.M., Sun, X.M., Wen, X.F., Han, S.J., Yan, J.H., 2010. Impact of cloudiness on net ecosystem exchange of carbon dioxide in different types of forest ecosystems in China. Biogeosciences 7, 711–722. https://doi.org/10.5194/bg-7-711-2010.
Zheng, L., Gaire, N.P., Shi, P., 2021. High-altitude tree growth responses to climate change across the Hindu Kush Himalaya. J. Plant Ecol. 14, 829–842. https://doi.org/10.1093/jpe/rtab035.
Zhu, Z., Wang, S., Woodcock, C.E., 2015. Improvement and expansion of the Fmask algorithm: cloud, cloud shadow, and snow detection for Landsats 4-7, 8, and sentinel 2 images. Remote Sens. Environ. 159, 269–277. https://doi.org/10.1016/j.rse.2014.12.014.
Zhu, M., Zhang, J., Zhu, L., 2021. Variations in growing season NDVI and its sensitivity to climate change responses to green development in mountainous areas. Front. Environ. Sci. 9, 1–11. https://doi.org/10.3389/fenvs.2021.678450.